

**GEORGIA DOT RESEARCH PROJECT 18-05**

**FINAL REPORT**

**UPDATED LAYER COEFFICIENTS FOR GDOT  
FLEXIBLE PAVEMENT DESIGN**



**OFFICE OF PERFORMANCE-BASED  
MANAGEMENT AND RESEARCH**

**600 WEST PEACHTREE STREET NW  
ATLANTA, GA 30308**

**March 2022**

## TECHNICAL REPORT DOCUMENTATION PAGE

<b>1. Report No.</b> FHWA-GA-22-1805	<b>2. Government Accession No.</b> N/A	<b>3. Recipient's Catalog No.</b> N/A	
<b>4. Title and Subtitle</b> Updated Layer Coefficients for GDOT Flexible Pavement Design		<b>5. Report Date</b> March 2022	
		<b>6. Performing Organization Code</b> N/A	
<b>7. Author(s)</b> S. Sonny Kim, Ph.D., P.E. <a href="https://orcid.org/0000-0002-3468-0230">https://orcid.org/0000-0002-3468-0230</a> ; Hyung S. Lee, Ph.D., P.E. <a href="https://orcid.org/0000-0003-1616-7449">https://orcid.org/0000-0003-1616-7449</a> ; Stephan A. Durham, Ph.D., P.E.; R. Benjamin Davis, Ph.D. <a href="https://orcid.org/0000-0003-4478-302X">https://orcid.org/0000-0003-4478-302X</a> ; Ryan Romeo <a href="https://orcid.org/0000-0002-5344-8883">https://orcid.org/0000-0002-5344-8883</a>		<b>8. Performing Organization Report No.</b> 18-05	
<b>9. Performing Organization Name and Address</b> University of Georgia, College of Engineering Driftmier Engineering Center, Athens, GA 30602 Phone: (706) 542-9804, Email: kims@uga.edu		<b>10. Work Unit No.</b> N/A	
		<b>11. Contract or Grant No.</b> PI# 0016337	
<b>12. Sponsoring Agency Name and Address</b> Georgia Department of Transportation Office of Performance-based Management and Research 600 West Peachtree Street NW Atlanta, GA 30308		<b>13. Type of Report and Period Covered</b> Final Report (Oct. 2018- March 2022)	
		<b>14. Sponsoring Agency Code</b> N/A	
<b>15. Supplementary Notes</b> Conducted in cooperation with the U.S. Department of Transportation, Federal Highway Administration.			
<b>16. Abstract</b> <p>Currently, the Georgia Department of Transportation (GDOT) uses the 1972 American Association of State Highway and Transportation Officials (AASHTO) empirical pavement design procedure for the structural design of highways. The layer coefficients used at this time by GDOT were empirically derived from pavement mixes more than 50 years ago. Since then, the asphalt mixtures and vehicle loads have seen significant changes. Based on the increased use of modern asphalt binders/mixtures, such as reclaimed asphalt pavement (RAP), ground tire rubber (GTR), and stone matrix asphalt (SMA), there is a need to update the layer coefficients as a means to account for these recent developments in the design and construction of Georgia (GA) pavements.</p> <p>In this project, a number of road segments with varying condition were identified in different GDOT districts across Georgia. Then, falling weight deflectometer (FWD) testing was conducted along the selected sites. At some of the FWD testing stations, pavement cores were also extracted and tested in an asphalt mixture performance tester (AMPT) to determine accurate dynamic modulus (<math>E^*</math>) curves for the locations.</p> <p>The <math>E^*</math> curves obtained from AMPT testing were used to calculate updated layer coefficient values for flexible GA pavements. To process the FWD data, a state-of-the-art dynamic backcalculation software, UGA-PAVE, was developed. The software was validated by comparing the <math>E^*</math> curves backcalculated for the core locations with those measured via AMPT testing. A few issues were observed during the validation; consequently, ground-penetrating radar (GPR) testing was performed along some of the sites where the FWD testing was conducted. From the GPR testing, high variations in subgrade density were observed in most of the problematic sites tested, highlighting the importance of accurate knowledge of material properties for pavement layers below the asphalt.</p>			
<b>17. Key Words</b> Asphalt Concrete, MEPDG, Layer Coefficients, FWD Backcalculation		<b>18. Distribution Statement</b> No Restrictions	
<b>19. Security Classification (of this report)</b> Unclassified	<b>20. Security Classification (of this page)</b> Unclassified	<b>21. No. of Pages</b> 118	<b>22. Price</b> Free

GDOT Research Project 18-05

Final Report

UPDATED LAYER COEFFICIENTS FOR GDOT  
FLEXIBLE PAVEMENT DESIGN

By

S. Sonny Kim, Ph.D., P.E., F.ASCE  
Associate Professor

Hyung S. Lee, Ph.D., P.E.  
Senior Civil Engineer, Applied Research Associates

Stephan A. Durham, Ph.D., P.E.  
Professor

R. Benjamin Davis, Ph.D.  
Associate Professor

Ryan Romeo  
Graduate Research Assistant

Civil Engineering, College of Engineering  
University of Georgia

Contract with  
Georgia Department of Transportation

In cooperation with  
U.S. Department of Transportation  
Federal Highway Administration

March 2022

The contents of this report reflect the views of the authors who are responsible for the facts and the accuracy of the data presented herein. The contents do not necessarily reflect the official views or policies of the Georgia Department of Transportation or the Federal Highway Administration. This report does not constitute a standard, specification, or regulation.

# SI\* (MODERN METRIC) CONVERSION FACTORS

## APPROXIMATE CONVERSIONS TO SI UNITS

Symbol	When You Know	Multiply By	To Find	Symbol
<b>LENGTH</b>				
in	inches	25.4	millimeters	mm
ft	feet	0.305	meters	m
yd	yards	0.914	meters	m
mi	miles	1.61	kilometers	km
<b>AREA</b>				
in <sup>2</sup>	square inches	645.2	square millimeters	mm <sup>2</sup>
ft <sup>2</sup>	square feet	0.093	square meters	m <sup>2</sup>
yd <sup>2</sup>	square yard	0.836	square meters	m <sup>2</sup>
ac	acres	0.405	hectares	ha
mi <sup>2</sup>	square miles	2.59	square kilometers	km <sup>2</sup>
<b>VOLUME</b>				
fl oz	fluid ounces	29.57	milliliters	mL
gal	gallons	3.785	liters	L
ft <sup>3</sup>	cubic feet	0.028	cubic meters	m <sup>3</sup>
yd <sup>3</sup>	cubic yards	0.765	cubic meters	m <sup>3</sup>
NOTE: volumes greater than 1000 L shall be shown in m <sup>3</sup>				
<b>MASS</b>				
oz	ounces	28.35	grams	g
lb	pounds	0.454	kilograms	kg
T	short tons (2000 lb)	0.907	megagrams (or "metric ton")	Mg (or "t")
<b>TEMPERATURE (exact degrees)</b>				
°F	Fahrenheit	5 (F-32)/9 or (F-32)/1.8	Celsius	°C
<b>ILLUMINATION</b>				
fc	foot-candles	10.76	lux	lx
fl	foot-Lamberts	3.426	candela/m <sup>2</sup>	cd/m <sup>2</sup>
<b>FORCE and PRESSURE or STRESS</b>				
lbf	poundforce	4.45	newtons	N
lbf/in <sup>2</sup>	poundforce per square inch	6.89	kilopascals	kPa

## APPROXIMATE CONVERSIONS FROM SI UNITS

Symbol	When You Know	Multiply By	To Find	Symbol
<b>LENGTH</b>				
mm	millimeters	0.039	inches	in
m	meters	3.28	feet	ft
m	meters	1.09	yards	yd
km	kilometers	0.621	miles	mi
<b>AREA</b>				
mm <sup>2</sup>	square millimeters	0.0016	square inches	in <sup>2</sup>
m <sup>2</sup>	square meters	10.764	square feet	ft <sup>2</sup>
m <sup>2</sup>	square meters	1.195	square yards	yd <sup>2</sup>
ha	hectares	2.47	acres	ac
km <sup>2</sup>	square kilometers	0.386	square miles	mi <sup>2</sup>
<b>VOLUME</b>				
mL	milliliters	0.034	fluid ounces	fl oz
L	liters	0.264	gallons	gal
m <sup>3</sup>	cubic meters	35.314	cubic feet	ft <sup>3</sup>
m <sup>3</sup>	cubic meters	1.307	cubic yards	yd <sup>3</sup>
<b>MASS</b>				
g	grams	0.035	ounces	oz
kg	kilograms	2.202	pounds	lb
Mg (or "t")	megagrams (or "metric ton")	1.103	short tons (2000 lb)	T
<b>TEMPERATURE (exact degrees)</b>				
°C	Celsius	1.8C+32	Fahrenheit	°F
<b>ILLUMINATION</b>				
lx	lux	0.0929	foot-candles	fc
cd/m <sup>2</sup>	candela/m <sup>2</sup>	0.2919	foot-Lamberts	fl
<b>FORCE and PRESSURE or STRESS</b>				
N	newtons	0.225	poundforce	lbf
kPa	kilopascals	0.145	poundforce per square inch	lbf/in <sup>2</sup>

\*SI is the symbol for the International System of Units. Appropriate rounding should be made to comply with Section 4 of ASTM E380. (Revised March 2003)

## TABLE OF CONTENTS

TABLE OF CONTENTS .....	iv
LIST OF FIGURES .....	vi
LIST OF TABLES .....	viii
EXECUTIVE SUMMARY .....	1
UPDATED LAYER COEFFICIENTS .....	2
FWD BACKCALCULATION SOFTWARE.....	3
CHAPTER 1. INTRODUCTION .....	4
CHAPTER 2. LITERATURE REVIEW .....	6
LAYER COEFFICIENTS .....	6
FWD BACKCALCULATION .....	9
Numerical Pavement Models.....	10
Optimization Routines .....	12
CHAPTER 3. SITE SELECTION.....	15
CHAPTER 4. UGA-PAVE DEVELOPMENT.....	21
DESCRIPTION OF METHODS.....	21
Numerical Pavement Model .....	21
Optimization Routine.....	34
SOFTWARE SUMMARY .....	40
CHAPTER 5. UPDATED LAYER COEFFICIENTS.....	47
PROCEDURE.....	47
RESULTS.....	51
Coefficients Calculated from AMPT Testing.....	52
Coefficients Calculated from FWD Backcalculation .....	57
Comparison with Updated Coefficients of Other State DOTs .....	61
CHAPTER 6. UGA-PAVE VALIDATION .....	63
PROCEDURE.....	63
VALIDATION RESULTS .....	66
CHAPTER 7. CONCLUSIONS AND RECOMMENDATIONS .....	77
UPDATED LAYER COEFFICIENTS .....	77
FWD BACKCALCULATION .....	77
APPENDICES .....	79

**APPENDIX A. PROPOSED STANDARD OPERATING PROCEDURE FOR  
CALCULATING NEW LAYER COEFFICIENTS FROM DYNAMIC MODULUS DATA ..... 79**

**APPENDIX B. PROPOSED STANDARD OPERATING PROCEDURE FOR OPERATION  
OF UGA-PAVE FOR DYNAMIC MODULUS BACKCALCULATION ..... 84**

**ACKNOWLEDGMENTS ..... 102**

**REFERENCES ..... 103**

## LIST OF FIGURES

Figure 1. Map. Statewide map of GDOT segment ratings $\geq 75$ . .....	16
Figure 2. Map. GDOT District 1 mapped for segment ratings $\geq 75$ . .....	17
Figure 3. Map. GDOT District 2 mapped for segment ratings $\geq 75$ . .....	17
Figure 4. Map. GDOT District 3 mapped for segment ratings $\geq 75$ . .....	18
Figure 5. Map. GDOT District 4 mapped for segment ratings $\geq 75$ . .....	18
Figure 6. Map. GDOT District 5 mapped for segment ratings $\geq 75$ . .....	19
Figure 7. Map. GDOT District 6 mapped for segment ratings $\geq 75$ . .....	19
Figure 8. Screen. UGA-PAVE Data Import Wizard page. ....	42
Figure 9. Screen. UGA-PAVE Material Properties input page. ....	42
Figure 10. Screen. UGA-PAVE FWD Backcalculation runtime page. ....	43
Figure 11. Screen. UGA-PAVE Pseudo-Level 1 Dynamic Modulus Mastercurve results page. ....	45
Figure 12. Screen. UGA-PAVE Level 2 Creep Compliance Curve results page. ....	46
Figure 13. Screen. UGA-PAVE Moduli Variation results page. ....	46
Figure 14. Graph. AMPT-measured dynamic modulus data for Lift 1 of Core 1 extracted from SR 11. ....	54
Figure 15. Graph. Above-4.5-inch layer coefficients calculated from AMPT data. ....	55
Figure 16. Graph. Below-4.5-inch layer coefficients calculated from AMPT data. ....	55
Figure 17. Graph. Full-depth layer coefficients calculated from AMPT data. ....	56
Figure 18. Photo. Composite Core 1 extracted from SR 26, featuring asphalt on top of PCC. ....	56
Figure 19. Graph. FWD backcalculated layer coefficients corresponding to the top 4.5 inches of asphalt for SR 10, SR 11, SR 22, SR 26, SR 57 (Johnson County), and SR 82. ....	58
Figure 20. Graph. FWD backcalculated layer coefficients corresponding to the asphalt portion below a depth of 4.5 inches for SR 10, SR 11, SR 22, SR 26, SR 57 (Johnson County), and SR 82. ....	59
Figure 21. Graph. FWD backcalculated layer coefficients representing the entire asphalt concrete layer for SR 10, SR 11, SR 22, SR 26, SR 57 (Johnson County), and SR 82. ....	60
Figure 22. Photo. Asphalt core after 38 mm specimens were extracted for AMPT testing. ....	64
Figure 23. Graph. Comparison of FWD backcalculated and lab-measured $ E^* $ for SR 10 Core 4. ....	67

Figure 24. Graph. Comparison of FWD backcalculated and lab-measured $ E^* $ for SR 10 Core 7. ....	68
Figure 25. Graph. Comparison of FWD backcalculated and lab-measured $ E^* $ for SR 11 Core 3. ....	68
Figure 26. Graph. Comparison of FWD backcalculated and lab-measured $ E^* $ for SR 22 Core 1. ....	69
Figure 27. Graph. Comparison of FWD backcalculated and lab-measured $ E^* $ for SR 26 Core 1. ....	69
Figure 28. Graph. Comparison of FWD backcalculated and lab-measured $ E^* $ for SR 57 (Johnson County) Core 3. ....	70
Figure 29. Graph. Comparison of FWD backcalculated and lab-measured $ E^* $ for SR 82 Core 1. ....	70
Figure 30. Graph. Comparison of FWD backcalculated and lab-measured $ E^* $ for SR 82 Core 3. ....	71
Figure 31. Graph. Comparison of FWD backcalculated and lab-measured $ E^* $ for SR 129 Core 5. ....	71
Figure 32. Graph. Subgrade density estimated by GPR for SR 26N. ....	73
Figure 33. Graph. Subgrade density estimated by GPR for SR 26S. ....	74
Figure 34. Graph. Subgrade density estimated by GPR for SR 129N. ....	74
Figure 35. Graph. Subgrade density estimated by GPR for SR 129S. ....	75
Figure 36. Graph. Subgrade density estimated by GPR for SR 10W. ....	75
Figure 37. Graph. Subgrade density estimated by GPR for SR 10E. ....	76
Figure 38. Screen. Initial Microsoft Access after opening FWD data database file. ....	93
Figure 39. Screen. Histories tab of the imported FWD data. ....	94
Figure 40. Screen. Example of the “Export – Excel Spreadsheet” window. ....	94
Figure 41. Screen. FWD data export confirmation window. ....	95
Figure 42. Screen. The UGA-PAVE starting page. ....	96
Figure 43. Screen. UGA-PAVE data import wizard prior to importing FWD data. ....	96
Figure 44. Screen. Import wizard after selecting and importing FWD data. ....	97
Figure 45. Screen. Example of setting material properties for Station 1. ....	98
Figure 46. Screen. Example of setting material properties for Station 55. ....	98
Figure 47. Screen. Example of runtime window prior to starting backcalculation. ....	99
Figure 48. Screen. Example of $ E^* $ results page after backcalculation completes. ....	99
Figure 49. Screen. Demonstration of exporting $ E^* $ result from UGA-PAVE. ....	100
Figure 50. Screen. Example of exported $ E^* $ data from UGA-PAVE to an Excel file. ....	101



## LIST OF TABLES

Table 1. Final selection of GA state routes for FWD, GPR, and core testing. ....	20
Table 2. Information for cores used in AMPT testing for updated layer coefficients. ....	52
Table 3. Statistical analysis of AMPT-derived layer coefficients. ....	57
Table 4. Seed moduli (initial guesses) for the backcalculation parameters of each pavement section.....	65
Table 5. Constant parameters for each pavement section used in the backcalculation. ....	65

## EXECUTIVE SUMMARY

Currently, the Georgia Department of Transportation (GDOT) uses the 1972 American Association of State Highway and Transportation Officials (AASHTO), including the 1981 Revisions, empirical pavement design procedure for the structural design of highways. The layer coefficients currently used by GDOT were empirically derived from pavement mixes more than 50 years ago. Since that time, asphalt mixtures and vehicle loads have seen significant changes. Based on the increased use of modern asphalt binders/mixtures, such as reclaimed asphalt pavement (RAP), ground tire rubber (GTR), and stone matrix asphalt (SMA), as well as newer manufacturing and construction techniques, such as cold in-place recycling, there is a need to update the layer coefficients to account for these recent developments in the design and construction of Georgia (GA) pavements.

In this project, a number of road segments with varying condition were identified in different GDOT districts across Georgia. Falling weight deflectometer (FWD) testing was conducted along the selected sites. At some of the FWD testing stations, pavement cores were also extracted and tested in an asphalt mixture performance tester (AMPT) to determine accurate dynamic modulus ( $|E^*|$ ) curves for the locations.

The  $|E^*|$  curves obtained from AMPT testing were used to calculate updated layer coefficient values for flexible GA pavements. To process the FWD data, a state-of-the-art dynamic backcalculation software, UGA-PAVE, was developed. The software was validated by comparing the  $|E^*|$  curves backcalculated for the core locations with those measured via AMPT testing. A few issues were observed during the validation; consequently, ground-penetrating radar (GPR) testing was performed along some of the sites where the FWD testing was conducted. From the GPR

testing, high variations in subgrade density were observed in most of the problematic sites tested, highlighting the importance of accurate knowledge of material properties for the foundation layers beneath the asphalt.

## **UPDATED LAYER COEFFICIENTS**

Key findings from the updated layer coefficients study include the following:

- Three types of layer coefficients are calculated:
  - The first two coefficients reflect current GDOT practice and represent the strength of the portion of the asphalt: (1) above 4.5 inches of depth, and (2) below 4.5 inches of depth.
  - The third coefficient represents the entire pavement layer, which is helpful for comparing to the convention of other state DOTs.
- For the first coefficient (i.e., top 4.5 inches of asphalt):
  - An average value of 0.50 was observed, with standard deviation of 0.03.
  - From statistical analysis of the samples, a coefficient of 0.44 can be used with 97.8 percent reliability (unchanged from current GDOT practice).
- For the second coefficient (i.e., asphalt below 4.5 inches):
  - An average value of 0.51 was recorded, with standard deviation of 0.06.
  - From statistical analysis, a coefficient of 0.39 can be used with 97.8 percent reliability (up from 0.33 in current GDOT practice).
- For the third coefficient (i.e., full asphalt layer):
  - An average value of 0.51 was determined, with standard deviation of 0.04.

- From statistical analysis, a coefficient of 0.43 can be used with 97.8 percent reliability.
- Higher layer coefficient values associated with lower reliabilities (i.e., 50 and 84.2 percent) are also provided for all three coefficients in the event less conservative designs are desired.

## **FWD BACKCALCULATION SOFTWARE**

Key findings from the FWD backcalculation study include the following:

- A new dynamic FWD backcalculation software, UGA-PAVE, has been developed and made available to GDOT as a deliverable for this project.
- A novel optimization algorithm was developed for UGA-PAVE, designed specifically for FWD backcalculation. Additionally, the software employs a state-of-the-art pavement modeling algorithm, ViscoWave.
- Issues were encountered in the backcalculations of some of the pavement sections during validation. As a result, GPR testing was conducted, and it was observed that accurate knowledge of material properties (e.g., density, Poisson's ratio, modulus) for the foundation layers below the asphalt is crucial for accurate backcalculation of the dynamic modulus.
- Future studies are recommended pertaining to the relationship between FWD-backcalculated dynamic modulus and foundation layer properties, such as the subgrade modulus. Furthermore, GPR testing can serve as an invaluable tool alongside FWD testing to quickly determine many pertinent properties, such as the foundation layer thicknesses and densities.

## CHAPTER 1. INTRODUCTION

The Georgia Department of Transportation (GDOT) uses the 1972 American Association of State Highway and Transportation Officials (AASHTO), including the 1981 revisions, empirical pavement design procedure for its structural design of asphalt concrete (AC) pavements.<sup>[1]</sup> In the involved procedure, each pavement layer is associated with a layer coefficient value, which is then used for thickness design of the pavement structure. The current layer coefficients used by GDOT are those proposed by AASHTO in the 1960s; however, asphalt mixtures and vehicle loads have changed substantially since that time. Furthermore, with the increased use of newer asphalt binders and mixtures, such as reclaimed asphalt pavement (RAP), ground tire rubber (GTR), and stone matrix asphalt (SMA), as well as newer manufacturing and construction techniques (e.g., cold in-place recycling), there is a need to update the layer coefficients for these recently developed materials that are currently being used for design and construction of Georgia (GA) pavements.

The primary objective of this research project is to evaluate the layer coefficients of asphalt concrete layers currently used by GDOT and provide updated values that more appropriately reflect the characteristics of modern materials. Since the early 2000s, other state DOTs have conducted similar studies, and thus far all have found that the coefficients determined by AASHTO lead to significant overdesigning of flexible pavements when using modern materials, which translates into higher construction costs than necessary. In this study, new layer coefficients are determined and recommended for GDOT to use in its flexible pavement designs. Although further studies are warranted, it is anticipated that the outcomes of this study can be used to improve GDOT's current flexible pavement design process (via the updated layer coefficients), in addition to GDOT's future design process as it transitions to the *Mechanistic–Empirical Pavement Design Guide* (MEPDG) and AASHTOWare Pavement ME Design (PMED) Software.

Current practice to determine  $|E^*|$  of a flexible pavement involves extracting cylindrical samples, or cores, from the pavement section and conducting expensive and time-consuming lab tests. As one part of this study, a state-of-the-art dynamic modulus backcalculation tool, UGA-PAVE, has been developed for *in situ* estimation of dynamic modulus ( $|E^*|$ ) via falling weight deflectometer (FWD) backcalculation, which is significantly faster than core extraction and testing. Furthermore, FWD backcalculation is a nondestructive testing (NDT) method, meaning the pavement is virtually unharmed in the process; conversely, core testing damages the pavement, where the hole left in the pavement after core extraction must be filled in. Given proper inputs for the geometry of the pavement structure, the backcalculation software analyzes FWD force and deflection data and then estimates the *in situ* dynamic modulus curve. As part of this study, the software was validated with lab-measured  $|E^*|$  from asphalt cores. The tool was used to backcalculate the dynamic modulus master curves from pavement sections selected from 10 Georgia roads of varying health, and the updated layer coefficients were computed using those backcalculated  $|E^*|$  curves.

It should be noted that the original layer coefficients were determined based on loss of pavement serviceability (or more specifically, the present serviceability index [PSI]), which is an indicator of the overall pavement performance, including cracking, rutting, and ride quality. Therefore, the layer coefficient used in the empirical AASHTO design represents the “overall quality” of a given material that contributes to the overall pavement performance, rather than a physical parameter with scientific units. Since the layer coefficient is not a physical parameter, it usually involves large-scale, long-term pavement experiments and/or calibration for determining the coefficients for different pavement layers. Nonetheless, the scope of this study is limited to evaluating the layer coefficient of GDOT’s AC mixtures based on a physical parameter, namely the dynamic modulus.

## CHAPTER 2. LITERATURE REVIEW

### LAYER COEFFICIENTS

The earliest significant techniques for calculating the structural number (SN) via FWD testing were established in the AASHTO 1986 *Guide for Design of Pavement Structures*, wherein two methods are given.<sup>[2]</sup> In the first procedure, the layer moduli are estimated using FWD backcalculation, after which the moduli are converted to layer coefficients (used to calculate SN) via the steps outlined in Volume 2 of the guide. The second procedure involves using the FWD deflection sensor measurements to estimate the SN of the pavement as a whole. However, both methods have notable disadvantages, with the first being time-consuming and requiring accurate backcalculation results, and the second being based upon Burmister's two-layer model, whereby the subgrade is assumed to be a halfspace with infinite thickness, which is not always a viable approximation for pavements in practice when the subgrade is shallow.

In 1992, the New Hampshire DOT (NHDOT) found that two pavement sections assumed to have approximately the same SN exhibited notably different deflections under equivalent loading. As a result, Janoo determined updated layer coefficients for base course materials using a novel technique based on FWD measurements, and the updated values were shown to have acceptable agreement with experimental Clegg Hammer (i.e., Clegg Impact Soil Tester) and dynamic cone penetrometer results.<sup>[3]</sup> In 1994, Rohde proposed new guidelines for calculating the SN from FWD tests, and developed a new approach based on the "deflection bowl," which can be determined from FWD measurements.<sup>[4]</sup> The approach was validated using data from 62 *in situ* pavement sections and was shown to have good agreement with the first procedure outlined in the 1986 AASHTO *Design Guide*. However, the equation Rohde developed was not entirely robust, as it

only required pavement thickness and FWD measurement data as inputs and assumed purely elastic materials for the pavement layers.<sup>[5]</sup>

Kim et al. later improved Rohde's approach by modifying it to consider depth to a rigid layer, as well as by enlarging the database's range of pavement structures and responses used to generate the equation.<sup>[6]</sup> In the study, they showed that Rohde's equation tends to underestimate the effective structural number; as a result, they determined new coefficients for Rohde's equation and showed their modified equation offers improved SN estimation. Because their modified approach only involves changing the coefficient values of the equation, it uses the same inputs as Rohde's—FWD deflections and pavement thickness—and therefore is no more difficult to implement in practice.

Bahia et al. conducted a study for the Wisconsin DOT (WisDOT) to generate layer coefficients for different asphalt mix types.<sup>[7]</sup> Using the traditional AASHTO technique based on resilient modulus, they compared backcalculated resilient modulus from nondestructive testing with lab-measured samples for pavements of varying levels of distress. Results from the study led to recommended layer coefficients ranging from 0.17 to 0.23 for asphaltic materials used in Wisconsin. Afterward, a new technique for determining layer coefficients was proposed, but its validity was not explored in the study. Peters-Davis and Timm updated asphalt layer coefficients for the Alabama DOT (ALDOT) in 2009.<sup>[8]</sup> They found that structural number, traffic loading, and resilient modulus were the most pertinent factors for good accuracy when using the 1993 AASHTO *Design Guide*, and their study targeted updating the SN values due to traffic loading and resilient modulus, which are typically given for a design problem. To calculate new coefficients, they tested eight pavement sections from the National Center for Asphalt Technology (NCAT) Pavement Test Track at Auburn University within two periods: 2003–2006 and



2006–2009. The sections were selected to have notably different thicknesses so as to promote a wide variety of pavement distresses over the testing periods. Their results suggested that the average layer coefficient for hot mix asphalt (HMA) sections at least 5 inches thick is 0.54 (with a standard deviation of 0.08 among the 14 pavement sections tested) rather than the traditional 0.44 determined by AASHTO in the 1960s, and this was estimated to lead to an HMA layer-thickness reduction of 18 percent. A 2019 Florida DOT (FDOT) study conducted by Taylor also concluded that the layer coefficient for high polymer (HP) asphalt concrete mixes should be 0.54.<sup>[9]</sup> The updated value was calculated using experimental methods and verified across a wide array of distress modes, such as rutting and reflective cracking. Results from the study suggested that using HP asphalt mixes with a structural number of 0.54 would lead to a 23 percent reduction in asphalt layer thickness over using polymer-modified asphalt (PMA) mixes under similar environments and loadings.<sup>[3]</sup>

Recently, Virginia DOT (VDOT) funded a research effort comparing the SNs estimated from FWD and traffic speed deflectometer (TSD) measurements for use in network-level applications.<sup>[10]</sup> The study found that TSD testing was as effective as the more common FWD testing at identifying pavement sections that *require* rehabilitation at the network level. The identification process used was to first calculate effective SNs from the FWD and TSD measurements; then pavement sections whose SN's fell within the lower 30<sup>th</sup> percentile were identified as “structurally weak.” The main conclusion of the study was that using one set of FWD data along with one set of TSD data was observed to have better agreement in general (i.e., more likely to identify the same amount of structurally weak pavement sections) compared to using two different sets of FWD data. A few important issues concerning the results/conclusions should be addressed. First, the analysis was only performed for interstate roads, as VDOT did not have

enough data for network-level analysis on primary roads for comparison with TSD. Second, the analyses performed did not consider whether the same pavement sections were identified as structurally weak; only the *number* of pavement sections below the 30<sup>th</sup> percentile were considered in regard to the quality of agreement. Finally, there were large gaps in time between the data collections of the first FWD, second FWD, and TSD data collections. The first set of FWD data was collected between years 2006 and 2008 and the second set was obtained in 2011, whereas the corresponding TSD testing was performed in 2015. In other words, the results from the study are inconclusive regarding whether conducting TSD and FWD testing *at the same time* is more effective than solely conducting FWD testing.

The most recent study involving updated layer coefficients for use with structural number was conducted for NHDOT by Nematy et al.<sup>[11]</sup> For their approach, they measured the international roughness index (IRI) for 17 pavements of varying conditions. Using those measurements, they backcalculated the change in PSI for each section. Then, inputting corresponding traffic data and typical design values, they used the 1993 AASHTO design equation to calculate the *in situ* structural number of the entire pavement section. Finally, they used the estimated SN to estimate layer coefficients for each site's AC layer. In their results, they proposed a layer coefficient of 0.41 for HMA, up from NHDOT's typically used values ranging between 0.34 and 0.38.

## **FWD BACKCALCULATION**

Pavement backcalculation methods are used to monitor the structural health of asphalt concrete pavements by inversely calculating the modulus parameters. The most popular approach involves using a falling weight deflectometer, which is a type of nondestructive testing equipment that rapidly impacts the pavement and measures the displacement response along the surface.<sup>[12]</sup> The

deflection sensors are arranged in a line extending from the point of loading to measure the displacement wave as it propagates through the pavement. FWD backcalculation methods comprise two essential parts: an optimization scheme and a computational model of the pavement structure. In short, the optimization scheme uses the pavement model to identify a set of layer moduli that most closely reproduces the experimentally measured deflection response. Thus, the literature review presented here will be separated into two sections—one pertaining to the development of robust numerical pavement models, and one to the optimization methodology.

### **Numerical Pavement Models**

Despite the load imparted by the deflectometer being transient, the traditional FWD backcalculation methods are static in nature. In such methods<sup>[13][14][15]</sup>, the deflections from each sensor are considered only for a single time point in the numerical model, which greatly reduces computational expense; however, static backcalculation methods are prone to inaccuracies due to the viscoelastic nature of flexible pavements.<sup>[16][17]</sup> Asphalt concrete is well known to be a viscoelastic material, which means its modulus varies with both temperature and the loading rate; thus, consideration of multiple time points is required to properly simulate the problem.

Over time, dynamic FWD backcalculation techniques have emerged, offering increases in accuracy via numerical models that consider multiple time points in the deflection responses.<sup>[17][18][19][20][21][22][23]</sup> The pavement models are most commonly constructed using the finite element method (FEM)<sup>[13][14][16]</sup>; however, when modeling dynamic pavement responses, significant errors can arise due to the reflection of waves at the edges of the model. Traditionally, the solution to this issue has been to increase the size of the model until the reflections do not occur within the time frame of interest. Often, the required size leads to an impractical, computationally

expensive model.<sup>[15]</sup> Recent efforts have made considerable progress in regard to the wave reflection issue using methods such as perfectly matched layer<sup>[24] [25] [26]</sup>, enriched FEM<sup>[27] [28]</sup>, and the layer transfer matrix method.<sup>[29] [30] [31]</sup> However, each of these techniques are notably computationally expensive, and are therefore not desirable for use in inverse methods such as FWD backcalculation.

An alternative numerical modeling approach is the spectral element method (SEM) originally devised by Rizzi and Doyle<sup>[32] [33]</sup>, which is essentially a derivative of the finite element method. Rather than using traditional finite elements built from polynomial shape functions, modern SEMs employ semi-infinite spectral elements (see: Al-Khoury et al.<sup>[34] [35] [36]</sup>) constructed from harmonic functions that are more efficient for simulating wave propagation. The method uses the discrete Fourier transform (DFT) to convert from the time domain and compute the solution in the frequency domain. Furthermore, spectral element models require dramatically less computational resources than comparable finite element models, because each layer of the pavement structure can be sufficiently modeled via a single spectral element. Furthermore, finite layer methods (FLMs) have been developed, which are similar to SEM in that they use the DFT to solve the system of equations in the frequency domain.<sup>[19] [37] [38]</sup>

A notable drawback associated with SEM and FLM is using the DFT to convert between the time and frequency domains. Time histories collected from FWDs are transient, nonperiodic signals and are prone to measurement errors (e.g., noise). Furthermore, due to their viscoelastic nature, a large number of harmonics are required to effectively model flexible pavements in the frequency domain, and it has been shown that the DFT is not ideal for converting signals with such characteristics.<sup>[19] [38] [39] [40] [41]</sup> Lee has recently developed ViscoWave, an FLM that avoids the use of the DFT by instead employing a combination of the Laplace and Hankel

transformations.<sup>[42][43]</sup> These transforms led ViscoWave to become a unique FLM, based on impulse load and responses that are more suitable for transient, nonperiodic FWD signals. Therefore, the ViscoWave algorithm was chosen for pavement modeling in UGA-PAVE.

## **Optimization Routines**

Despite the improvements in forward modeling of flexible pavement systems discussed previously, dynamic backcalculation remains challenging due to various difficulties in optimization.<sup>[17]</sup> The most troublesome issues with the optimization arise from the inverse nature of the problem. When the pavement is modeled with high accuracy, the backcalculation becomes distinctly “ill-posed.”<sup>[44]</sup> This is primarily because the optimization is carried out with fewer input variables (i.e., pavement layer moduli) than output variables (i.e., displacement sensor time histories), thereby creating the possibility of non-unique solutions.<sup>[17][45]</sup> In an FWD backcalculation analysis, the ill-posedness manifests as multiple sets of dynamic moduli for which the model generates near-identical deflection time histories. The optimization is further challenged due to the numerical model having different levels of sensitivity for different layer moduli. Additionally, inherent noise within the FWD measurements<sup>[19]</sup> and other uncertainties (e.g., layer thickness) further complicate the analysis.

A popular choice for optimizing the FWD backcalculation is nonlinear least-squares, which seeks to minimize the squared norm of the error between the measured and predicted dynamic deflections.<sup>[12][15][46][47]</sup> Such problems are usually solved via Newton’s method; however, the classical Newton’s method has a tendency to converge locally and exhibits poor performance when the initial guess is far from the global minimum.<sup>[48]</sup> Trust-region (TR) methods were developed to refine the convergence properties of Newton’s method and have improved nonlinear least-squares

optimization in a wide range of applications.<sup>[49] [50] [51] [52] [53]</sup> A popular Newton-based method is the subspace trust-region interior reflective (STIR) algorithm for its efficiency and reliability.<sup>[54]</sup> The most notable aspect of the STIR method involves its subspace implementation. Original trust-region methods calculate the Newton step within the full-size Hilbert space (i.e., with dimensions equal to the number of updating variables). The STIR algorithm's subspace modification limits the number of dimensions during computation to just two, thereby reducing computational expense for little cost to accuracy.

Perhaps the most notable alternative to Newton-based trust-region methods is the Levenberg–Marquardt algorithm (LMA), which is essentially a Tikhonov-regularized Gauss–Newton algorithm (GNA) that operates similarly to a trust-region method. Because the objective function in the optimization is a sum of squares, it has unique properties that allow Newton's method to be re-posed in a manner such that computation of second-order derivatives can be avoided. This is advantageous for problems consisting of many variables (e.g., 100 or more) or with computationally expensive second derivatives. The latter advantage is useful in particular for FWD backcalculation because their second-order derivatives must be calculated using finite-difference approximations, which involve numerous costly function evaluations. Recently, Bellavia and Riccietti developed an LMA specifically tailored for solving ill-posed nonlinear least-squares problems by modifying the Gauss–Newton algorithm to resemble the structure of Newton-based trust-region methods.<sup>[55]</sup>

To improve the performance of the ill-posed optimization in dynamic FWD backcalculation, a tandem trust-region (TTR) algorithm has been developed, which combines both the STIR and LMA techniques into a hybrid scheme. The STIR and LMA methods have been observed to outperform each other in different situations that commonly arise in a given backcalculation

problem; by using them simultaneously, the strengths of one can be used to cover the other's weaknesses.

### CHAPTER 3. SITE SELECTION

A number of pavement sections across Georgia were selected for FWD and ground-penetrating radar (GPR) testing, as well as for asphalt core collection. The FWD data are intended to be used with UGA-PAVE to backcalculate the *in situ*  $|E^*|$  curves (ultimately leading to the updated layer coefficients). The GPR testing is intended to estimate the layer thicknesses and densities of the involved pavement sections. Finally, the asphalt cores were obtained for use in validating the UGA-PAVE software.

To assist the research team with the site selection, GDOT provided the project-level Pavement Condition Evaluation System (PACES) ratings for all the state-maintained highways. To identify the location information as well as the highway functional types (e.g., interstate, primary, etc.), the research team downloaded the geographic information system (GIS) data for the roadway inventory from GDOT's website.<sup>[56]</sup> The rating data were then merged with the GIS data, and the pavement sections with ratings greater than or equal to 75 were mapped out for initial evaluation. Figure 1 shows the statewide segment rating mapped to GDOT's GIS data.



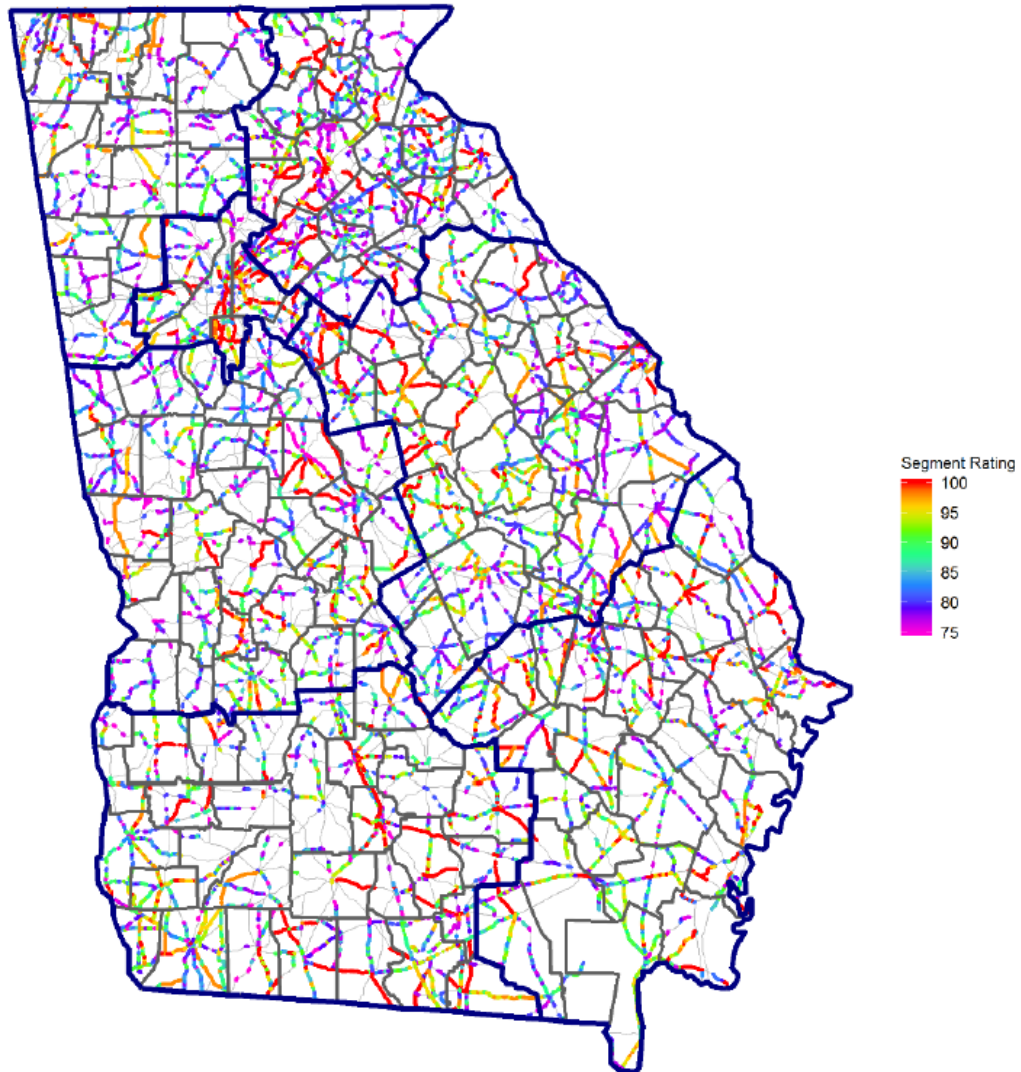


**Figure 1. Map. Statewide map of GDOT segment ratings  $\geq 75$ .**

For a closer evaluation of the mapped segment ratings, the map in figure 1 was broken down into each GDOT district. To avoid the high amount of traffic in the Atlanta area, District 7 was removed from the district-level analysis. Figure 2 through figure 7 show the district-level rating maps for the remaining GDOT districts that were carefully evaluated for the preliminary site selection.

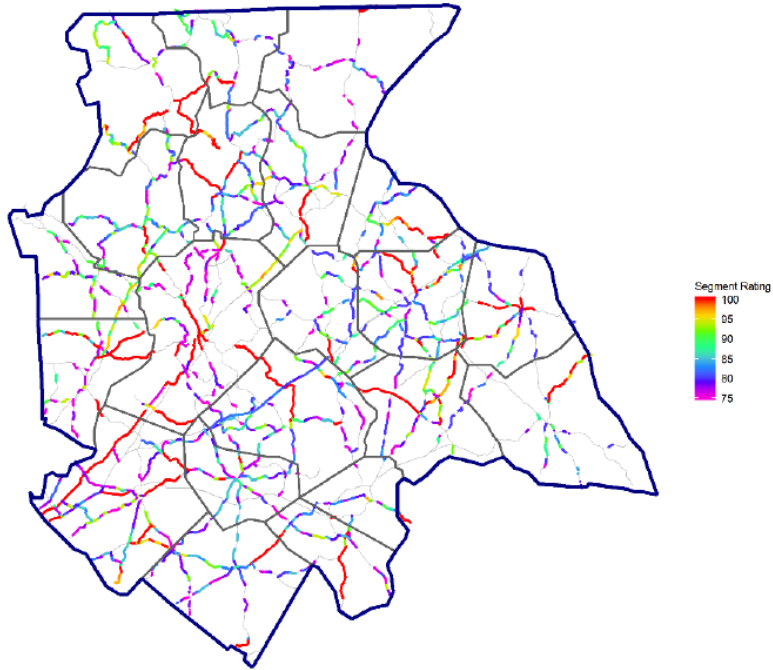


**Figure 2. Map. GDOT District 1 mapped for segment ratings  $\geq 75$ .**

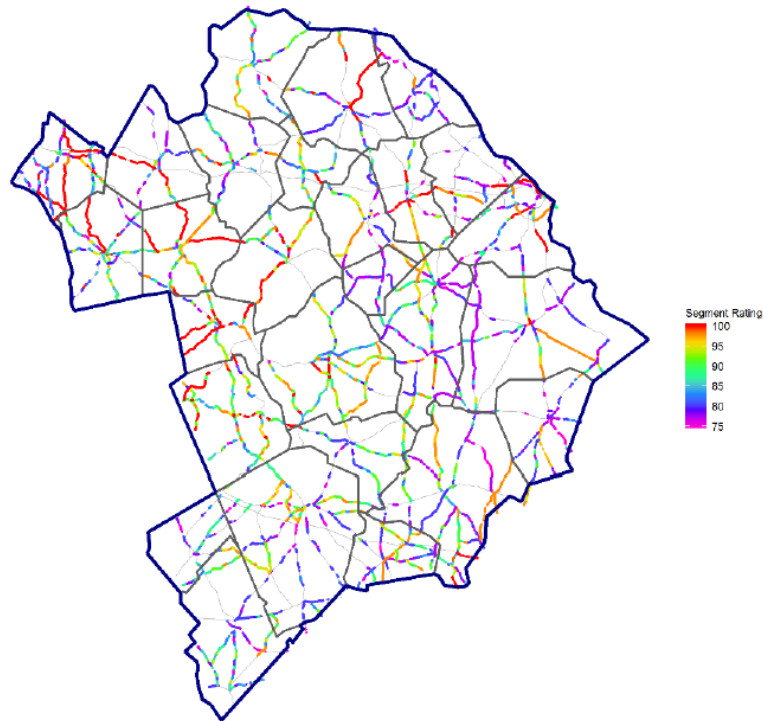


**Figure 3. Map. GDOT District 2 mapped for segment ratings  $\geq 75$ .**

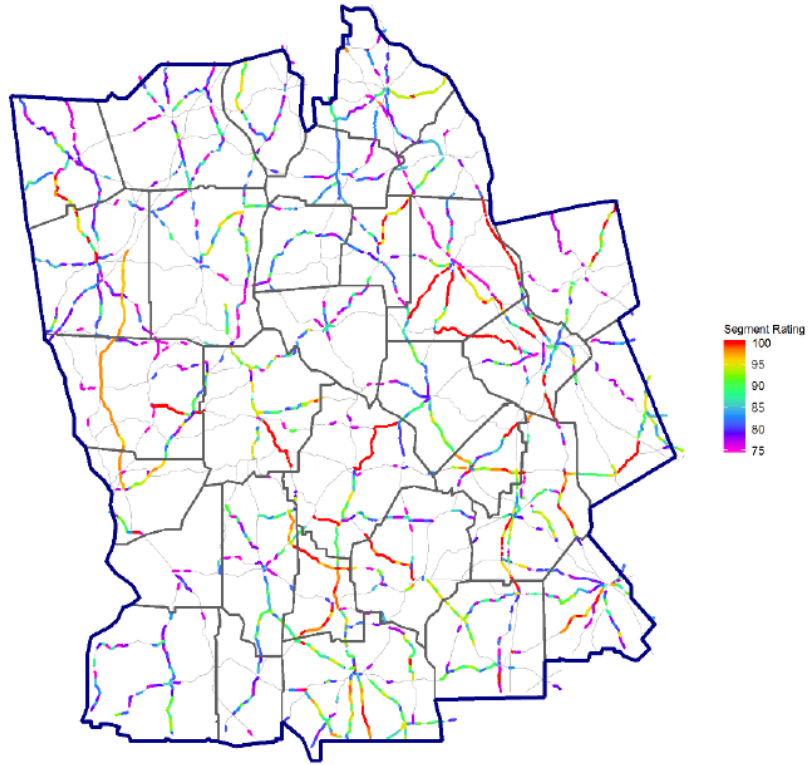


**Figure 4. Map. GDOT District 3 mapped for segment ratings  $\geq 75$ .**

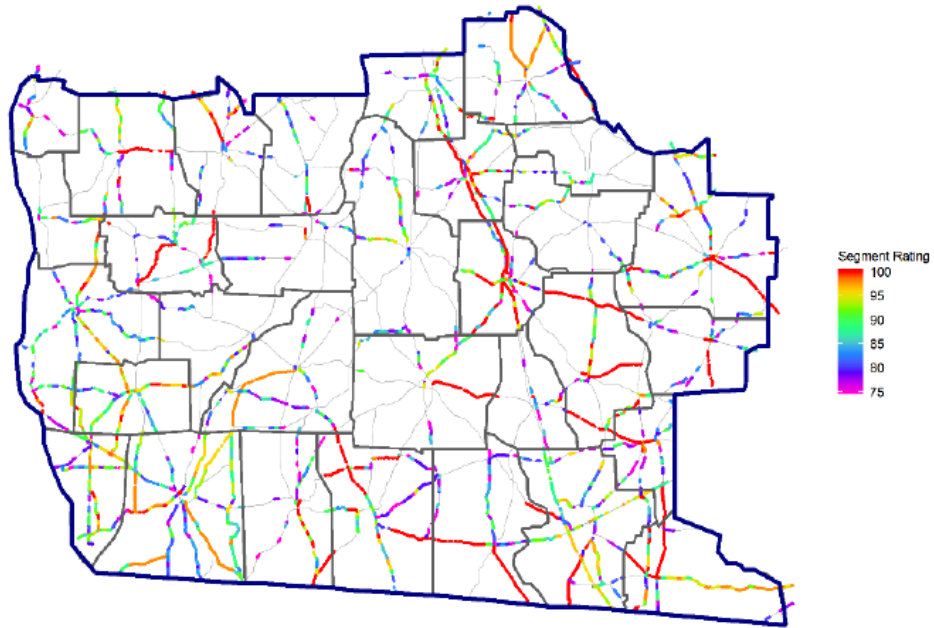


**Figure 5. Map. GDOT District 4 mapped for segment ratings  $\geq 75$ .**

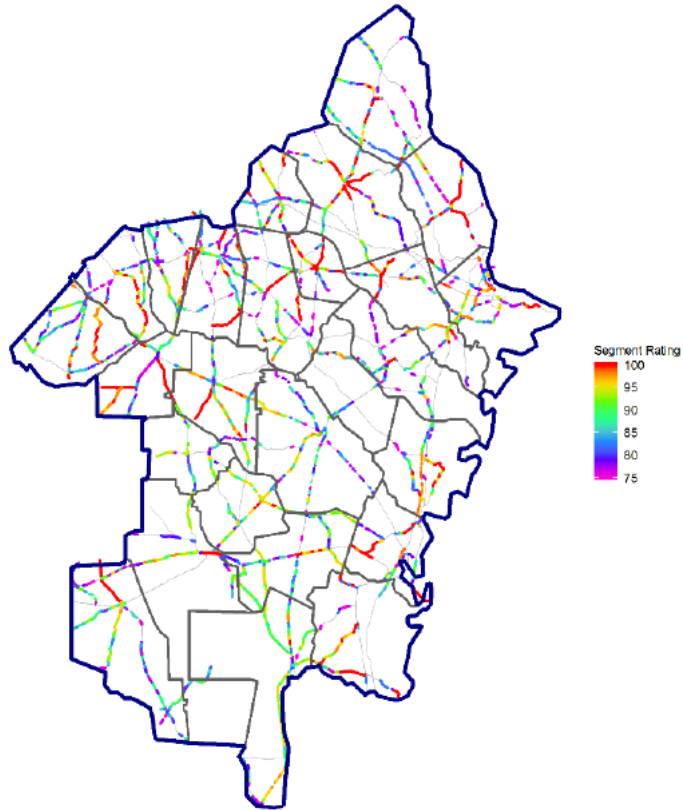


**Figure 6. Map. GDOT District 5 mapped for segment ratings  $\geq 75$ .**

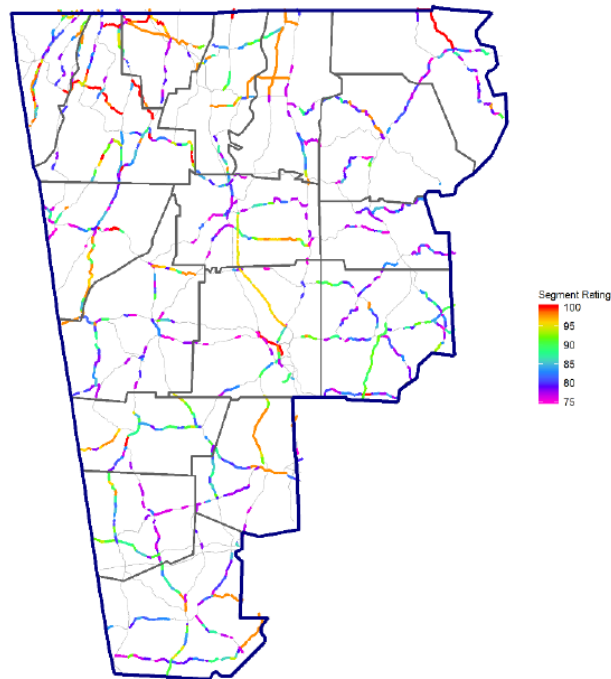


**Figure 7. Map. GDOT District 6 mapped for segment ratings  $\geq 75$ .**

The maps in figure 2 through figure 7 were evaluated to select three pavement sections within each district: one section with a high rating value (close to 100), one section with a medium rating value (between 80 and 90), and one section with a low rating value (below 80). Furthermore, the research team looked for pavement sections with relatively uniform rating values for at least a length of 5.0 miles, while excluding the interstate routes in an attempt to avoid busy (i.e., high-traffic) highways. Nine sites were selected in total, as listed in table 1.

**Table 1. Final selection of GA state routes for FWD, GPR, and core testing.**

District	Route ID	Route No.	County	Starting MP	Ending MP	Avg. Rating
1	1000100008200INC	SR 82	Jackson	6.00	21.54	100.0
	1000100001000INC	SR 10	Walton	0.00	13.60	86.3
	1000100001100INC	SR 11	Walton	2.70	9.00	78.2
2	1000100002200INC	SR 22	Hancock	0.00	12.00	99.2
	1000100005700INC	SR 57	Johnson	13.00	25.89	89.1
	1000100005700INC	SR 57	Emanuel	0.00	8.53	77.0
5	1000100007300INC	SR 73	Evans	6.75	14.86	100.0
	1000100012900INC	SR 129	Candler	0.00	8.00	91.4
	1000100002600INC	SR 26	Bulloch	34.00	42.64	79.0

## CHAPTER 4. UGA-PAVE DEVELOPMENT

### DESCRIPTION OF METHODS

UGA-PAVE is a dynamic FWD backcalculation technique and comprises state-of-the-art computational methods for the forward model (which simulates the FWD displacement response) and optimization routine (which calculates the pavement layer moduli). For the forward model, UGA-PAVE employs the ViscoWave algorithm; for the optimization routine, it uses the tandem trust-region technique, which was developed as part of GDOT Research Project (RP) 18-05 and combines both the STIR and LMA techniques into a hybrid scheme.

### Numerical Pavement Model

In this section, Lee's ViscoWave algorithm developed for dynamic FWD backcalculation of flexible pavements is detailed. The method is extremely complex and, thus, a slightly abbreviated discussion of the major aspects is provided here. The method's full formulation is detailed extensively in other literature. <sup>[42] [43]</sup>

### *Equations of Motion*

First, the pavement section is modeled in cylindrical coordinates and assumed to be axisymmetric around the  $z$ -axis (i.e., perpendicular to the pavement surface). Following this assumption, the displacements can be derived as:

$$u = \frac{\partial \varphi}{\partial r} + \frac{\partial^2 \gamma}{\partial r \partial z} \quad (1)$$

$$w = \frac{\partial \varphi}{\partial z} - \frac{\partial^2 \gamma}{\partial r^2} - \frac{1}{r} \frac{\partial \gamma}{\partial r} \quad (2)$$

where,  $u$  is displacement in the radial direction  $r$ ,  $w$  is the displacement in the vertical direction  $z$ , and  $\varphi$  and  $\gamma$  are scalar potentials for the translational and rotational components of motion, respectively. Substituting equations (1) and (2) into the balance of linear momentum yields the compression and shear wave equations for the medium:

$$\frac{\partial^2 \varphi}{\partial r^2} + \frac{1}{r} \frac{\partial \varphi}{\partial r} + \frac{\partial^2 \varphi}{\partial z^2} = \frac{\ddot{\varphi}}{c_p^2} \quad (3)$$

$$\frac{\partial^2 \gamma}{\partial r^2} + \frac{1}{r} \frac{\partial \gamma}{\partial r} + \frac{\partial^2 \gamma}{\partial z^2} = \frac{\ddot{\gamma}}{c_s^2} \quad (4)$$

where, the notation  $\ddot{\cdot}$  denotes the second partial derivative with respect to time. The constants  $c_p$  and  $c_s$  are the speeds of sound of the compression ( $p$ ) and shear ( $s$ ) waves propagating through the medium, and are defined as:

$$c_p = \sqrt{\frac{\lambda + 2\mu}{\rho}} \quad (5)$$

$$c_s = \sqrt{\mu/\rho} \quad (6)$$

where,  $\lambda$  and  $\mu$  are the Lamé constants for the medium, and  $\rho$  is its density.

Solutions to equations (3) and (4) can be obtained by first applying the Laplace transform, given by:

$$\mathcal{L}[f(t)] = \hat{f}(s) = \int_0^{\infty} f(t) e^{-st} dt \quad (7)$$

and subsequently the Hankel transform of a  $\nu^{th}$ -order Bessel function  $J_\nu$ , given by:

$$\mathcal{H}_\nu[\hat{f}(r)] = \bar{f}_\nu(k) = \int_0^\infty r \hat{f}(r) J_\nu(kr) dr \quad (8)$$

Applying these two transforms to equations (3) and (4) yields the wave equations for the axisymmetric in the Laplace–Hankel domain:

$$\frac{\partial^2 \bar{\varphi}}{\partial z^2} - \left( k^2 + \frac{s}{\hat{c}_p^2} \right) \bar{\varphi} = 0 \quad (9)$$

$$\frac{\partial^2 \bar{\gamma}}{\partial z^2} - \left( k^2 + \frac{s}{\hat{c}_s^2} \right) \bar{\gamma} = 0 \quad (10)$$

where,  $s$  is the complex Laplace variable representing frequency/decay, and  $k$  is the Hankel variable pertaining to Bessel function scaling. Additionally, the speed of sound constants from equations (5) and (6) have become:

$$\hat{c}_p = \sqrt{\frac{\hat{\lambda} + 2\hat{\mu}}{\rho}} \quad (11)$$

$$\hat{c}_s = \sqrt{\hat{\mu}/\rho} \quad (12)$$

Finally, solving equations (9) and (10) yields expressions for the waves traveling in the  $r$  and  $z$  directions:

$$\bar{\varphi} = A_1 e^{-\bar{p}z} \quad (13)$$

$$\bar{\gamma} = B_1 e^{-\bar{q}z} \quad (14)$$

where,  $A_1$  and  $B_1$  are arbitrary constants determined from the boundary conditions, and:



$$\bar{p} = \sqrt{k^2 + \frac{s}{\hat{c}_p^2}} \quad (15)$$

$$\bar{q} = \sqrt{k^2 + \frac{s}{\hat{c}_s^2}} \quad (16)$$

It should be noted that for linearly elastic materials, the speeds of sound in the Laplace domain ( $\hat{c}_p, \hat{c}_s$ ) are equal to those in the time domain ( $c_p, c_s$ ) because  $\lambda$  and  $\mu$  are directly related to a constant elastic modulus,  $E$ . However, the definitions in equations (11) and (12) are necessary when modeling viscoelastic materials such as asphalt, because the elastic modulus is no longer constant and is instead a function of time,  $E(t)$ , often referred to as the relaxation modulus.

### ***Stress and Displacement***

To make use of the solutions given in equations (13) and (14), the displacements and stresses must be determined and likewise transformed into the Laplace–Hankel domain. The axisymmetric stresses in the radial and vertical directions due to a vertical loading can be derived in cylindrical coordinates from continuum mechanics as:

$$\sigma_{zr} = \mu \left( \frac{\partial u}{\partial z} + \frac{\partial w}{\partial r} \right) \quad (17)$$

$$\sigma_{zz} = \lambda \left( \frac{\partial u}{\partial r} + \frac{\partial w}{\partial z} + \frac{u}{r} \right) + 2\mu \frac{\partial w}{\partial z} \quad (18)$$

Substituting equation (17) into equation (1) and equation (18) into equation (2) produces expressions for the stresses in relation to the scalar potentials as:

$$\sigma_{zr} = \mu \frac{\partial}{\partial r} \left( 2 \frac{\partial \varphi}{\partial z} - \frac{\partial^2 \gamma}{\partial r^2} - \frac{1}{r} \frac{\partial \gamma}{\partial r} + \frac{\partial^2 \gamma}{\partial z^2} \right) \quad (19)$$

$$\sigma_{zz} = \lambda \left( \frac{\partial^2 \varphi}{\partial r^2} + \frac{\partial^2 \varphi}{\partial z^2} + \frac{1}{r} \frac{\partial \varphi}{\partial r} \right) + 2\mu \frac{\partial}{\partial z} \left( \frac{\partial \varphi}{\partial z} - \frac{\partial^2 \gamma}{\partial r^2} - \frac{1}{r} \frac{\partial \gamma}{\partial r} \right) \quad (20)$$

Before applying the Laplace and Hankel transforms to the stresses and displacements, it is useful to make note of two Hankel identities. The first,  $\mathcal{H}_\nu \left[ \frac{d^2 \hat{f}}{dr^2} + \frac{1}{r} \frac{d\hat{f}}{dr} - \frac{\nu^2}{r^2} \hat{f} \right] = -k^2 \bar{f}_\nu(\mathbf{k})$ , is relevant for transforming differential equations that include their first and second radial derivatives. The second,  $\mathcal{H}_1 \left[ \frac{d\hat{f}}{dr} \right] = -k \mathcal{H}_0 [\hat{f}(r)] = -k \bar{f}_\nu(\mathbf{k})$ , is useful for relating a function's zeroth-order Hankel transform to the first-order transform of its radial derivative. With these identities, the Laplace–Hankel transformed stresses can be modified to:

$$\bar{\sigma}_{zr} = -sk\hat{\mu} \left[ 2 \frac{\partial \bar{\varphi}}{\partial z} + (k^2 + \bar{q}^2) \bar{\gamma} \right] \quad (21)$$

$$\bar{\sigma}_{zz} = s\hat{\mu}(k^2 + \bar{q}^2) \bar{\varphi} + 2sk^2 \hat{\mu} \frac{\partial \bar{\gamma}}{\partial z} \quad (22)$$

Similarly, applying the Laplace and Hankel transforms to the displacements in equations (1) and (2) yields:

$$\bar{u} = -k\bar{\varphi} - k \frac{\partial \bar{\gamma}}{\partial z} \quad (23)$$

$$\bar{w} = \frac{\partial \bar{\varphi}}{\partial z} + k^2 \bar{\gamma} \quad (24)$$

It should be noted that Hankel transforms of orders one and zero were used to convert the radial and vertical displacements, respectively, due to the nature of the loading. For FWD

backcalculation, the displacements are used to calculate the impulse response of the pavement; that is, a vertical impulse loading is applied instantaneously at time  $t = 0$  and at location  $r = 0$ , after which the system is unloaded for  $t > 0$ . This means that  $w(t = 0) \neq 0$ , whereas  $u(t = 0) = 0$ . Similarly, the first-order Bessel function,  $J_1$ , begins at a nonzero value, whereas the zeroth-order Bessel function,  $J_0$ , begins at zero.

### *Derivation of Stiffness Matrices*

A typical pavement section comprises several layers of different materials, and the equations for stress and displacement presented hitherto are only valid for one homogeneous layer. Therefore, they need to be applied in a manner suitable for a medium of multiple distinct layers. The approach discussed here was originally developed by Al-Khoury et al. <sup>[34] [35] [36]</sup>, which extends Doyle's <sup>[33]</sup> two-dimensional (2D) spectral element method to axisymmetric-layered media. The technique operates much the same as the finite element method; however, the stiffness matrices are constructed using spectral element theory as opposed to a traditional finite element formulation. Compared to finite elements, spectral elements are highly computationally efficient for modeling wave propagation in layered structures, because only one element is needed to model each layer of material.

The stiffness matrices for two types of spectral elements are derived here: one for an element with finite thickness, and one with the form of a semi-infinite half-space. Once obtained, the stiffness matrices of each element can be connected to form the global stiffness matrix for the entire system in the same manner as performed in the finite element method.

### *Finite-Layer Element*

An axisymmetric finite-layer element with a finite thickness can be imagined as a cylinder with infinite radius. It consists of two nodes—one on its top surface and one on its bottom surface—with each having one radial and one vertical degree of freedom (DOF). These vertical DOFs are defined with their positive directions oriented downward. The response at any location inside the element can be calculated by a superposition of the incident waves (introduced by the load) and reflected waves (induced by the top/bottom element boundaries) traveling through the element. This response can be dissected into a compression wave traveling at speed  $c_p$  and a shear wave with speed  $c_s$ .

To account for the vertical waves reflecting from the bottom boundary, additional terms are added to equations (13) and (14), yielding:

$$\bar{\varphi} = A_1 e^{-\bar{p}z} + A_2 e^{-\bar{p}(h-z)} \quad (25)$$

$$\bar{\gamma} = B_1 e^{-\bar{q}z} + B_2 e^{-\bar{q}(h-z)} \quad (26)$$

where,  $h$  is the vertical thickness of the layer, and  $A_2$  and  $B_2$  are additional arbitrary constants. Inserting equation (25) into equation (23) and equation (26) into equation (24) then gives the displacement within the finite-layer element as:

$$\bar{u} = -kA_1 e^{-\bar{p}z} - kA_2 e^{-\bar{p}(h-z)} + k\bar{q}B_1 e^{-\bar{q}z} - k\bar{q}B_2 e^{-\bar{q}(h-z)} \quad (27)$$

$$\bar{w} = -\bar{p}A_1 e^{-\bar{p}z} + \bar{p}A_2 e^{-\bar{p}(h-z)} + k^2 B_1 e^{-\bar{q}z} + k^2 B_2 e^{-\bar{q}(h-z)} \quad (28)$$

Similarly, substituting the Laplace–Hankel transformed potentials into equations (21) and (22) gives:

$$\begin{aligned}\bar{\sigma}_{zr} = & 2sk\bar{p}\hat{\mu}A_1e^{-\bar{p}z} - 2sk\bar{p}\hat{\mu}A_2e^{-\bar{p}(h-z)} - sk(k^2 + \bar{q}^2)\hat{\mu}B_1e^{-\bar{q}z} \\ & - sk(k^2 + \bar{q}^2)\hat{\mu}B_2e^{-\bar{q}(h-z)}\end{aligned}\quad (29)$$

$$\begin{aligned}\bar{\sigma}_{zz} = & s\hat{\mu}(k^2 + \bar{q}^2)A_1e^{-\bar{p}z} + s\hat{\mu}(k^2 + \bar{q}^2)A_2e^{-\bar{p}(h-z)} - 2sk^2\bar{q}\hat{\mu}B_1e^{-\bar{q}z} \\ & + 2sk^2\bar{q}\hat{\mu}B_2e^{-\bar{q}(h-z)}\end{aligned}\quad (30)$$

Equations (29) and (30) can be arranged into two sets of matrix systems (i.e., one for displacement, one for stress) with a common vector containing the arbitrary constants. For both systems, the two nodes of the finite-layer element must be considered. The stresses and displacements of the top node, represented by subscript 1, are obtained by inserting  $z = 0$  into the equations. Likewise, those of the bottom node, represented by subscript 2, are found by setting  $z = h$ . Using this approach, the sets of equations take the form:

$$\begin{Bmatrix} \bar{u}_1 \\ \bar{w}_1 \\ \bar{u}_2 \\ \bar{w}_2 \end{Bmatrix} = \begin{bmatrix} -k & -ke^{-\bar{p}h} & k\bar{q} & -k\bar{q}e^{-\bar{q}h} \\ -\bar{p} & \bar{p}e^{-\bar{p}h} & k^2 & k^2e^{-\bar{q}h} \\ -ke^{-\bar{p}h} & -k & k\bar{q}e^{-\bar{q}h} & -k\bar{q} \\ -\bar{p}e^{-\bar{p}h} & \bar{p} & k^2e^{-\bar{q}h} & k^2 \end{bmatrix} \begin{Bmatrix} A_1 \\ A_2 \\ B_1 \\ B_2 \end{Bmatrix}$$

$$\bar{U} \equiv \mathbf{Q}_d \mathbf{A} \quad (31)$$

$$\begin{Bmatrix} \bar{\sigma}_{zr,1} \\ \bar{\sigma}_{zz,1} \\ \bar{\sigma}_{zr,2} \\ \bar{\sigma}_{zz,2} \end{Bmatrix} = s\hat{\mu} \begin{bmatrix} 2k\bar{p} & -k\bar{p}e^{-\bar{p}h} & -k(k^2 + \bar{q}^2) & -k(k^2 + \bar{q}^2)e^{-\bar{q}h} \\ (k^2 + \bar{q}^2) & (k^2 + \bar{q}^2)e^{-\bar{p}h} & -2k^2\bar{q} & 2k^2\bar{q}e^{-\bar{q}h} \\ 2k\bar{p}e^{-\bar{p}h} & -2k\bar{p} & -k(k^2 + \bar{q}^2)e^{-\bar{q}h} & -k(k^2 + \bar{q}^2) \\ (k^2 + \bar{q}^2)e^{-\bar{p}h} & (k^2 + \bar{q}^2) & -2k^2\bar{q}e^{-\bar{q}h} & 2k^2\bar{q} \end{bmatrix} \begin{Bmatrix} A_1 \\ A_2 \\ B_1 \\ B_2 \end{Bmatrix}$$

$$\bar{\mathbf{S}} \equiv s\hat{\mu} \mathbf{Q}_s \mathbf{A} \quad (32)$$

From the finite element, the stiffness matrix of an element,  $\mathbf{K}$ , is the relationship between the displacements and surface tractions, defined as:

$$\bar{\mathbf{T}} = \mathbf{K} \bar{\mathbf{U}} \quad (33)$$

where,  $\bar{\mathbf{T}}$  is the vector of surface tractions. This traction vector comes from the Cauchy stress theorem and is obtained by multiplying the unit vector normal to each boundary of the element with the stress vector at that boundary. For an axisymmetric element of finite thickness with positive z-direction oriented downward, the tractions are defined as:

$$\begin{Bmatrix} \bar{T}_{r,1} \\ \bar{T}_{z,1} \\ \bar{T}_{r,2} \\ \bar{T}_{z,2} \end{Bmatrix} = \begin{bmatrix} -1 & 0 & 0 & 0 \\ 0 & -1 & 0 & 0 \\ 0 & 0 & 1 & 0 \\ 0 & 0 & 0 & 1 \end{bmatrix} \begin{Bmatrix} \bar{\sigma}_{zr,1} \\ \bar{\sigma}_{zz,1} \\ \bar{\sigma}_{zr,2} \\ \bar{\sigma}_{zz,2} \end{Bmatrix}$$

$$\bar{\mathbf{T}} \equiv \mathbf{N}_f \bar{\mathbf{S}} \quad (34)$$

Finally, the stiffness matrix for the finite-thickness spectral element,  $\mathbf{K}_f$ , is determined by combining equations (31), (32), and (34) into equation (33), canceling  $\mathbf{A}$  on both sides, and post-multiplying by  $\mathbf{Q}_d^{-1}$ , yielding:

$$K_f = s\hat{\mu}N_fQ_sQ_d^{-1} \quad (35)$$

### *Semi-Infinite Element*

Similar to the previous element type, a radially symmetric element with a semi-infinite thickness takes the form of a half-space cylinder spanning infinite distance in the radial direction and extends semi-infinitely in the  $z$ -direction. Implementation of this element is useful for avoiding the issue of wave reflections that occur at the bottom surface of the model, as the only horizontal boundary is the top surface. As a result, the element has only one node, located on its top surface, and its response can be treated much the same as the finite-thickness variant.

Because wave reflections need not be considered, equations (9) and (10) are sufficient for describing wave propagation within the element, which can be verified by setting  $h = \infty$  in the corresponding equations for the previous element type. The displacements for the semi-infinite element can therefore be obtained by substituting those equations into equations (23) and (24) to obtain:

$$\bar{u} = -kA_1e^{-\bar{p}z} + k\bar{q}B_1e^{-\bar{q}z} \quad (36)$$

$$\bar{w} = -\bar{p}A_1e^{-\bar{p}z} + k^2B_1e^{-\bar{q}z} \quad (37)$$

Likewise, inserting them into equations (21) and (22) yields the stresses for the half-space element in the Laplace–Hankel domain as:

$$\bar{\sigma}_{zr} = 2sk\bar{p}\hat{\mu}A_1e^{-\bar{p}z} - sk(k^2 + \bar{q}^2)\hat{\mu}B_1e^{-\bar{q}z} \quad (38)$$

$$\bar{\sigma}_{zz} = s(k^2 + \bar{q}^2)\hat{\mu}A_1e^{-\bar{p}z} - 2sk^2\bar{q}\hat{\mu}B_1e^{-\bar{q}z} \quad (39)$$

When arranging the semi-infinite element's displacements and stresses into matrix form, only the node at the top surface ( $z = 0$ ) needs to be considered. Employing the same strategy as used for the previous element yields:

$$\begin{aligned} \begin{Bmatrix} \bar{u}_1 \\ \bar{w}_1 \end{Bmatrix} &= \begin{bmatrix} -k & k\bar{q} \\ -\bar{p} & k^2 \end{bmatrix} \begin{Bmatrix} A_1 \\ B_1 \end{Bmatrix} \\ \bar{\mathbf{U}} &\equiv \mathbf{Q}_d \mathbf{A} \end{aligned} \quad (40)$$

$$\begin{aligned} \begin{Bmatrix} \bar{\sigma}_{zr,1} \\ \bar{\sigma}_{zz,1} \end{Bmatrix} &= s\hat{\mu} \begin{bmatrix} 2k\bar{p} & -k(k^2 + \bar{q}^2) \\ (k^2 + \bar{q}^2) & -2k^2\bar{q} \end{bmatrix} \begin{Bmatrix} A_1 \\ B_1 \end{Bmatrix} \\ \bar{\mathbf{S}} &\equiv s\hat{\mu} \mathbf{Q}_s \mathbf{A} \end{aligned} \quad (41)$$

To determine the stiffness matrix, the Cauchy stress theorem is once again applied to define the surface tractions. For the axisymmetric semi-infinite thickness spectral element with positive  $z$ -direction defined downward, the boundary tractions are related to the stresses by:

$$\begin{aligned} \begin{Bmatrix} \bar{T}_{r,1} \\ \bar{T}_{z,1} \end{Bmatrix} &= \begin{bmatrix} -1 & 0 \\ 0 & 1 \end{bmatrix} \begin{Bmatrix} \bar{\sigma}_{zr,1} \\ \bar{\sigma}_{zz,1} \end{Bmatrix} \\ \bar{\mathbf{T}} &\equiv -\bar{\mathbf{S}} \end{aligned} \quad (42)$$

By inserting equations (40)–(42) into equation (33) and rearranging as for the finite-thickness element, the stiffness matrix for the semi-infinite spectral element,  $\mathbf{K}_s$ , is then:



$$\mathbf{K}_s = -s\hat{\mu}\mathbf{Q}_s\mathbf{Q}_d^{-1} \quad (43)$$

### *Numerical Laplace–Hankel Inversion*

After the system response due to the FWD impulse load is calculated in the Hankel–Laplace domain, the result must be converted to the time domain. This is accomplished by using the inverse Hankel transform followed by the inverse Laplace transform. For the purposes of FWD backcalculation, only the vertical displacements at the very surface of the model are of interest; thus, the inverse Hankel transform of order zero will be used. The analytical form of this transform is:

$$\widehat{W}_j(r) = \int_0^{\infty} k\bar{W}_j(k)J_0(kr) dk \quad (44)$$

where,  $W_j$  is the vertical deflection of the model at the  $j^{th}$  surface location. Although the upper limit of the integrand in the inverse Hankel transform is infinity, it has been shown that the solution converges well when integrating over only the first five roots of the derivative of the Bessel function used in the transform.<sup>[42] [57] [58]</sup> Because  $J_0$  is used in equation (44) to transform the vertical displacements from equation (24), the roots of its derivative,  $J_1$ , are used to subdivide the integration, replacing it with a finite series of integrals as:

$$\begin{aligned} \widehat{W}_j(r) = & \int_{b_0}^{b_1} k\bar{W}_j(k)J_0(kr) dk + \int_{b_1}^{b_2} k\bar{W}_j(k)J_0(kr) dk \\ & + \dots + \int_{b_4}^{b_5} k\bar{W}_j(k)J_0(kr) dk \end{aligned} \quad (45)$$

where,  $b_n$  is the  $n^{th}$  root of  $J_1$ , and  $b_0 = 0$ . Each sub-integration can then be numerically computed using 6-point Gaussian quadrature via:

$$\int_{b_{n-1}}^{b_n} k \bar{W}_j(k) J_0(kr) dk = \frac{b_n - b_{n-1}}{2} \sum_{p=1}^6 w_p \beta_p \bar{W}_j J_0(\beta_p) \quad (46)$$

With,

$$\beta_p = \left( \frac{b_n - b_{n-1}}{2} \right) x_p + \left( \frac{b_n + b_{n-1}}{2} \right) \quad (47)$$

where,  $w_p$  is the weight of the  $p^{th}$  node,  $x_p$ , in the quadrature rule.

Next, the closed form of the inverse Laplace transform is given by:

$$W_j(t) = \frac{1}{2\pi i} \int_B \widehat{W}_j(s) e^{st} ds \quad (48)$$

where,  $i = \sqrt{-1}$ . The fixed Talbot algorithm (FTA) by Abate and Valko <sup>[59]</sup> In the FTA, the contour path,  $B$ , is defined as:

$$s(\theta) = \alpha \theta (\cot(\theta) + i), \quad -\pi < \theta < \pi \quad (49)$$

where,

$$\alpha = \frac{2M}{5t} \quad (50)$$

Parameter  $\alpha$  is introduced to control the precision of the numerical integration. This is accomplished by specifying the number of subdivisions of the contour path,  $M$ , which is equal to

the number of precision decimal places. By inserting equation (49) into equation (48), the analytical form of the inverse Laplace transform becomes:

$$W_j(t) = \frac{\alpha}{\pi} \int_0^\pi \Re[\widehat{W}_j(s(\theta))e^{s(\theta)t}(1 + i\xi(\theta))] d\theta \quad (51)$$

where,  $\Re[\circ]$  takes the real part of complex quantity  $\circ$ , and:

$$\xi(\theta) = \theta - \cot(\theta) + \theta \cot^2(\theta) \quad (52)$$

Finally, using the trapezoidal rule, equation (51) can be numerically approximated as:

$$W_j(t) = \frac{\alpha}{M} \left( \frac{1}{2} \widehat{W}_j(\alpha) e^{\alpha t} + \sum_{q=1}^{M-1} \Re[\widehat{W}_j(s(\theta_q)) e^{s(\theta_q)t} (1 + i\xi(\theta_q))] \right) \quad (53)$$

where,

$$\theta_q = \frac{q\pi}{M} \quad (54)$$

## Optimization Routine

The optimization for FWD backcalculation analyses is most commonly posed as a constrained nonlinear least-squares curve-fitting problem, which has the form:

$$\min_{\mathbf{x}} f(\mathbf{x}) = \|\mathbf{F}(\mathbf{x}) - \mathbf{y}\|^2 \equiv \boldsymbol{\epsilon}(\mathbf{x})^T \boldsymbol{\epsilon}(\mathbf{x}), \quad \mathbf{b}^L \leq \mathbf{x} \leq \mathbf{b}^U \quad (55)$$

where,  $\mathbf{x}$  is the vector of  $n$  input variables,  $\mathbf{y}$  is the set of  $m$  experimentally measured data points,  $\mathbf{F}(\mathbf{x})$  is a vector function of the input variables (here, it is the deflections produced from

ViscoWave),  $\boldsymbol{\epsilon}(\boldsymbol{x}) = \boldsymbol{F}(\boldsymbol{x}) - \boldsymbol{y}$  is the residual error function,  $f(\boldsymbol{x})$  is the sum of errors squared, and  $\|\bullet\|^2$  is the Euclidean norm operator. The vectors  $\boldsymbol{b}^L$  and  $\boldsymbol{b}^U$  are the lower and upper bounds used to constrain the input variables.

The values of  $x$  are adjusted such that the value of  $f(\boldsymbol{x})$  decreases relative to the previous iteration; this procedure of repetitively varying  $\boldsymbol{x}$  is called the *step calculation*, and it is written mathematically as:

$$\boldsymbol{x}_{k+1} = \boldsymbol{x}_k + \boldsymbol{p}_k \quad (56)$$

where,  $\boldsymbol{x}_k$  is the set of values at the current iteration  $k$ ,  $\boldsymbol{x}_{k+1}$  is the subsequent iterate, and  $\boldsymbol{p}_k$  is the *step vector*. A new step is computed every iteration until the differences between the measured and predicted data (i.e.,  $f(\boldsymbol{x})$ ) are minimized; the final, or optimal, parameters are denoted  $\boldsymbol{x}^*$ .

As discussed in **Error! Reference source not found.**, the most popular class of optimization techniques used to solve nonlinear least-squares optimization problems is those of the trust-region variety. TR methods determine solutions to equation (55) by conducting a *secondary optimization* of the step vector from equation (56) during each iteration of the primary optimization. Traditional TR methods define the objective of this step vector optimization via a constrained second-order Taylor series approximation of  $f(\boldsymbol{x}_k + \boldsymbol{p}_k)$  about  $\boldsymbol{p}_k$ . Thus, the secondary, *step optimization* problem has the form:

$$\min_{\boldsymbol{p}_k} \phi(\boldsymbol{p}_k) = f(\boldsymbol{x}_k) + \boldsymbol{g}_k^T \boldsymbol{p}_k + \frac{1}{2} \boldsymbol{p}_k^T \boldsymbol{H}_k \boldsymbol{p}_k, \quad \|\boldsymbol{p}_k\| \leq \Delta_k \quad (57)$$

where,  $\boldsymbol{g}_k$  and  $\boldsymbol{H}_k$  are the gradient and Hessian of  $f(\boldsymbol{x}_k)$ , and  $\phi(\boldsymbol{p}_k)$  is the value of the Taylor series approximation of  $f(\boldsymbol{x}_k + \boldsymbol{p}_k)$ . The constraint,  $\|\boldsymbol{p}_k\| \leq \Delta_k$ , is an  $n$ -dimensional sphere of

radius  $\Delta_k$ , and this *hypersphere* is called the trust-region. The inequality constraint (i.e.,  $\leq$ ) restricts the step vector,  $p_k$ , to exist on or within the region.

In least-squares minimization problems, the gradient is computed as:

$$\mathbf{g}_k = 2\mathbf{J}_k\epsilon_k \quad (58)$$

where,  $\epsilon_k$  is shorthand for  $\epsilon(x_k)$ , and  $\mathbf{J}_k = \left[ \frac{\delta\epsilon_k}{\delta x_1}, \frac{\delta\epsilon_k}{\delta x_2}, \dots, \frac{\delta\epsilon_k}{\delta x_n} \right]$  is the Jacobian of  $\epsilon_k$ . Additionally, the Hessian is calculated by:

$$\mathbf{H}_k = 2\mathbf{J}_k^T\mathbf{J}_k + 2\epsilon_k^T\nabla^2\epsilon_k \quad (59)$$

where,  $\nabla^2$  denotes the vector Laplacian operator. The residuals become progressively smaller as the optimization is conducted, so the second term in equation (59) is often dropped to yield the approximate Hessian calculation:

$$\mathbf{H}_k \approx 2\mathbf{J}_k^T\mathbf{J}_k \quad (60)$$

The above formulation considerably reduces the computational expense of each iteration at the cost of higher error early in the optimization when values of  $\epsilon_k$  are relatively high. The calculations for  $\mathbf{g}_k$  and  $\mathbf{H}_k$  depend on computing the partial derivatives of  $\epsilon_k$  with respect to  $x_k$ . However, these derivatives are not formulated analytically for FWD backcalculation models. Thus, forward finite difference approximations are used instead to approximate the partial derivatives, which are computed as:

$$\frac{\partial \epsilon_k}{\partial x_j} \approx \frac{F(x_k + d_k) - F(x_k)}{\delta_j} \quad (61)$$

where,  $x_j$  is the  $j^{th}$  variable in  $x_k$ ,  $\delta_j$  is the finite difference step size, and the  $i^{th}$  element of  $d_k$  is determined by:

$$d_{k,i} = \begin{cases} \delta_j, & i = j \\ \mathbf{0}, & i \neq j \end{cases} \quad (62)$$

The tandem trust-region method uses two optimization techniques simultaneously: subspace trust-region interior reflective and a modified Levenberg–Marquardt algorithm. The STIR method was originally developed by Branch et al.<sup>[54]</sup> and makes use of a so-called *affine-scaling* transformation, which rearranges equation (57) as:

$$\min_{\bar{p}_k} \bar{\phi}(\bar{p}_k) = f(x_k) + \bar{g}_k^T \bar{p}_k + \frac{1}{2} \bar{p}_k^T \bar{H}_k \bar{p}_k, \quad \|\bar{p}_k\| \leq \Delta_k \quad (63)$$

where,  $\bar{g}_k = D_k g_k$ ,  $\bar{H}_k = D_k (H_k + C_k) D_k$ , and  $\bar{p}_k = D_k^{-1} p_k$ . The quantities  $D_k$  and  $C_k$  are known as the affine-scaling matrices. The first affine-scaling matrix,  $D_k$ , applies weights to each variable in  $x_k$  based on how far it is from its upper/lower bound (closer to bound  $\rightarrow$  lower weight). The basis for this weight is first determined from the boundary-distance vector,  $\sigma(x_k)$ , with its  $i^{th}$  element computed according to:

$$\sigma_i = \begin{cases} x_i - b_i^L, & g_i \geq \mathbf{0} \text{ \& } b_i^L > -\infty \\ \mathbf{1}, & g_i \geq \mathbf{0} \text{ \& } b_i^L = -\infty \\ b_i^U - x_i, & g_i < \mathbf{0} \text{ \& } b_i^U < \infty \\ -\mathbf{1}, & g_i < \mathbf{0} \text{ \& } b_i^U = \infty \end{cases} \quad (64)$$

Afterward, the first matrix is calculated as:

$$\mathbf{D}_k = \mathbf{diag}\left(|\sigma_k|^{-\frac{1}{2}}\right) \quad (65)$$

where,  $\mathbf{diag}(\circ)$  converts an input vector to a diagonal matrix. The second affine-scaling matrix,  $\mathbf{C}_k$ , adjusts the diagonal elements of the Hessian based on the same principle as  $\mathbf{D}_k$ , defined by:

$$\mathbf{C}_k = \mathbf{D}_k(\mathbf{diag}(\mathbf{g}_k)\mathbf{J}_k^\sigma)\mathbf{D}_k \quad (66)$$

where,  $\mathbf{J}_k^\sigma$  is the Jacobian of  $\sigma_k$  with respect to  $x_k$  that is a diagonal matrix with values  $\pm 1$  and 0.

Levenberg–Marquardt optimization approaches are a popular alternative to trust-region–based methods. Although not formally defined as a trust-region, LMAs operate similarly to TR techniques. The Levenberg–Marquardt formulations of the secondary, step-optimization problem takes a slightly different approach than the traditional TR variety; because both the gradient and (approximated) Hessian are defined relative to  $J_k$ , the objective function can be posed as a first-order Taylor series approximation of  $\epsilon(x_k + p_k)$  with respect to  $p_k$ , giving:

$$\min_{p_k} \psi(p_k) = \|\epsilon_k + J_k p_k\|^2, \quad \|p_k\| \leq \Delta_k \quad (67)$$

In the above formulation,  $\psi(p_k)$  serves as an alternative approximation to equation (63)’s  $\phi(p_k)$  for estimating  $f(x_k + p_k)$ . The specific Levenberg–Marquardt approach employed by TTR uses the variation devised by Bellavia and Riccietti<sup>[55]</sup>, which has the form:

$$\min_{p_k} \psi(p_k) = \|\epsilon_k + \mathbf{B}_k^{1/2} p_k\|^2, \quad \|\mathbf{B}_k^{-1/2} p_k\| \leq \Delta_k \quad (68)$$

Here,  $B_k$  is called the *effective Hessian* and is analogous to  $H_k$  in equation (60); however, it is instead calculated via singular value decomposition (SVD) of  $J_k$ , which is detailed below. Similarly,  $B_k^{1/2}$  is the *effective Jacobian*, because  $J_k^T J_k \equiv B_k^{1/2,T} B_k^{1/2} \equiv B_k^{1/2} B_k^{1/2}$ . The tandem trust-region technique applies one further modification to Bellavia and Riccietti's formulation: a variable weighting scheme from Conn et al. (section 6.7.3).<sup>[60]</sup> The form of the LMA objective function then becomes:

$$\min \tilde{\psi}(\tilde{\mathbf{p}}_k) = \|\epsilon_k + \tilde{\mathbf{B}}_k^{1/2} \tilde{\mathbf{p}}_k\|^2, \quad \|\tilde{\mathbf{B}}_k^{-1/2} \tilde{\mathbf{p}}_k\| \leq \Delta_k \quad (69)$$

where,  $\tilde{B}_k^{1/2} = W_k B_k^{1/2}$ ,  $\tilde{B}_k^{-1/2} = W_k^{-1} B_k^{-1/2}$ ,  $\tilde{\mathbf{p}}_k = W_k^{-1} \mathbf{p}_k$ , and  $W_k = \text{diag}(\log_{10}|x_k|)$  is the weighting matrix. When solving for the LMA step in equation (69),  $\tilde{B}_k$  and its cohorts are computed directly from the weighted Jacobian,  $\tilde{J}_k = J_k W_k$ , instead of using the relationships defined in the previous sentence. First, the SVD of the weighted Jacobian is computed according to:

$$\mathbf{U}_k \Sigma_k \mathbf{V}_k^T = \tilde{J}_k \quad (70)$$

where,  $U_k$  and  $V_k$  are the  $m$ -by- $m$  and  $n$ -by- $n$  unitary matrices, respectively, and  $\Sigma_k$  is the  $m$ -by- $n$  diagonal matrix of singular values corresponding to  $\tilde{J}_k$ . From this decomposition, the weighted effective Jacobian, weighted gradient, and weighted effective Hessian are, respectively,

$$\tilde{B}_k^{1/2} = V_k (\Sigma_k^T \Sigma_k)^{1/2} V_k^T \quad (71)$$

$$\tilde{\mathbf{g}}_k = V_k \Sigma_k^T \Sigma_k \epsilon_k \quad (72)$$



$$\tilde{\mathbf{B}}_k = \mathbf{V}_k(\boldsymbol{\Sigma}_k^T \boldsymbol{\Sigma}_k) \mathbf{V}_k^T \quad (73)$$

Finally, Bellavia and Riccietti's technique calls for a reparameterizing  $\tilde{\psi}$  with respect to  $\tilde{\mathbf{z}}_k = \tilde{\mathbf{B}}_k^{-1/2} \tilde{\mathbf{p}}_k$  so that the constraint takes a similar form as in equation (57), yielding:

$$\min_{\tilde{\mathbf{z}}_k} \tilde{\psi}(\tilde{\mathbf{z}}_k) = f(\mathbf{x}_k) + 2(\tilde{\mathbf{B}}_k^{1/2} \tilde{\mathbf{g}}_k)^T \tilde{\mathbf{z}}_k + \tilde{\mathbf{z}}_k^T (\tilde{\mathbf{B}}_k^T \tilde{\mathbf{B}}_k) \tilde{\mathbf{z}}_k, \quad \|\tilde{\mathbf{z}}_k\| \leq \boldsymbol{\Delta}_k \quad (74)$$

where, the solution is related to the full-space LMA step by  $\mathbf{p}_k = \mathbf{W}_k \tilde{\mathbf{B}}_k^{1/2} \tilde{\mathbf{z}}_k$ .

## SOFTWARE SUMMARY

The primary deliverable of UGA-PAVE is to estimate the dynamic modulus ( $|E^*|$ ) master curve of the AC layers using the FWD data. The dynamic modulus master curve can be considered as “Level 1.5” inputs with regard to the MEPDG input hierarchy. The  $|E^*|$  curves generated by UGA-PAVE resemble (but are not actually) Level 1 inputs. Obtaining true Level 1 inputs for a dynamic modulus master curve requires site-specific data tested at different temperatures; however, FWD testing can only feasibly be conducted at a single temperature *in situ*. To counteract this, a general time–temperature superposition (TTS) model for HMA is developed using results from GDOT Research Project (RP) 16-19, yielding:

$$\beta(T) = \alpha_1 T^2 + \alpha_2 T + \alpha_3 \quad (75)$$

where,  $T$  is the desired temperature to shift to,  $\alpha_i$  is the  $i^{\text{th}}$  TTS model coefficient, and  $\beta$  is the time–temperature superposition factor used to construct the  $|E^*|$  master curve. The general TTS

coefficients determined from RP 16-19 are  $\alpha_1 = 0.0012$ ,  $\alpha_2 = -0.1773$ , and  $\alpha_3 = 3.2262$ . Using the above model, the time–temperature superposition shifting is performed according to:

$$\log_{10}f_R = \log_{10}f - \log_{10}\beta(T) \quad (76)$$

where,  $f$  is the frequency of the pre-shift  $|E^*|$  curve, and  $f_R$  is its corresponding reduced frequency for the master curve. In summary, using the above procedure allows UGA-PAVE to estimate full Level 1  $|E^*|$  inputs (dynamic modulus master curve) from an incomplete set of Level 1  $|E^*|$  data (i.e., FWD testing conducted at a single temperature) and Level 2 data (i.e., the HMA time–temperature superposition model derived from RP 16-19).

The first input page of the software is the Data Import Wizard, shown in figure 8. Additionally, a viewing pane that shows the current selections has been added for ease of viewing for large data sets. The second page is for Material Properties management, shown in figure 9. Here, the geometry and guesses for the layer moduli are entered into the software. Little has changed since the last reporting period, except that the values that are being optimized by the backcalculation software have been highlighted in magenta.

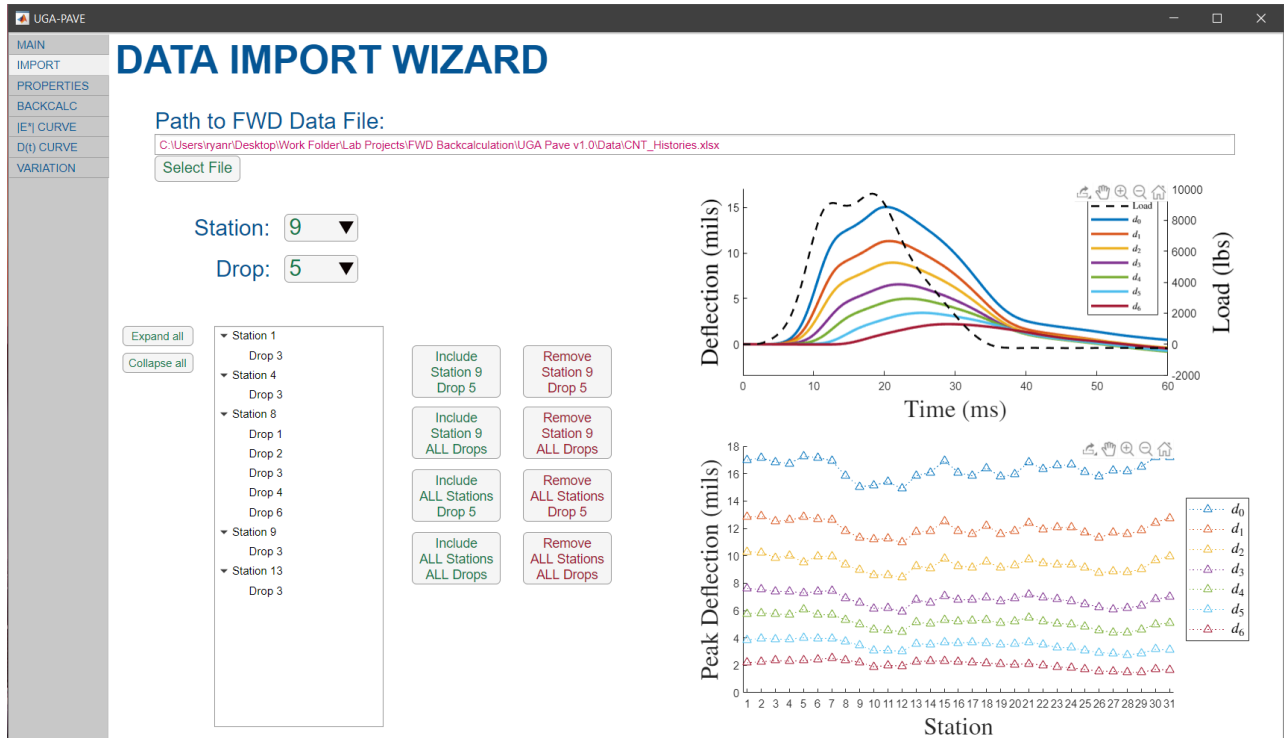


Figure 8. Screen. UGA-PAVE Data Import Wizard page.

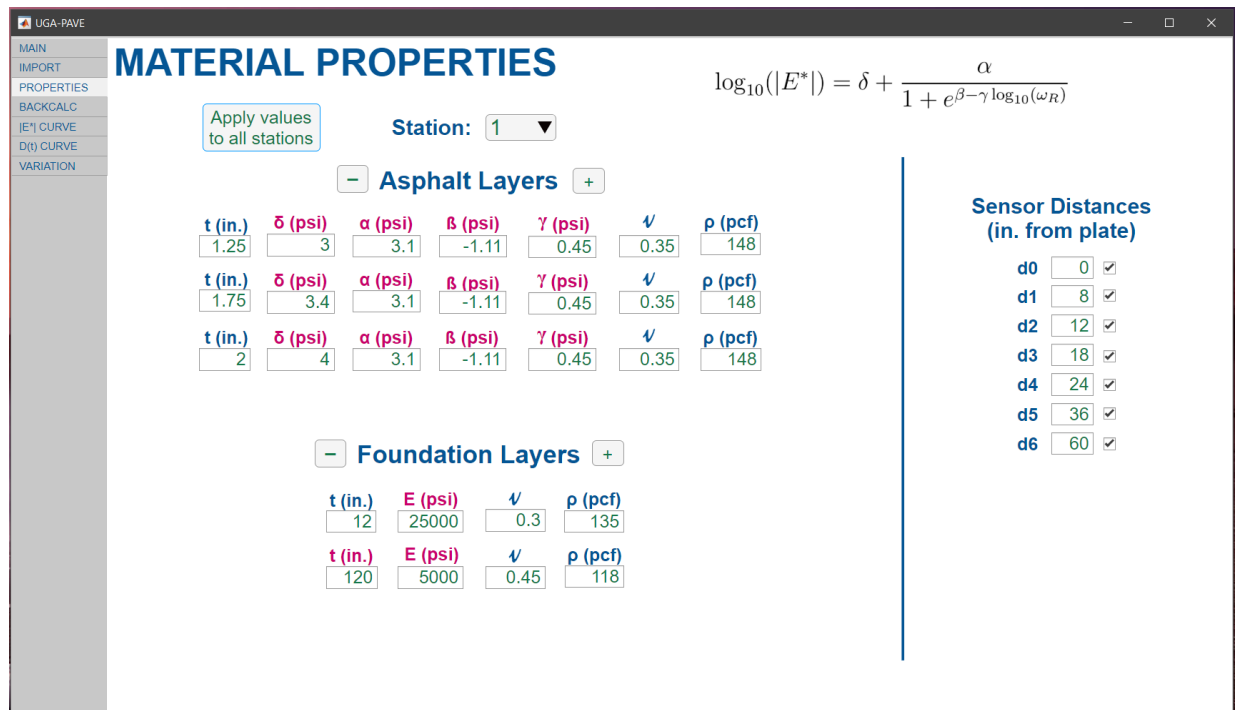
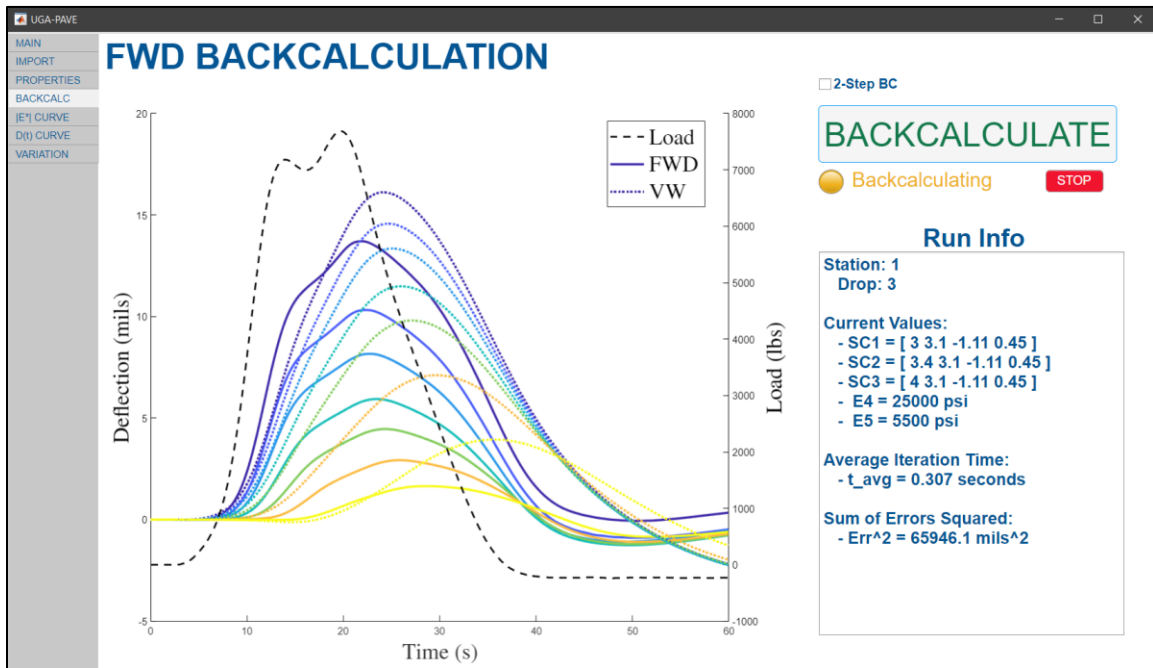


Figure 9. Screen. UGA-PAVE Material Properties input page.

The third pertinent page is shown in figure 10 and is used to run and observe the FWD backcalculation. A notable feature has been implemented: an *optional* “2-Step BC” checkbox that is placed above the BACKCALCULATE button. Essentially, the first of the two steps performs the backcalculation by assuming all the asphalt lifts are equivalent; for example, if three lifts are specified on the material properties input page, all three are aggregated into one layer. Then, the second step segments the asphalt layer into the number of lifts specified on the Material Properties input page and conducts the backcalculation as intended, and the starting values for the dynamic moduli are set as the result obtained in the first step for the aggregate asphalt layer. This method increases the time each backcalculation takes but can potentially improve the accuracy of the backcalculation.



**Figure 10. Screen. UGA-PAVE FWD Backcalculation runtime page.**

The following pages are for the software outputs. The first is the Dynamic Modulus Mastercurve results page in figure 11. The interface allows the user to view the entire backcalculated result for

a selected station. For each station, there are five input fields for temperatures. In the primary input field “Station Temp:”, the user should input the temperature of the pavement when the FWD test was performed. The other four temperature inputs correspond to the shifting temperatures used to construct the master curve, and they are already preset to AASHTOWare Pavement ME Design (PMED) software specifications.

Below the temperature inputs are a number of time–temperature superposition factors. These allow the user to control the characteristics of the shifting used to construct the master curve; however, this is quite an arduous process and predetermined values are provided by default. The values are valid for a large range of HMA mixes and were determined by averaging the lab results from asphalt cores tested in RP 16-19.

Finally, at the bottom right is a table of  $|E^*|$  values that are taken from the master curve, which are automatically set to the arrangement used by PMED, and an Export button that will output the values directly to the .xml file format used by PMED to be as user-friendly as possible. Each asphalt lift will have its own master curve generated, and a dropdown box is used to view and export the tabulated result.

It should be noted that the master curves generated are currently referred to by the UGA research team as “Pseudo-Level 1” inputs. This name is adopted because the data at each temperature were not directly obtained through FWD testing at the temperatures. In other words, to have true Level 1 inputs, an FWD test would have to be performed at four different temperatures. However, for Pseudo-Level 1 inputs, an FWD test is only performed at one temperature, and the time–temperature superposition factors obtained from a database are used to extrapolate what the FWD test results would be at all the other temperatures. One of the validation efforts conducted later in

this study determined how accuracy between Pseudo-Level 1 inputs compares to traditional Level 1 inputs.

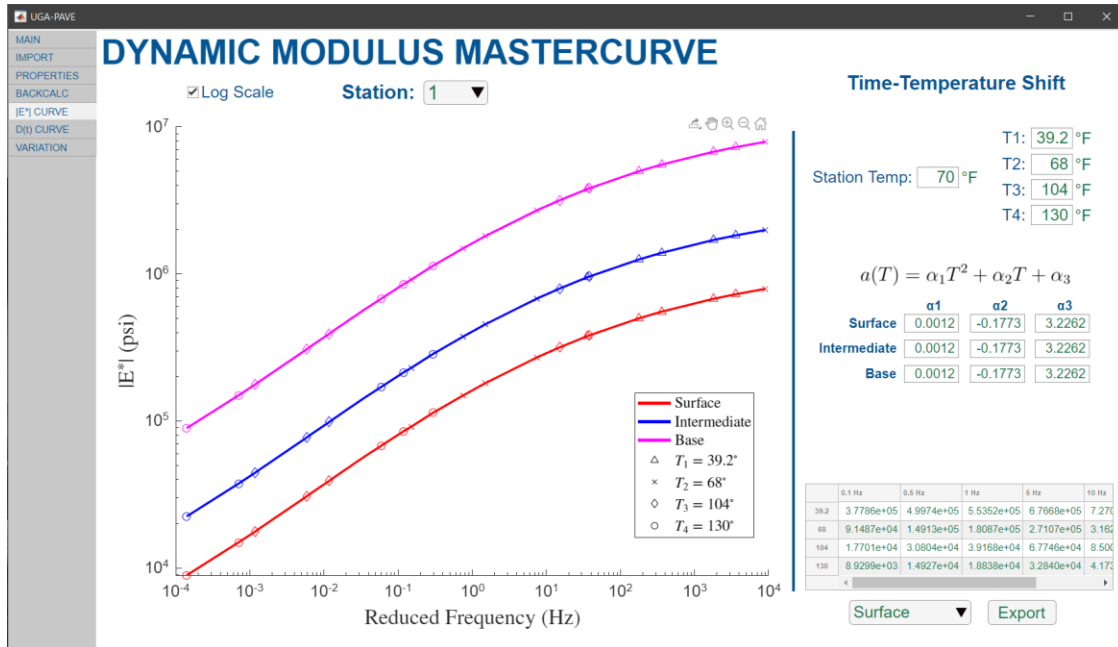


**Figure 11. Screen. UGA-PAVE Pseudo-Level 1 Dynamic Modulus Mastercurve results page.**

The next-to-last page provides the Creep Compliance Curve. As shown in figure 12, this page shares many similarities with the Dynamic Modulus Mastercurve page. The primary difference is that the result on this page is only of Level 2 input for the MEPDG. An interconversion technique developed by S.W. Park and Y.R. Kim is used to create the D(t) curves corresponding to the backcalculated  $|E^*|$  data. An internal study was performed by the research team to determine these inputs drastically improve PMED’s predictions for the terminal IRI and AC thermal cracking performance criteria compared to using regional-averaged Level 3 inputs.

Finally, figure 13 shows the last results page: Moduli Variation. This page plots the moduli resulting from the backcalculation at all road stations to identify the locations of the weakest and

strongest points of the pavement section. Values used to plot the variation of  $|E^*|$  curves are taken using the dynamic modulus estimated at a loading frequency of 1 Hz.

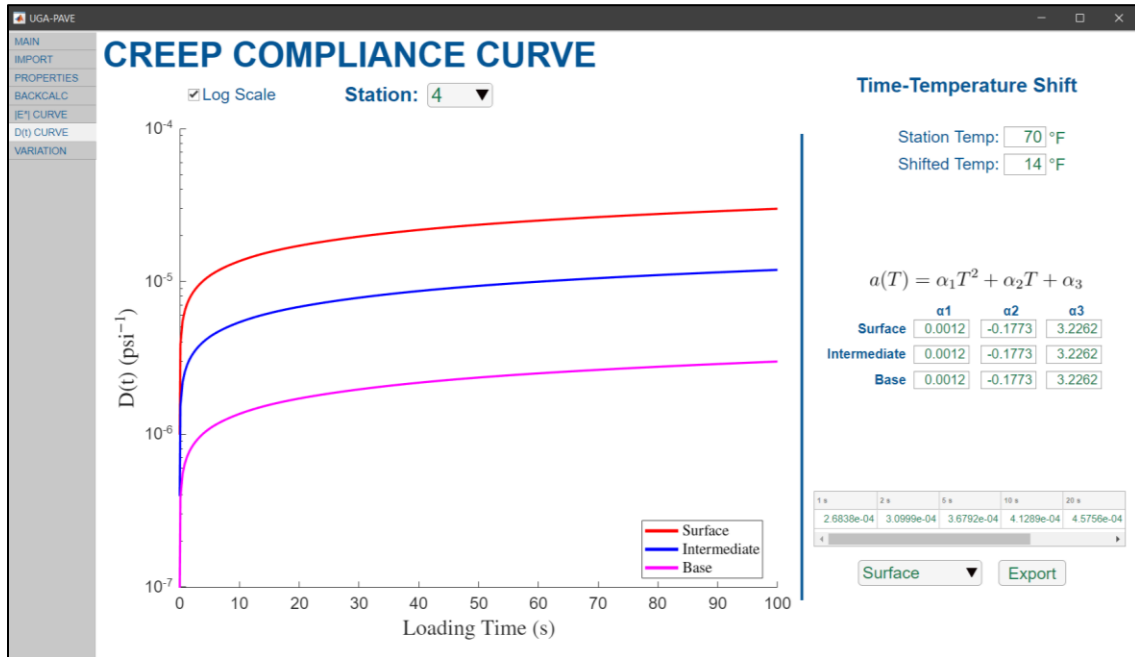


Figure 12. Screen. UGA-PAVE Level 2 Creep Compliance Curve results page.

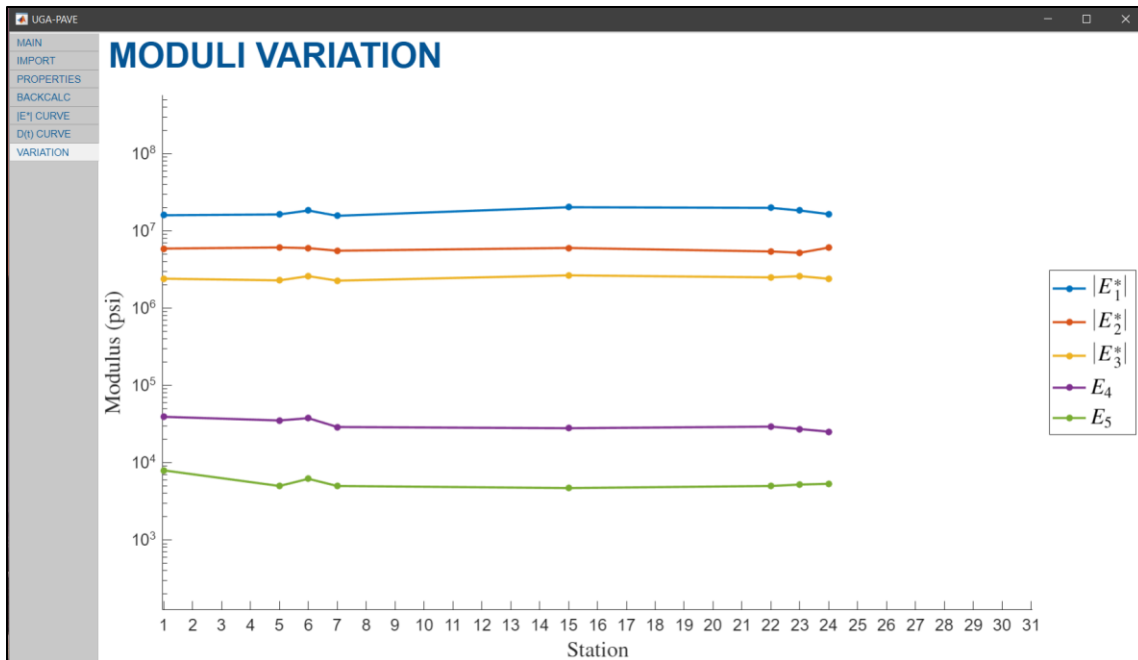


Figure 13. Screen. UGA-PAVE Moduli Variation results page.

## CHAPTER 5. UPDATED LAYER COEFFICIENTS

### PROCEDURE

Road sections for collecting field data were identified in three regions of Georgia; they are located in GDOT districts 1, 2, and 5. The identified sections span a wide range of characteristics (e.g., soil support values, degree of anticipated deterioration) and were expected to be good candidates for determining new layer coefficients.

Layer coefficients are used to determine a pavement section's structural number, which is a technique for quantifying its strength. In the technique, the SN is calculated by:

$$SN = \sum_{i=1}^n a_i D_i \quad (77)$$

where,  $a_i$  and  $D_i$  are the layer coefficient and thickness of the  $i^{\text{th}}$  layer, respectively, and  $n$  is the number of pavement layers above the subgrade.

Currently, GDOT uses 0.44 as the value for HMA. However, this number is based on the AASHTO 1972 *Pavement Design Guide*, which derived this value using statistical fitting of empirical data taken in the 1960s. The quality and composition of AC mixes has changed significantly in the last 50 years, and as a result, modern flexible pavements designed using the 1972 AASHTO guide tend to be oversized for their intended life cycles.

Out of the literature pertaining to using FWD data for updating layer coefficient values, two techniques were identified as the leading candidates. The first technique is taken from the 1993 AASHTO *Pavement Design Guide*, which provided an empirically derived relationship between dynamic modulus and the AC layer coefficients as:



$$a_{AC} = 0.171 \cdot \ln|E^*| - 1.784 \quad (78)$$

where,  $|E^*|$  is the value of the dynamic modulus at a given loading frequency. This technique was recently recommended for use in updating layer coefficients by Lanotte and Kutay.<sup>[61]</sup> They demonstrated that using a layer coefficient of 0.44 for HMA tends to underestimate its material strength, and showed that using the 1993 AASHTO equation yields higher values for the layer coefficients that are in the range of what has been observed from studies in other U.S. states that updated their values through means other than FWD data.

The second candidate was proposed by Abd El-Raof et al.<sup>[62]</sup> Rather than determining the layer coefficient via the dynamic modulus curve backcalculated from the FWD data, this technique directly uses the experimentally measured FWD deflections. The equation was derived using a statistical regression and takes the form:

$$a_{AC} = \frac{4.056 \cdot SIP^{-0.407} \cdot H_p^{0.546} + 0.006 \cdot A_2^{2.443}}{0.203 \cdot D_1} \quad (79)$$

where,  $SIP = D_0 - D_{1.5H_p}$  is the structural index of the pavement in microns,  $H_p$  is the pavement thickness in mm,  $A_2 = \frac{6}{D_0}(D_{300} + 2D_{450} + D_{600})$ , and the  $D_i$  parameters refer to the peak deflections measured by the FWD sensors at the radial distance specified in the subscript in mm (e.g.,  $D_{300}$  is the peak deflection measured by the sensor 300 mm from the FWD load). The authors compared this technique with that of the 1993 AASHTO *Pavement Design Guide* and showed the two methods have a decent correlation of  $R^2=0.83$  when estimating layer coefficients for the same sections.

The primary advantage of Abd El-Raof et al.'s technique is that it can be calculated entirely from the experimental FWD data, meaning the layer coefficient can be performed without backcalculation. Because the 1993 AASHTO method involves using data from the dynamic modulus curve, it can only be used after the pavement layer moduli have been backcalculated, thereby leading to a more time-consuming layer coefficient determination process.

However, there are notable limitations to Abd El-Raof et al.'s technique that make it less effective for layer coefficient estimation. Firstly, it can only calculate a single layer coefficient for the entire AC layer, whereas the 1993 AASHTO method can determine a layer coefficient for each individual asphalt lift for which a dynamic modulus curve is obtained. It has become apparent to the research team that asphalt pavements with significantly different layer moduli (i.e., different dynamic modulus curves) can produce near-exact FWD deflection time histories. Thus, it is reasoned that it is more reliable to calculate asphalt layer coefficients using a technique that is based on dynamic modulus values rather than deflection measurements. Consequently, the research team has selected the technique used in the 1993 AASHTO *Flexible Pavement Design Guide* (as outlined by Lanotte and Kutay <sup>[61]</sup>) for updating GDOT's HMA layer coefficient values for structural number calculation.

For this study, three types of coefficients were calculated. The first,  $a_{4.5-}$ , denotes the layer coefficient for the portion of the AC layer that spans from the surface to a depth of 4.5 inches. Conversely, coefficient  $a_{4.5+}$  represents the remaining portion of the AC layer below a depth of 4.5 inches. These coefficients were calculated from UGA-PAVE by dividing the AC layer into two sublayers above and below the 4.5-inch depth. After the backcalculation was conducted, the software generated two  $|E^*|$  curves, each corresponding to one of the two sublayers. Then, the values of both dynamic modulus curves at a frequency of 1 Hz were inserted into equation (78) to

calculate  $a_{4.5^-}$  and  $a_{4.5^+}$ . (The reasoning for this choice of loading frequency is explained at the end of this subsection.) The third and final coefficient calculated was  $a_{Full}$ , which represents the entire AC layer as a whole. This coefficient was calculated using a thickness-weighted average of the first two coefficients, given by:

$$a_{Full} = \frac{(a_{4.5^-})(4.5in) + (a_{4.5^+})(h_{AC} - 4.5 in)}{h_{AC}} \quad (80)$$

where,  $h_{AC}$  is the thickness of the entire AC layer.

Finally, the method for determining which loading frequency point on the dynamic modulus curves to use when calculating  $a_{4.5^-}$  and  $a_{4.5^+}$  is explained. Lanotte and Kutay [61] do not specify which frequency to use for the dynamic modulus in their equation given in equation (78). The dynamic modulus is a continuous curve that varies with frequency; however, the equation only allows for the input of dynamic modulus from a single frequency. Therefore, a single value of dynamic modulus that best represents the traffic loading should be used; thus, the UGA research team decided to use a loading frequency of 1 Hz, which is approximately at the center of the range of frequencies used as Level 1  $|E^*|$  inputs to PMED (i.e., 0.1 Hz to 25 Hz). The corresponding dynamic modulus value was taken from the master curve, which exists in reduced frequency space at some reference temperature, which in this study was 70°F, or 21.1°C. The  $|E^*|$  curves backcalculated from the FWD data therefore required conversion to reduced frequency.

The relationship between *in situ* loading frequency and reduced frequency is:

$$f_R = a(T)f_{FWD} \quad (81)$$

where,  $f_R$  is reduced frequency corresponding to  $f_{FWD}$ , which is the frequency domain of the  $|E^*|$  curve obtained immediately after backcalculation. The parameter  $a(T)$  is the time–temperature superposition factor, which depends on the current temperature of the pavement,  $T$ . For example, if the pavement has a temperature of 100°F during backcalculation, the frequency points of the backcalculated  $|E^*|$  curve are multiplied by a factor of  $a(T = 100^\circ\text{F})$  to convert the curve to reduced frequency domain at the reference temperature of 70°F; this procedure can be visualized solely as a horizontal shift to the curve. The most common approach used to calculate  $a(T)$  is to create a time–temperature superposition model for the AC mix in question. The UGA research team has several such models for HMA available from a separate GDOT research project (RP 16-19), and an average of all the models was used here to calculate the factor for shifting FWD backcalculated curves as:

$$\log_{10} a(T) = 0.0012T^2 - 0.1773T + 3.2262 \quad (82)$$

where, the temperature,  $T$ , has units of degrees Celsius. Note that at the reference temperature,  $T = 21.1^\circ\text{C}$ , the superposition factor is approximately equal to 1, which corresponds to no shift between the *in situ* and reduced frequency domains.



## RESULTS





The updated layer coefficients were determined using a two-part approach. First, an asphalt performance mixture tester device was used to determine the dynamic modulus curves of the individual lifts of the cores extracted from field testing. Second, the AMPT testing results were used to validate the  $|E^*|$  curves backcalculated from the FWD deflection data.

## Coefficients Calculated from AMPT Testing

AMPT testing was conducted with cores taken from SR 10, SR 11, SR 22, SR 26, SR 57, and SR 129; descriptions of each core used are given in table 2. For each core, two specimens were extracted from each distinct lift of the asphalt layer. The dynamic modulus of each specimen was then experimentally measured for loading rates of 0.1, 0.5, 1, 5, 10, and 25 Hz at three temperatures: 39.2, 68, and 104°F (4, 20, and 40°C). For each lift, a time-temperature superposition model was constructed from the data, and the data were shifted to a reference temperature of 70°F (21.1°C). Finally, a sigmoidal fitting function was applied to the shifted data to construct the master curve for the lift. An example set of dynamic modulus data measured from AMPT testing is shown in figure 14.

**Table 2. Information for cores used in AMPT testing for updated layer coefficients.**

Road	Core	Thickness (in.)	Location	Picture
SR 10 EB Lane 2	4	10.75	MP 4.32	
SR 11 SB	3	15	MP 7.40	

SR 22 EB	1	13.75	MP 6.605	
SR 26 NB	1	4.75 (+7 in. PCC)	MP 0.04	
SR 57 NB	3	5.5	MP 15.72	
SR 129 SB	5	6.25	MP 7.62	

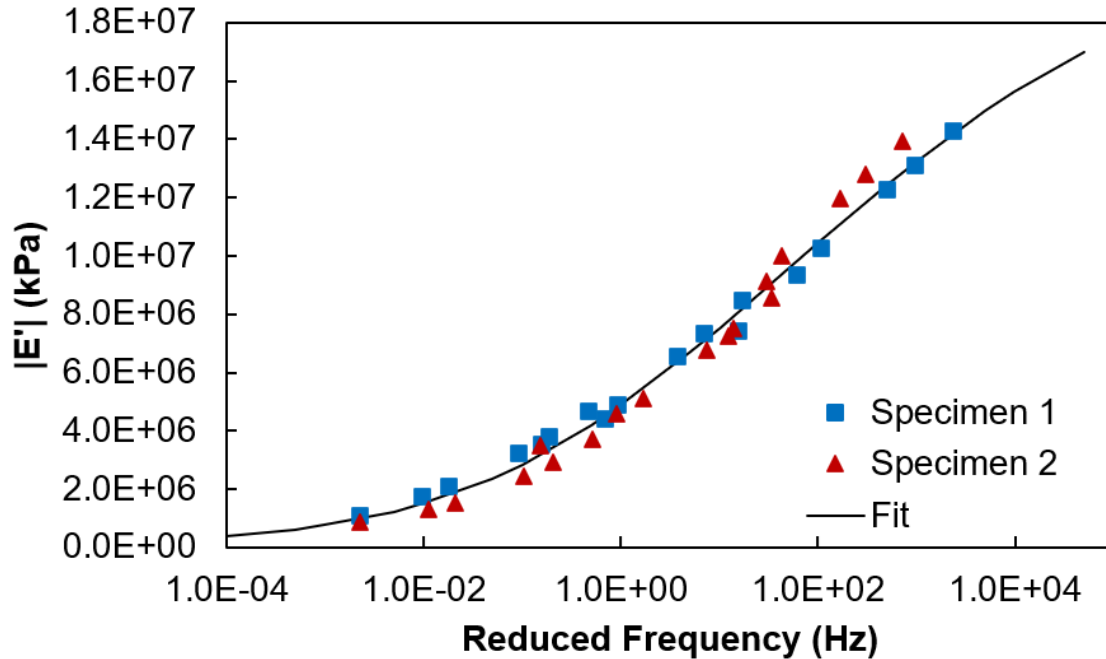


**Figure 14. Graph. AMPT-measured dynamic modulus data for Lift 1 of Core 1 extracted from SR 11.**

To calculate updated values for  $a_{4.5^-}$ , the dynamic modulus curves of each lift *above* 4.5-inch depth were averaged, and the dynamic modulus value at  $f_R = 1$  Hz on that averaged curve was input to equation (78). This procedure was repeated for  $a_{4.5^+}$ , except the  $|E^*|$  curves for each lift *below* 4.5 inch were averaged. Then, the full-depth coefficient,  $a_{Full}$ , was calculated using equation (80). The *in situ* layer coefficients calculated from the AMPT data are given in figure 15, figure 16, and figure 17. Note that no  $a_{4.5^+}$  could be calculated for the cores taken from SR 26 and SR 129. For the case of SR 26, the pavement layer was composite, comprising 4.75 inches of asphalt on top of 7 inches of Portland cement concrete (PCC), as shown in figure 18. For SR 129, the specimens extracted for the lift below 4.5-inch depth crumbled and could not be used in the AMPT device.

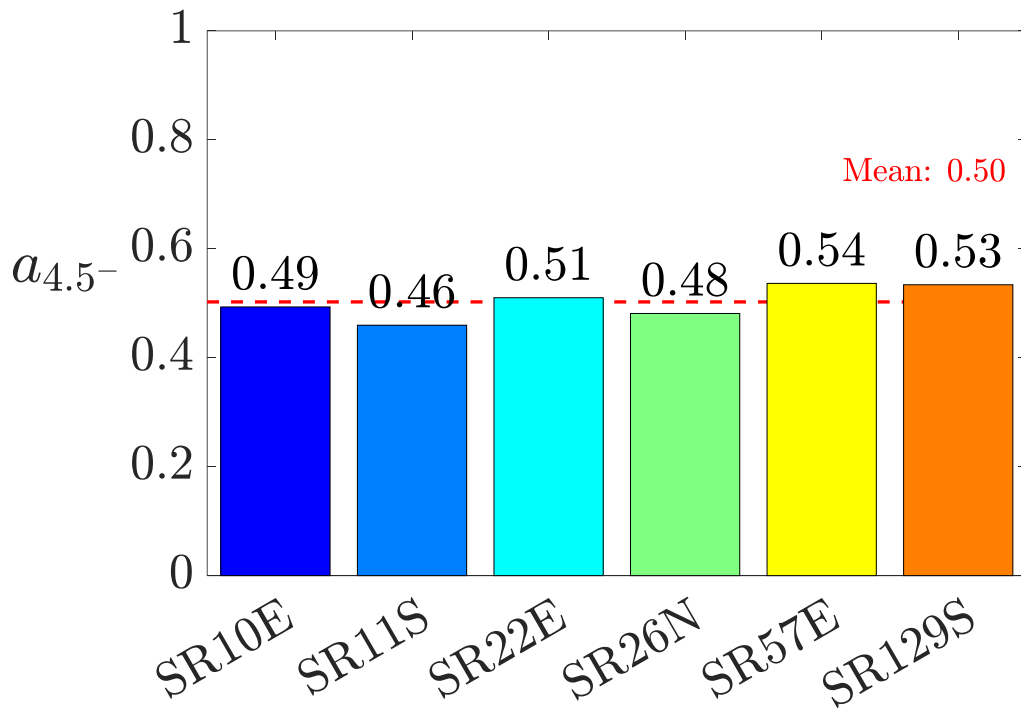


Figure 15. Graph. Above-4.5-inch layer coefficients calculated from AMPT data.

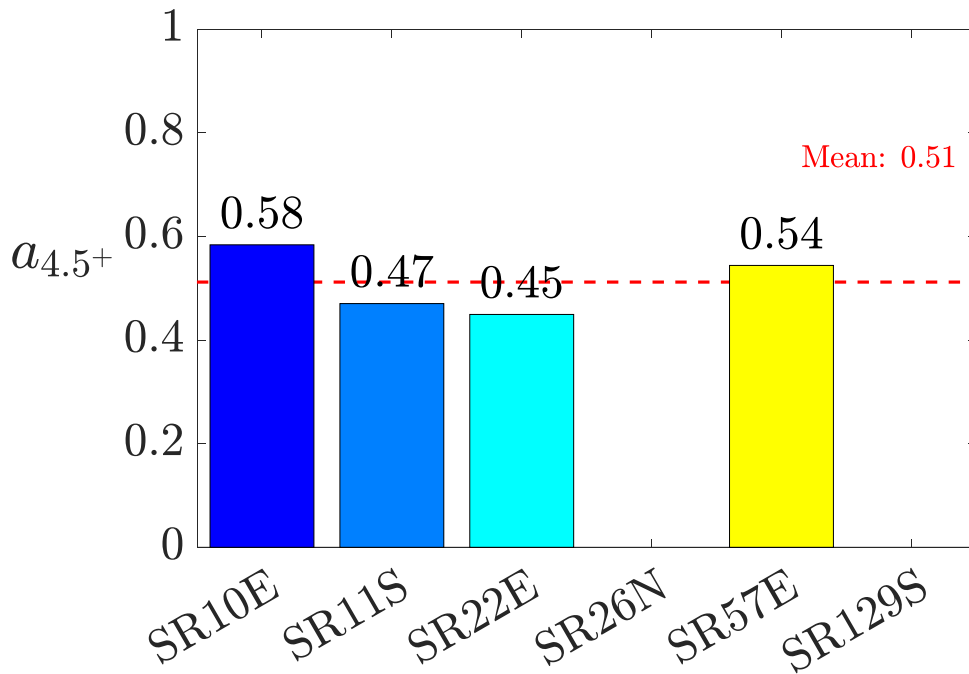


Figure 16. Graph. Below-4.5-inch layer coefficients calculated from AMPT data.



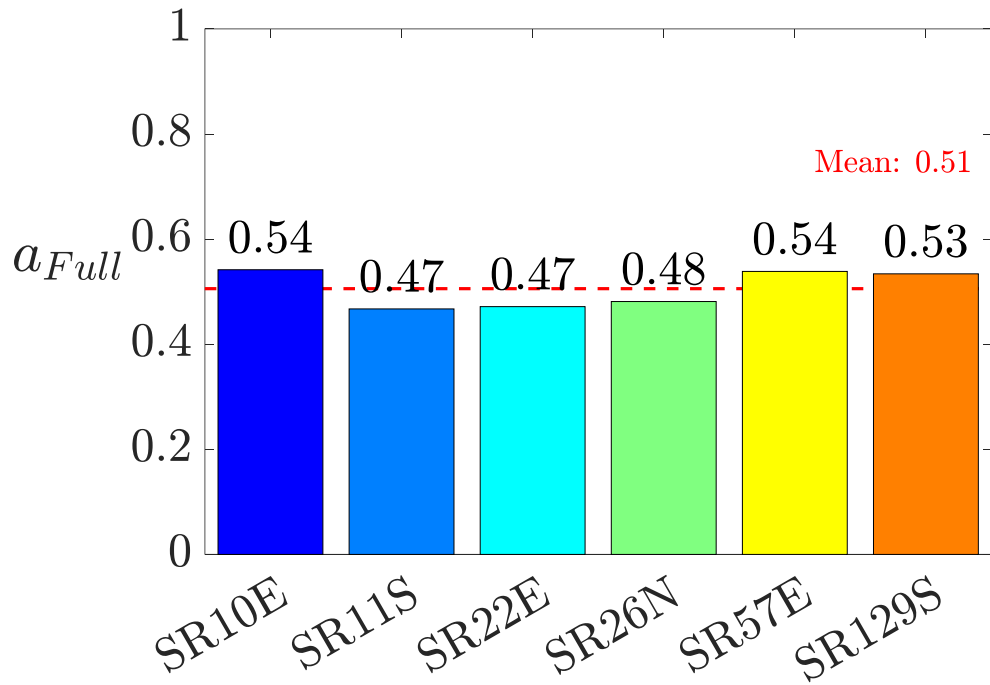


Figure 17. Graph. Full-depth layer coefficients calculated from AMPT data.



Figure 18. Photo. Composite Core 1 extracted from SR 26, featuring asphalt on top of PCC.

A statistical analysis of the AMPT-derived layer coefficients was conducted, and the results are contained in table 3. From the analysis, it was determined that the average layer coefficient value

was consistently between 0.50 and 0.51 for all three. However, a notable amount of variability existed in the coefficients, specifically with  $a_{4.5+}$ . To account for this, multiples of the standard deviation were subtracted from the mean to offer updated layer coefficients with higher statistical reliabilities. For example, subtracting two standard deviations ( $\sigma = 0.06$ ) from the mean of  $a_{4.5+}$  ( $\mu = 0.51$ ) yields a layer coefficient of  $a_{4.5+} = 0.39$  with a reliability of 97.8 percent. In other words, based on the set of AMPT data from this study, it can be expected that  $a_{4.5+} \geq 0.39$  for 97.8 percent of *in situ* GA pavements. Using this approach suggests updated layer coefficient values of  $a_{4.5-} = 0.44$  and  $a_{4.5+} = 0.39$ . In comparison with the values currently used by GDOT, i.e., 0.44 and 0.33, respectively, these results suggest the current value (0.44) used for the top 4.5 inches of asphalt is sufficient, but the below-4.5-inch coefficient (0.33) is lower than necessary.

**Table 3. Statistical analysis of AMPT-derived layer coefficients.**

	$a_{4.5-}$	$a_{4.5+}$	$a_{Full}$	Reliability (%)
$\sigma$ (Std. Dev.)	0.03	0.06	0.04	—
$\mu$ (Mean)	0.50	0.51	0.51	50
$\mu - \sigma$	0.47	0.45	0.47	84.2
$\mu - 2\sigma$	0.44	0.39	0.43	97.8

### **Coefficients Calculated from FWD Backcalculation**

To support the results of the previous subsection, layer coefficients were backcalculated from FWD data collected on SR 10, SR 11, SR 22, SR 26, SR 57 (Johnson County), and SR 82, and the results are given in figure 19, figure 20, and figure 21. Backcalculations were also conducted for

SR 11N, 73N/S, 82W, and 129N/S; however, they failed to reach an acceptable error tolerance of 200 mils<sup>2</sup> (determined by the research team as the highest error where the backcalculated deflections still resemble the experimentally measured deflections) and have, therefore, been excluded from the results.

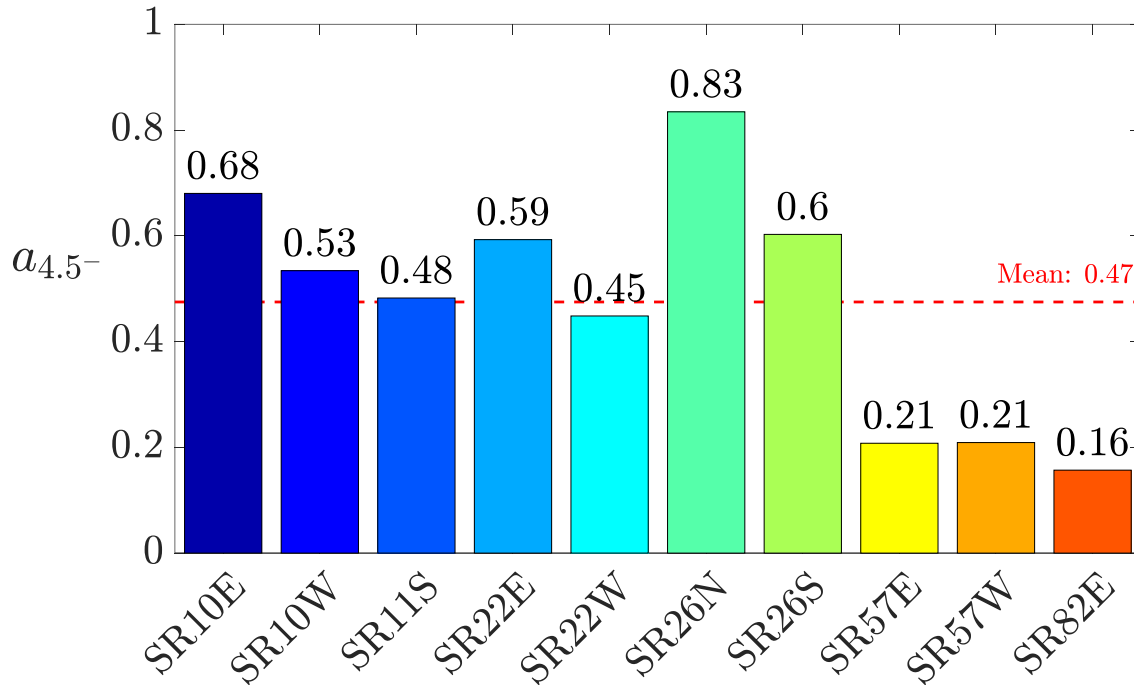


**Figure 19. Graph. FWD backcalculated layer coefficients corresponding to the top 4.5 inches of asphalt for SR 10, SR 11, SR 22, SR 26, SR 57 (Johnson County), and SR 82.**

The coefficients calculated for the top 4.5 inches of asphalt ( $a_{4.5^-}$  in figure 19) have an average of 0.47. With the exception of SR 57E/W and SR 82E, each of the top-4.5-inch layer coefficients satisfied the 97.8 percent reliability criterion of  $a_{4.5^-} \geq 0.44$  from table 3. Inspection of their corresponding  $a_{4.5^+}$  coefficients reveals the cause of the low layer coefficient values for the excepted roads.

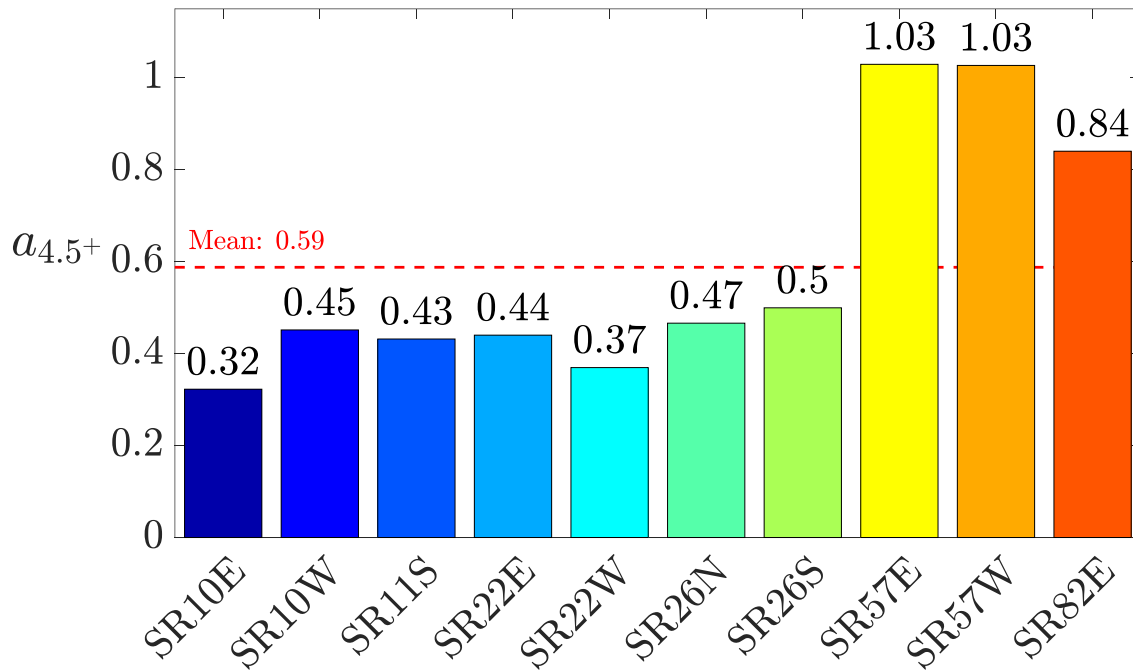


**Figure 20. Graph. FWD backcalculated layer coefficients corresponding to the asphalt portion below a depth of 4.5 inches for SR 10, SR 11, SR 22, SR 26, SR 57 (Johnson County), and SR 82.**

Figure 20 contains the FWD backcalculated layer coefficients revealed corresponding to the asphalt layer below 4.5 inches. For this set, only two roads fell below the 97.8 percent reliability criterion of  $a_{4.5+} \geq 0.39$  from table 3—SR 10E and SR 22W. For SR 22W, it is believed that the backcalculation is estimating the foundation layers (i.e., aggregate base and subgrade) to have higher elastic moduli than in actuality, thereby decreasing the backcalculated dynamic moduli of the asphalt layers. Most cores taken from SR 22 were observed to have been on top of a soil-aggregate base material, which was unique among all the roads surveyed for this project, leading the research team to be uncertain of how to best represent the material in the pavement model for FWD backcalculation.

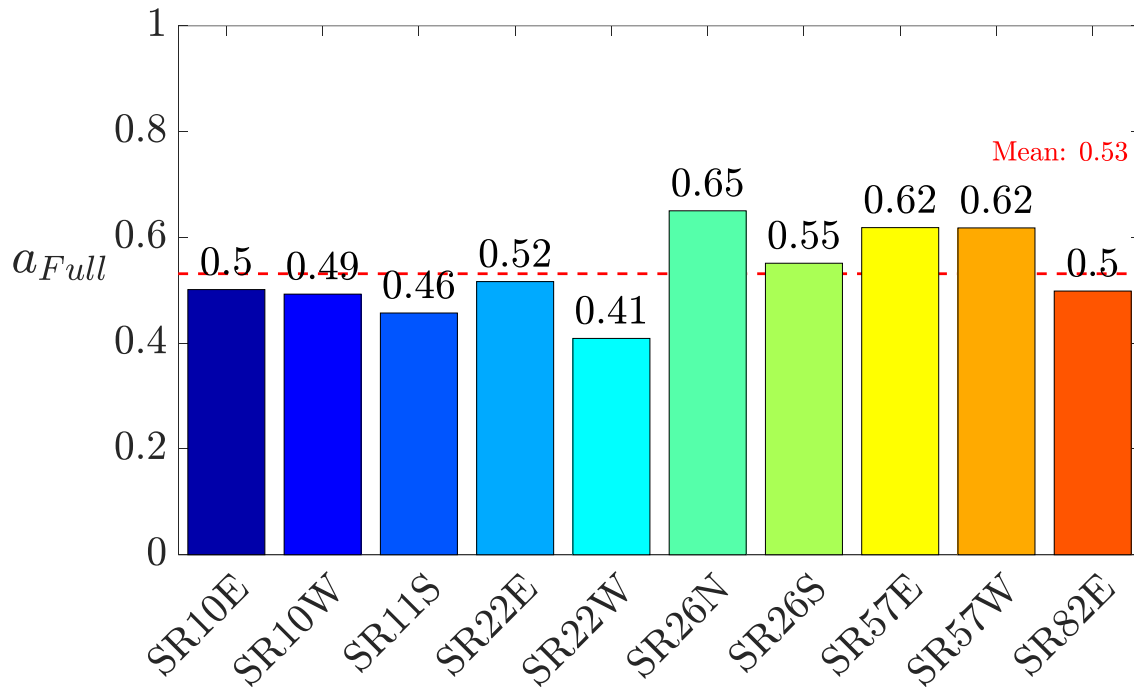


**Figure 21. Graph. FWD backcalculated layer coefficients representing the entire asphalt concrete layer for SR 10, SR 11, SR 22, SR 26, SR 57 (Johnson County), and SR 82.**

In the case of SR 10E, its corresponding top-4.5-inch coefficient was considerably higher with a value of backcalculation of  $a_{4.5-} = 0.68$ ; a value this high for the coefficient corresponds to the mean plus *six standard deviations*, which is statistically improbable to be realistic. Therefore, the issue is believed to be associated with the optimization in the backcalculation procedure. Although the asphalt layer used in the backcalculation is modeled with a division at 4.5 inches into two distinct lifts, their individual dynamic moduli do not necessarily need to be equal to their strength in reality due to a phenomenon known as the “compensating layer effect.” For instance, the combination of a stronger  $|E^*|$  above 4.5 inch and a weaker  $|E^*|$  below 4.5 inch than in actuality can lead to similar simulated deflections, and due to the nature of the optimization used in backcalculation, this is considered to be an equally valid result by the algorithm. This same issue with the converse situation (i.e., weaker-than-reality  $a_{4.5-}$  and stronger-than-reality  $a_{4.5+}$ ) is

believed to be the reason for the problematic results previously noted for SR 57E/W and SR 82E. For all three roads, their considerably low  $a_{4.5-}$  coefficients correspond to dramatically high  $a_{4.5+}$  values. Thus, the research team believes the backcalculation software converged to a result where the dynamic moduli corresponding to the below-4.5-inch asphalt were much stronger than reality, and as a consequence removed that stiffness from its estimate for the respective above-4.5-inch portions.

Inspection of the  $a_{Full}$  coefficients from figure 21 supports the reasoning for the previous issue. The full-layer coefficient effectively reflects the thickness-weighted average modulus of the entire asphalt layer, and the values of the problematic roads (i.e., SR 10E, SR 57E/W, and SR 82E) are all much closer to statistically probable values than their constituent 4.5-inch coefficients. Furthermore, all roads except for SR 22W meet the 97.8 percent reliability criterion from table 3. As mentioned previously, the research team was uncertain of how to properly model the soil-aggregate base material for this road, which is the likely cause for the discrepancy.

### **Comparison with Updated Coefficients of Other State DOTs**

In a study conducted by ALDOT in 2009<sup>[8]</sup>, it was recommended to replace the traditional value of 0.44 used for HMA mixes with an increased value of 0.54, and in a recent study by FDOT in 2019<sup>[9]</sup>, researchers recommended use of a coefficient of 0.54 for high polymer asphalt mixes. In the most recent study conducted by NHDOT<sup>[11]</sup>, the layer coefficient for HMA was recommended to be increased from 0.34–0.38 to 0.41, an increase of approximately 0.06.

The results from the present study indicate comparable results to other state DOTs for flexible pavements in GA. That is, the layer coefficients currently used by GDOT (i.e.,  $a_{4.5-} = 0.44$  and  $a_{4.5+} = 0.33$ ) are likely lower than necessary to sufficiently represent modern

asphalt mixes. For example, based on the 97.8 percent reliability criterion from table 3, coefficient values of  $a_{4.5^-} = 0.44$  and  $a_{4.5^+} = 0.39$  would be more accurate for GA pavements. Effectively, this corresponds to no change in the top-4.5-inch coefficient, and an increase in the below-4.5-inch coefficient of 0.06—a similar change as recommended in the cited ALDOT and NHDOT studies. However, the other DOTs use a single coefficient to represent the entire asphalt layer, hence the use of  $a_{Full}$  in the previous subsections. From these results, an average full-layer coefficient for GA pavements of 0.51 was concluded with a standard deviation of 0.04, which is similar to the results from the ALDOT study observing an average of 0.54 for HMA with a standard deviation of 0.08.

## CHAPTER 6. UGA-PAVE VALIDATION

### PROCEDURE

To validate the UGA-PAVE backcalculation tool, core samples were extracted by GDOT from each selected site (see table 1). The core specimens were then provided to the research team, who used an asphalt mixture performance tester to experimentally determine the dynamic modulus at specific stations. All cores were extracted from an FWD testing station (i.e., a location where FWD drops were performed). Apropos, FWD backcalculation was conducted for each station corresponding to a core, and the results were compared as validation.

The detailed validation procedure is as follows. First, the core was cut along the interface between distinct asphalt lifts, separating it into multiple stout cylinders. Then, two 38 mm diameter specimens were extracted from each of the stout cylinders. The 38 mm–specimens were then AMPT tested at various frequencies and temperatures to determine the dynamic modulus master curve of each lift. A picture of a core after being cut between lifts and having the 38 mm specimens removed is shown in figure 22.

The dynamic modulus master curve from AMPT testing was determined using the following process. First, two 38 mm–diameter specimens were extracted from each lift of the core. The specimens were then individually tested on the AMPT at three temperatures—39.2, 68, and 104°F (4, 20, and 40°C)—and six loading frequencies—0.1, 0.5, 1, 5, 10, and 25 Hz; the resulting data points were grouped together based on temperature. A time–temperature superposition model was the master curve then created from the data, and the data points were shifted to a reference temperature of 70°F (21.1°C). Finally, a sigmoidal function (see: top right of figure 9) was fit to



the grouped data set using an optimization scheme. This process was repeated for each lift of all cores used for validation.



**Figure 22. Photo. Asphalt core after 38 mm specimens were extracted for AMPT testing.**

The FWD backcalculations were conducted using pavement models comprising one asphalt layer and either one or two foundation layers, depending on the particular road. Each asphalt layer was modeled in UGA-PAVE with a total thickness equal to the corresponding core. A lack of information was available for the foundation layers (i.e., aggregate base, subgrade); therefore, regional averages were used for their material properties. Most aggregate base layers were assumed to comprise 12 inches of graded aggregate base (GAB) unless otherwise noted (e.g., some cores, such as for SR 10, were marked as having 10-inch GAB layers), and for the subgrade, the layer thickness was used as an optimization parameter and therefore did not need to be known. The backcalculation requires seed moduli (i.e., starting guesses for unknown parameters), and the selection of the seed moduli has a moderate effect in the optimized result. Thus, each pavement

section was backcalculated using different sets of seed moduli values as shown in table 4; similarly, due to regional variances, the parameters that remain constant during the backcalculation were also tuned for each pavement section based on regional averages, with the values in table 5.

**Table 4. Seed moduli (initial guesses) for the backcalculation parameters of each pavement section.**

Road	Core	$a_1$ ( $\log_{10} psi$ )	$a_2$	$a_3$	$a_4$	$E_{UAB}$ (ksi)	$E_{sub}$ (ksi)	$h_{sub}$ (ft)
SR 10	4	3.5	3.5	-1.5	0.5	20	5	10
	7	3.5	3.5	-1.5	0.5	20	5	10
SR 11	3	3.5	3.5	-1	0.4	20	5	5
SR 22	1	3.5	3.5	-1	0.4	20	5	10
SR 26	1	3.5	3.5	-1	0.4	4000	5	10
SR 57	3	3.5	3.5	-1	0.4	—	6.5	10
SR 82	1	3.5	3.5	-1.5	0.5	20	5	10
	3	3.5	3.5	-1.5	0.5	20	5	10
SR 129	5	3.5	3.5	-1.5	0.5	20	5	10

**Table 5. Constant parameters for each pavement section used in the backcalculation.**

Road	Core	$h_{AC}$ (in.)	$h_{UAB}$ (in.)	$\rho_{AC}$ (pcf)	$\rho_{UAB}$ (pcf)	$\rho_{sub}$ (pcf)	$\nu_{AC}$	$\nu_{UAB}$	$\nu_{sub}$
SR 10	4	10.875	10	140	120	100	0.3	0.35	0.4
	7	11.75	10	140	120	100	0.3	0.35	0.4
SR 11	3	15	12	140	120	70	0.3	0.35	0.35
SR 22	1	13.75	—	140	—	75	0.3	—	0.4
SR 26	1	4.5	6	140	145	100	0.3	0.2	0.4
SR 57	3	7.5	—	140	—	75	0.3	—	0.4
SR 82	1	8.5	10	140	120	75	0.3	0.35	0.4
	3	8.75	10	140	120	75	0.3	0.35	0.4
SR 129	5	6.5	12	140	120	100	0.3	0.35	0.4

The default model configuration was three layers: HMA on top, GAB in the center, and subgrade soil at the bottom. However, a few pavement sections had notable deviations from the default configuration. SR 11, SR 57 (Johnson County), and SR 82 were recorded to lie on top of a sand-clay material, and were modeled as HMA on top of a 12-inch GAB layer with a notably less dense subgrade layer. SR 22 consisted of a soil-aggregate base layer; thus, these roads were modeled using an HMA layer on top of a single foundation layer. Finally, no information was provided to the research team about SR 129, and it was modeled using the default configuration; however, it is possible that the section was modeled incorrectly due to the lack of available information.

After the FWD backcalculation was conducted for a given core, the resulting dynamic modulus curve needed to be converted to reduced frequency using the approach discussed in the PROCEDURE of chapter 5. The time–temperature superposition model takes the same form as in equation (82); however, the three coefficients are changed to match the time–temperature superposition model measured for the core via AMPT testing to provide more accurate matching.

## **VALIDATION RESULTS**

The results from the core-backcalculation validation study are contained in figure 23 to figure 31. In the graphs, the dynamic modulus curves of each lift measured from the AMPT testing are plotted in dotted gray lines, and the average of the curves are plotted in red for easier comparison with the FWD backcalculated  $|E^*|$  plotted in blue. Because the falling weight deflectometer cannot impart a perfect impulse load to the pavement in reality, there is a limited range of frequencies that it can excite; this regime was dubbed the “effective frequency range” (EFR) by Fu et al.<sup>[63]</sup>, and it is depicted in each figure using dashed green lines. Note that the EFR must be shifted using TTS along with the backcalculated  $|E^*|$  curve because the FWD load is imparted at a different

temperature from the master curve's reference temperature. For this reason, only the points within or near the EFR should be considered when determining the matching quality, because frequencies outside the range cannot be properly analyzed during backcalculation.

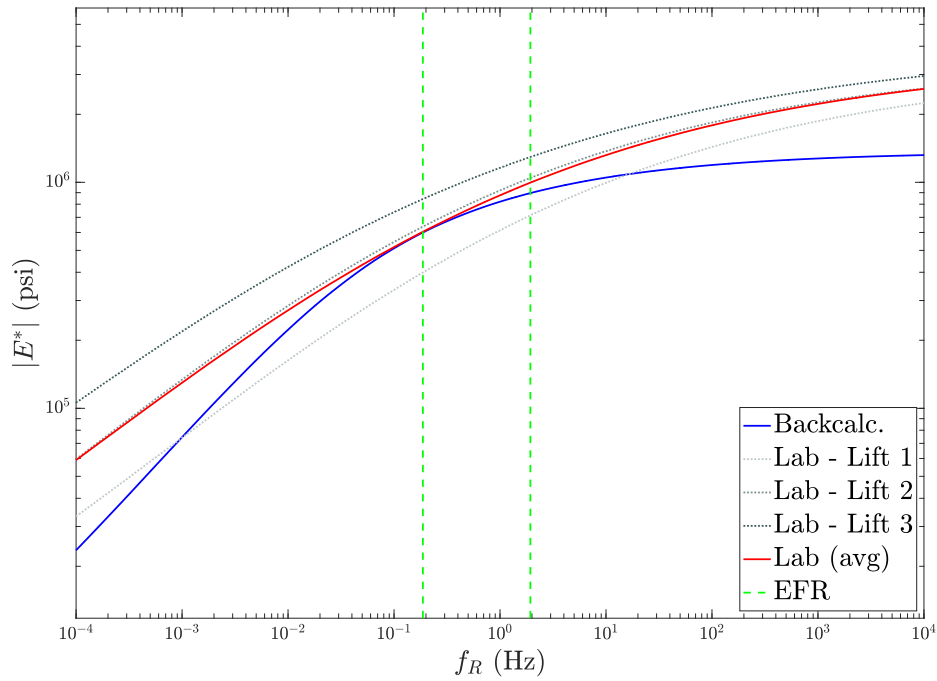


**Figure 23. Graph. Comparison of FWD backcalculated and lab-measured  $|E^*|$  for SR 10 Core 4.**

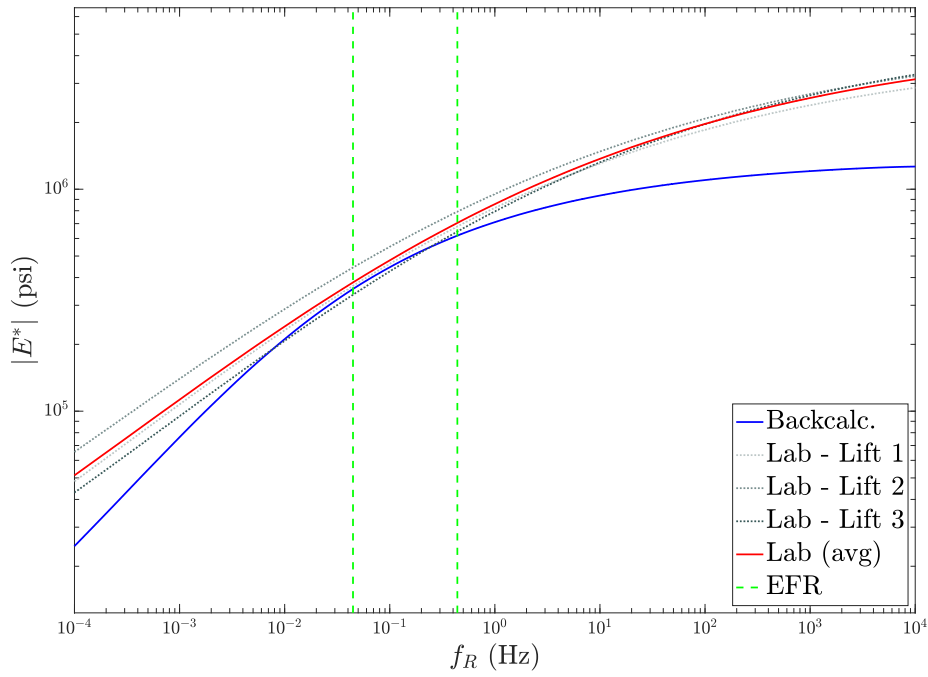


**Figure 24. Graph. Comparison of FWD backcalculated and lab-measured  $|E^*|$  for SR 10 Core 7.**

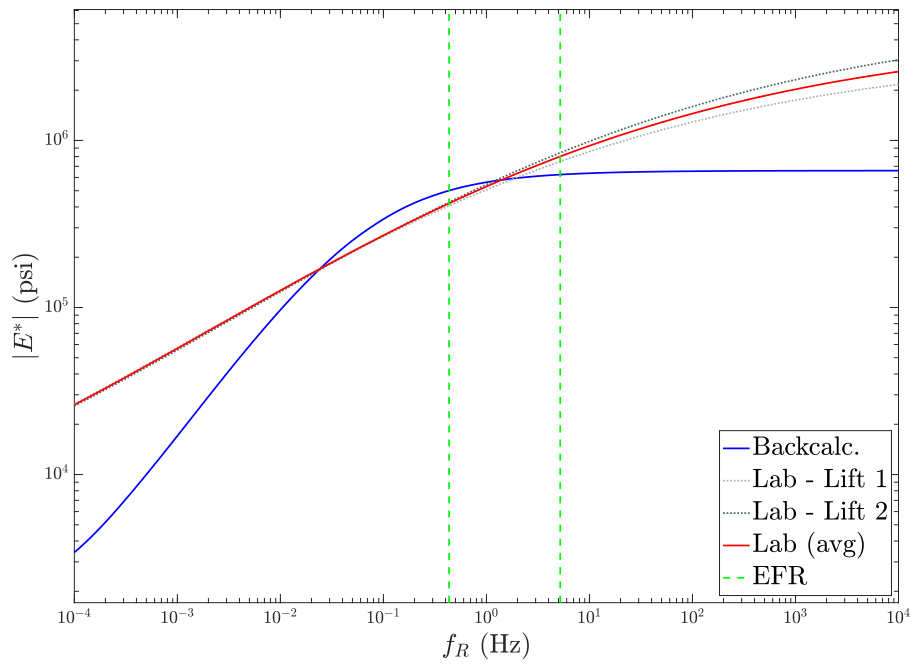


**Figure 25. Graph. Comparison of FWD backcalculated and lab-measured  $|E^*|$  for SR 11 Core 3.**

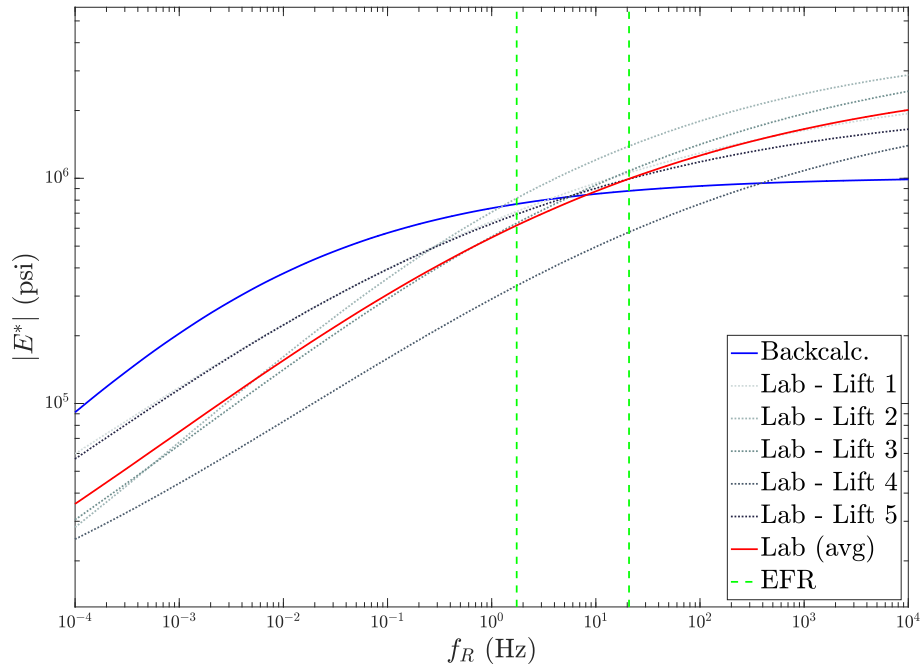


**Figure 26. Graph. Comparison of FWD backcalculated and lab-measured  $|E^*|$  for SR 22 Core 1.**

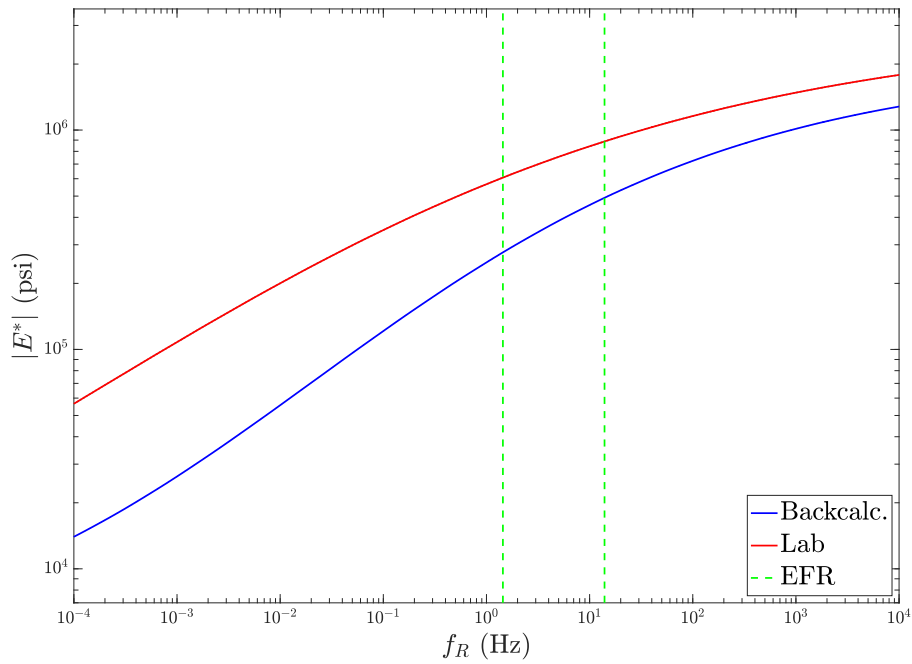


**Figure 27. Graph. Comparison of FWD backcalculated and lab-measured  $|E^*|$  for SR 26 Core 1.**

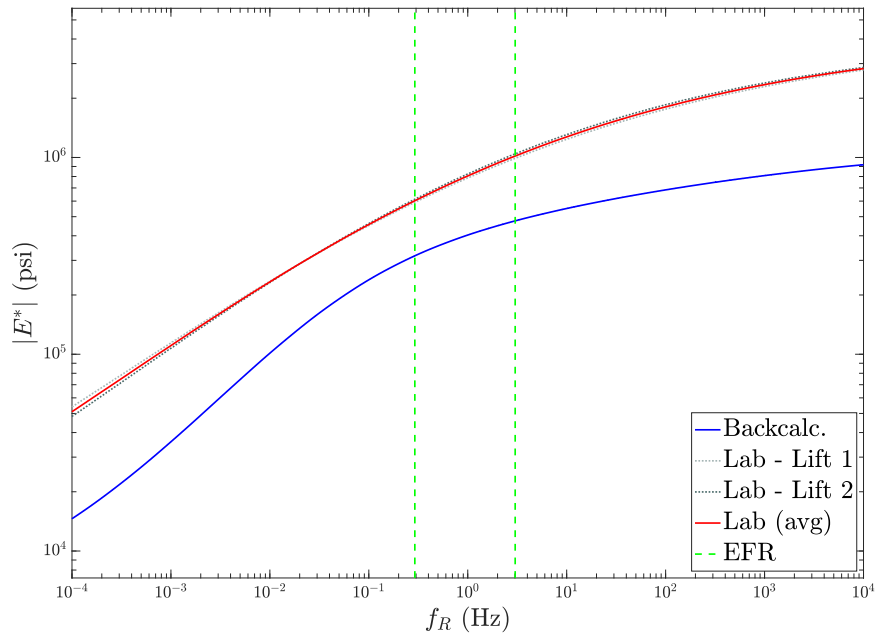


**Figure 28. Graph. Comparison of FWD backcalculated and lab-measured  $|E^*|$  for SR 57 (Johnson County) Core 3.**

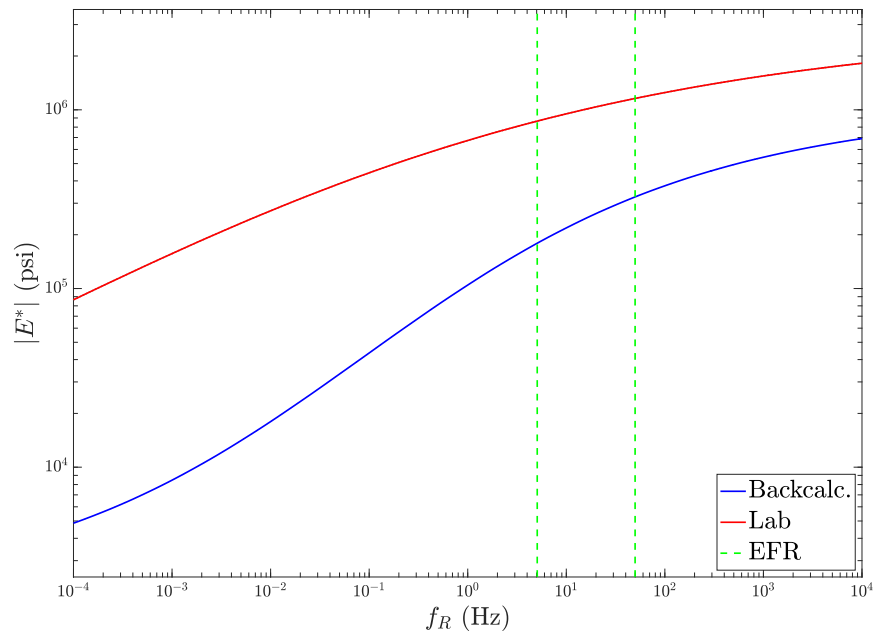


**Figure 29. Graph. Comparison of FWD backcalculated and lab-measured  $|E^*|$  for SR 82 Core 1.**

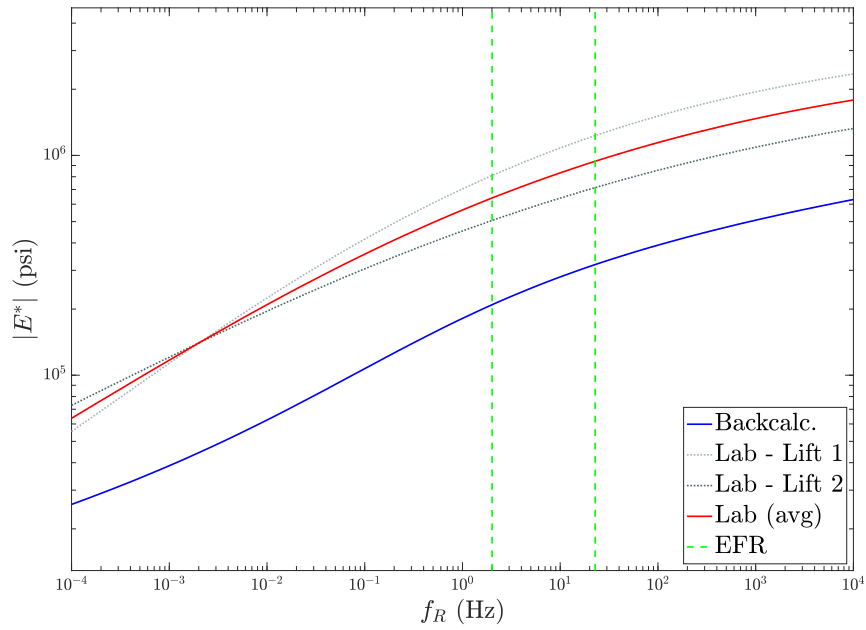


**Figure 30. Graph. Comparison of FWD backcalculated and lab-measured  $|E^*|$  for SR 82 Core 3.**

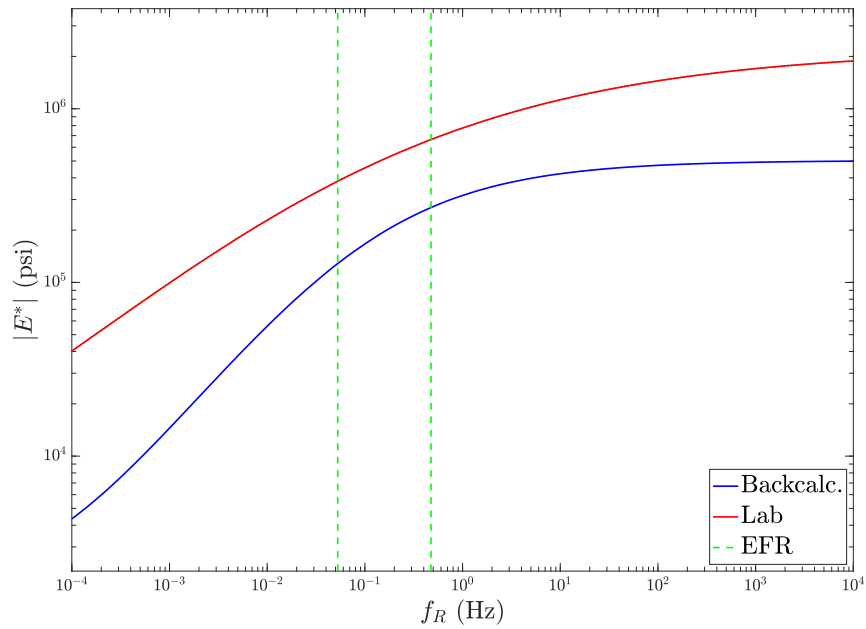


**Figure 31. Graph. Comparison of FWD backcalculated and lab-measured  $|E^*|$  for SR 129 Core 5.**



The backcalculated  $|E^*|$  curves for SR 10, SR 11, and SR 22 agreed well with the corresponding lab-measured curves, with percent differences within the EFR of 4.33 percent for SR 10 Core 4, 8.27 percent for SR 10 Core 7, 10.75 percent for SR 11 Core 3, and 9.54 percent for SR 22 Core 1. However, the results for SR 26, SR 57 (Johnson County), SR 82, and SR 129 demonstrated poor matching, having percent differences of 49.46 percent for SR 26 Core 1, 49.97 percent for SR 57 Core 3, 75.5 percent for SR 82 Core 1, 66.61 percent for SR 82 Core 3, and 62.17 percent for SR 129 Core 5.

The difference in backcalculation effectiveness differed substantially among the cores. The research team suspects two reasons as being the primary root causes. First, it is possible for a given pavement section to contain distresses that affect the structure's response when tested by FWD (e.g., bottom-up fatigue cracking, erosion of the aggregate base layer) but were not able to be detected in the core sample extracted from the road. In such scenarios, the AMPT-measured dynamic modulus should be higher than its FWD-backcalculated counterpart because the distress will reduce the pavement's strength as a whole but not necessarily for the specimens used in the AMPT device.

The second suspicion for the discrepancies between the AMPT and backcalculated  $|E^*|$  curves within the EFR is a lack of sufficient knowledge pertaining to the foundation layer characteristics, such as their densities, Poisson ratios, and elastic moduli. For instance, if the foundation layers are estimated with density or elastic modulus values that are higher than reality during FWD backcalculation, the dynamic modulus for the asphalt layer will be estimated lower to compensate for the strength.

To provide insight on the suspected issues, GPR testing was conducted along a few of the problematic sections where the FWD testing was conducted. The primary focus of the GPR

analysis was to determine the subgrade density variation underneath each road, and the measurements are plotted for SR 26N in figure 32, SR 26S in figure 33, SR 129N in figure 34, and SR 129S in figure 35. The subgrade varies significantly for each section of road by more than 30 pcf, with the exception of SR 129S, which remained remarkably consistent across the tested distance. Compared to the range of densities of each road, the constant inputs used for the backcalculations in table 5 are likely to differ significantly across the FWD testing stations. Thus, the subgrade density, as well as other similar material properties, assumed for the location where the core was extracted could be inaccurate by more than 10 pcf, significantly reducing the ability for UGA-PAVE to accurately backcalculate the  $|E^*|$  from the FWD data.

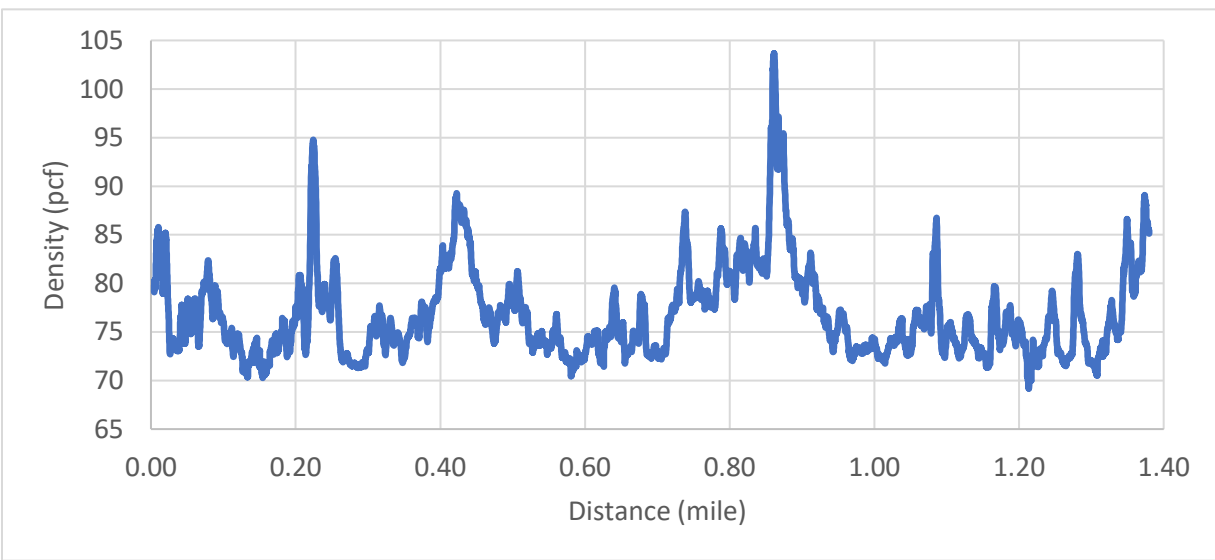


**Figure 32. Graph. Subgrade density estimated by GPR for SR 26N.**

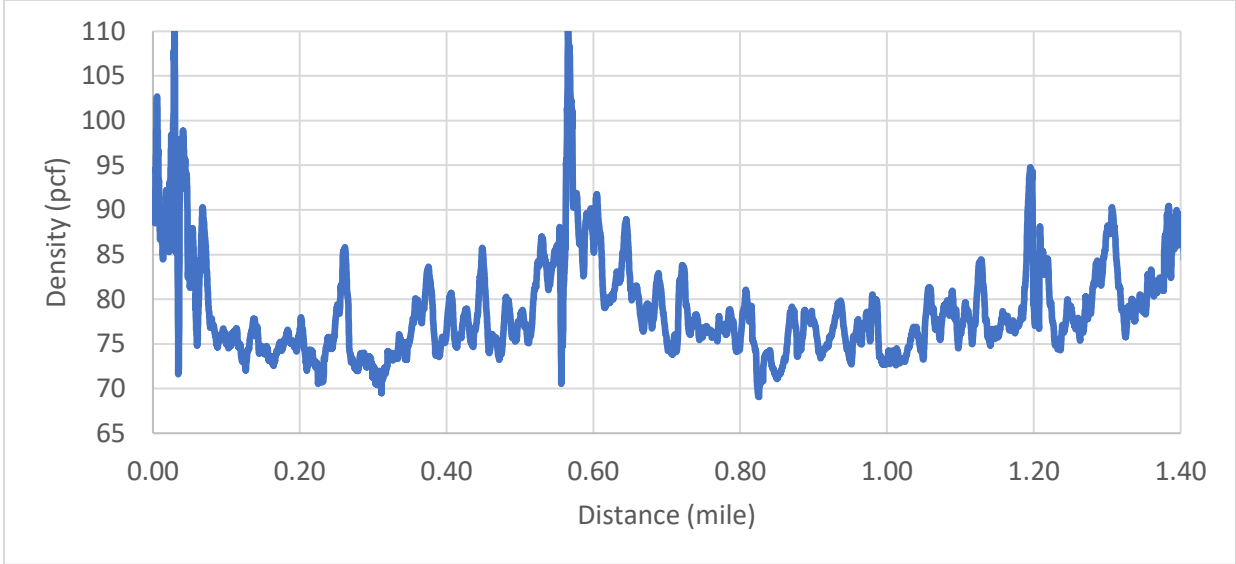


**Figure 33. Graph. Subgrade density estimated by GPR for SR 26S.**

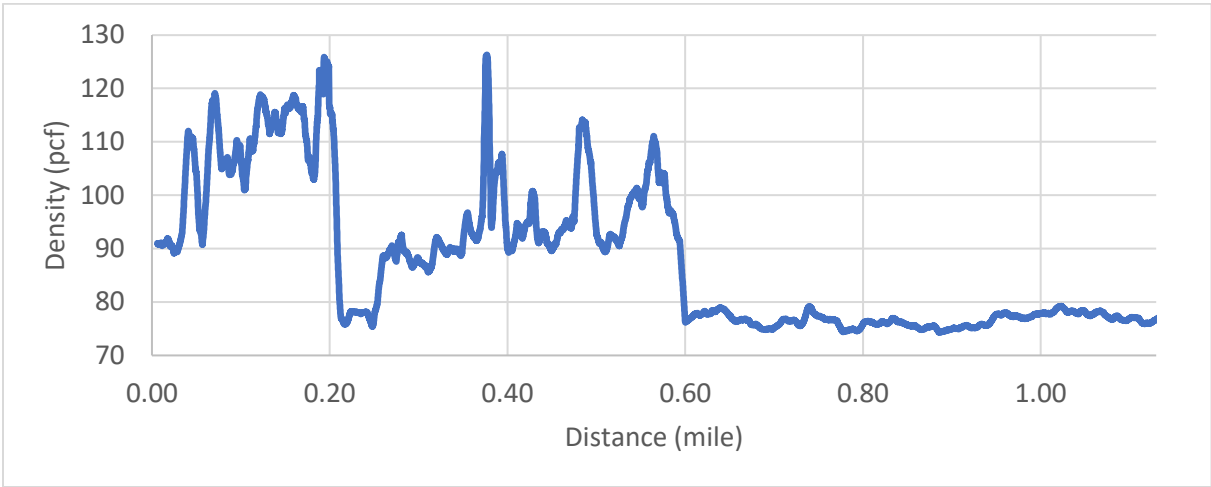


**Figure 34. Graph. Subgrade density estimated by GPR for SR 129N.**

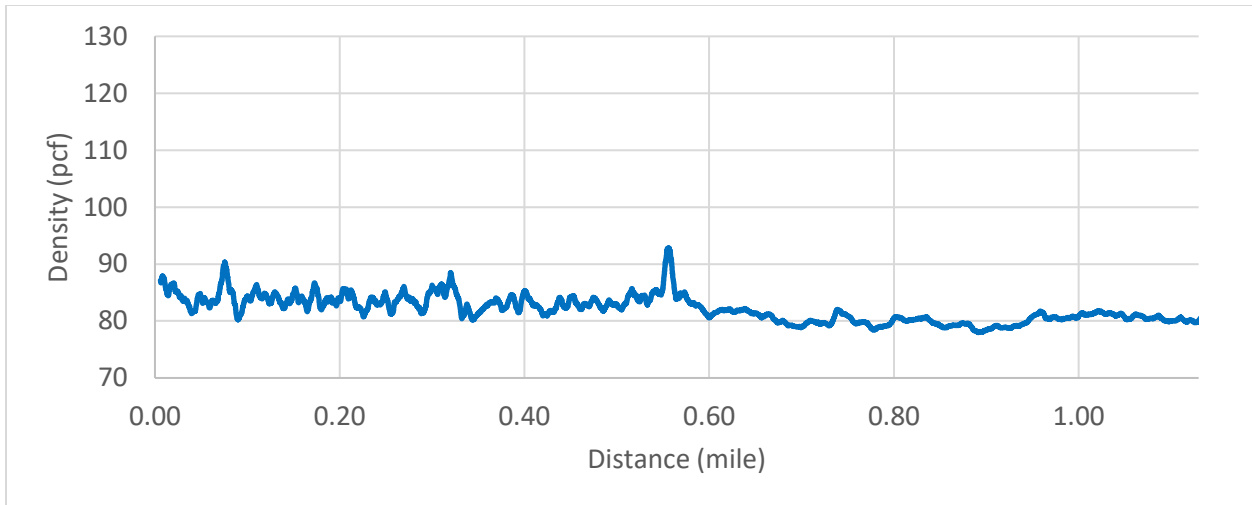


**Figure 35. Graph. Subgrade density estimated by GPR for SR 129S.**

To compare with the subgrade variation of one of the better validations, GPR testing was also conducted for some of the less problematic roads; these results are given for SR 10W in figure 36 and for SR 10E in figure 37. The dynamic modulus curves backcalculated for these two pavement sections had the lowest percent differences with their AMPT-measured counterparts among all the cores; incidentally, they had substantially lower subgrade variations than was measured for SR 82 and SR 129.

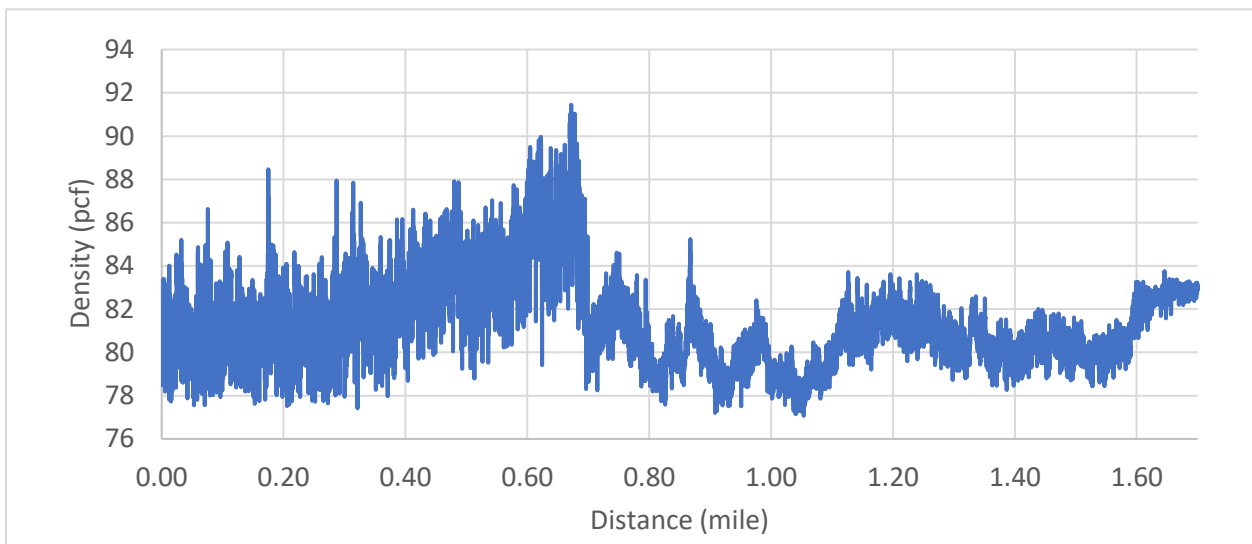


**Figure 36. Graph. Subgrade density estimated by GPR for SR 10W.**

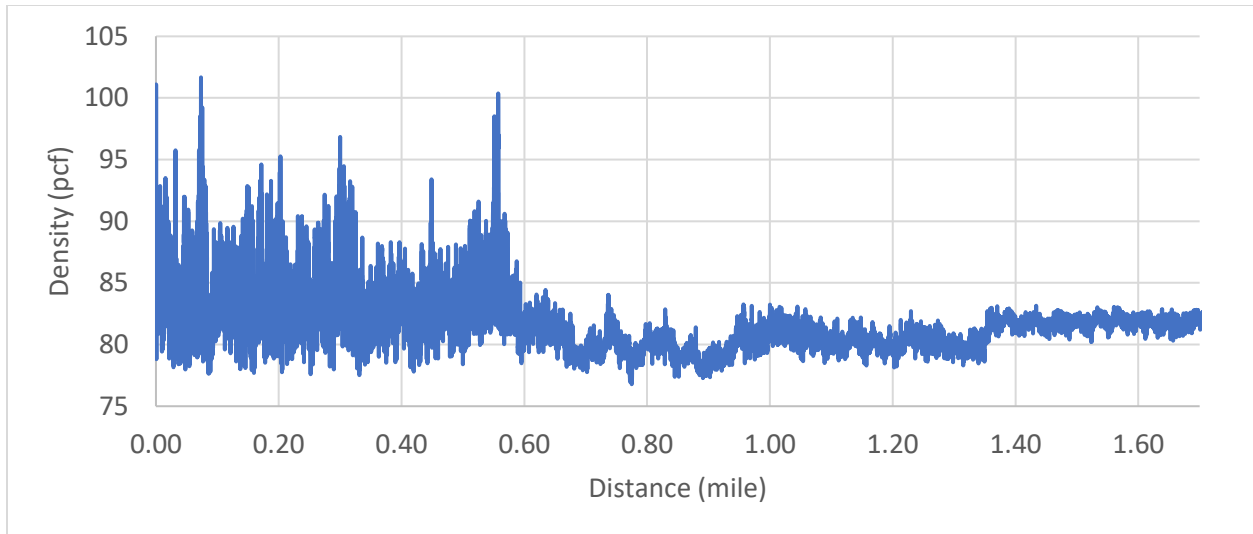


**Figure 37. Graph. Subgrade density estimated by GPR for SR 10E.**

The variations in subgrade density plotted in the figures above highlight the importance of ascertaining as much knowledge about the pavements' layers as possible for FWD backcalculation. The results suggest that even a small variation of 5–10 pcf in density between the pavement model and reality may introduce difficulties in the FWD backcalculation if the frequency of the variation is high. Further investigation is recommended in future studies to determine the sensitivity of FWD backcalculation to inaccurate values of the pavement layer material properties, such as the aggregate base and subgrade densities and Poisson ratios.

## CHAPTER 7. CONCLUSIONS AND RECOMMENDATIONS

### UPDATED LAYER COEFFICIENTS

New layer coefficients were calculated for asphalt concrete pavements using dynamic modulus curves obtained via AMPT testing of cores extracted from several locations across Georgia, and the updated values were validated using FWD backcalculation. GDOT currently uses two layer coefficients for flexible pavements based on the 1972 AASHTO *Pavement Design Guide*—0.44 for the portion above 4.5 inches, and 0.33 for the remainder below 4.5 inches. The updated layer coefficients calculated for the top-4.5-inch portion had an average value of 0.50 with a standard deviation of 0.03, and the below-4.5-inch portion was determined to have a mean of 0.51 with a standard deviation of 0.06.

From the analysis, three sets of layer coefficients were calculated based on the statistical reliability desired for the pavement design: 50, 84.2, and 97.8 percent. The coefficients corresponding to the highest reliability are recommended for pavement design despite being the most conservative, because the study used here to calculate them only measured strength and did not directly account for variations in distresses and mix type. Based on the most conservative confidence of 97.8 percent, the above-4.5-inch coefficient should remain at 0.44, whereas the below-4.5-inch layer coefficient should be increased to 0.39. Alternatively, the entire pavement layer can be modeled using a single-layer coefficient with a value of 0.43.

### FWD BACKCALCULATION

A state-of-the-art dynamic FWD backcalculation tool, UGA-PAVE, was developed as part of this study. The software was validated for dynamic modulus estimation by conducting FWD testing at the locations where cores were extracted for AMPT testing in the updated layer coefficients study.

In the validation, good agreement (<11 percent difference) was seen between the AMPT-measured and FWD-backcalculated  $|E^*|$  curves for four of nine tested cores. However, the remaining five cores/locations lacked convincing agreement, ranging from 49.46 to 75.50 percent difference.

Two primary causes are suspected for the poor backcalculations. First, certain distresses could exist in the pavement sections that affect the pavement section as a whole during FWD testing but were not contained in the extracted core. The section suspicion pertains to a lack of accurate knowledge of various material properties, such as the densities, moduli, and Poisson ratios of the foundation layers. A brief GPR analysis was conducted for some of the pavement sections, and it was observed that most of the roads with poor matching were associated with high volatility in the subgrade density, whereas the road with good matching had a comparatively low variation. This observation highlights the importance of having accurate information of the thicknesses and material properties of the various layers in the pavement structure for FWD backcalculation. Future investigation is recommended to provide insight on the sensitivity of backcalculated dynamic modulus to inaccuracies in such material properties.

Lastly, it is recommended that GPR is used as an initial “widetooth comb” that can quickly identify locations of atypical/abnormal/unexpected pavement characteristics, followed by FWD testing at those locations to serve as a “fine-tooth comb” that takes more time to conduct/process but has higher accuracy.

## APPENDICES

### APPENDIX A. PROPOSED STANDARD OPERATING PROCEDURE FOR CALCULATING NEW LAYER COEFFICIENTS FROM DYNAMIC MODULUS DATA

#### GENERAL

The purpose of this Standard Operating Procedure is to outline the methodology for calculating flexible layer coefficients from dynamic modulus ( $|E^*|$ ) curves. This technique is intended to determine coefficients *in situ*, such as from an  $|E^*|$  estimated from FWD backcalculation. The layer coefficients can then be used to determine the pavement section's structural number (SN) using the design procedures outlined in the GDOT Pavement Design Guide.

#### PROCEDURE

This test procedure is used when a dynamic modulus curve has been measured/estimated for an asphalt concrete pavement. The following instructions detail how to calculate a layer coefficient using the dynamic modulus curve.

1. If the dynamic modulus curve is a mastercurve (i.e., at the reference temperature of 70°F, or 21.1°C), skip this step and go to Step 2. Otherwise, convert the  $|E^*|$  curve to reduced frequency using Time-Temperature Superposition (TTS).
  - a. TTS shifting procedure:
    - i. Calculate the TTS factor,  $a(T)$ .



1. If no Time-Temperature Superposition model is available, the user can use the following equation which was developed from averages of numerous asphalt mixtures:

$$\log_{10}(a(T)) = 0.0022T^2 - 0.2363T + 4.0065,$$

where  $T$  is the temperature corresponding to the dynamic modulus curve, measured in Celsius.

- ii. Shift the  $|E^*|$  curve to reduced frequency using the relationship

$$f_R = a(T) \cdot f,$$

where  $f$  is the original frequency point of the  $|E^*|$  curve, and  $f_R$  is the corresponding reduced frequency point.

2. With the curve shifted to reduced frequency, determine the dynamic modulus value for  $f_R = 1$  Hz in psi.
3. Use the following equation from the 1993 AASHTO Pavement Design Guide to calculate the new layer coefficient:

$$a = 0.171 \cdot \ln(|E^*(f_R = 1 \text{ Hz})|) - 1.784,$$

where  $|E^*|$  is measured in psi.

### EXAMPLE CALCULATION

The following example calculation is provided to demonstrate the procedure outlined in previous section for calculating a layer coefficient from a dynamic modulus curve. For the example, an  $|E^*|$  curve is used that was obtained via a sigmoidal fitting function applied to AMPT-measured dynamic modulus data, given by

$$\log_{10}|E^*| = 3.9412 + \frac{2.7590}{1 + e^{-0.2964 - 0.4089 \log_{10}(f)}}.$$

Because  $|E^*|$  curves obtained from AMPT testing are typically already mastercurves; however, the above equation has been shifted to a non-reference temperature of 86°F (30°C) to demonstrate the Time-Temperature Superposition shifting procedure. From the AMPT testing, a TTS model of the example asphalt mixture was determined as

$$\log_{10} a(T) = 0.0015T^2 - 0.1769T + 3.0722.$$

Now, using the given sigmoidal function for dynamic modulus, expression for Time-Temperature Superposition, and starting temperature of 86°F (30°C), the layer calculation procedure from the previous section is applied. For convenience, the mathematical operations are shown in gray font to more clearly indicate when technical steps are applied.

1. The given  $|E^*|$  expression is not a mastercurve; therefore, it must be shifted to reduced frequency.
  - a. Apply Time-Temperature Superposition procedure:
    - i. Calculate the TTS factor,  $a(T)$ .

$$\log_{10} a(T) = 0.0015T^2 - 0.1769T + 3.0722$$

$$\log_{10} a(T = 30^\circ\text{C}) = 0.0015(30^\circ\text{C})^2 - 0.1769(30^\circ\text{C}) + 3.0722$$

$$\log_{10} a(T = 30^\circ\text{C}) = -0.8848$$

$$a(T = 30^\circ\text{C}) = 0.1304$$

ii. Shift the  $|E^*|$  curve to reduced frequency.

$$f_R = a(T) \cdot f$$

$$\log_{10} f_R = \log_{10} a(T) + \log_{10} f$$

$$\log_{10} |E^*(f)| = 3.9412 + \frac{2.7590}{1 + e^{-0.2964 - 0.4089 \log_{10}(f)}}$$

$$\log_{10} |E^*(f_R)| = 3.9412 + \frac{2.7590}{1 + e^{-0.2964 - 0.4089 (\log_{10}(f_R) - \log_{10} a(T))}}$$

$$\log_{10} |E^*(f_R)| = 3.9412 + \frac{2.7590}{1 + e^{-0.2964 - 0.4089 \log_{10}(f_R) + 0.4089 \log_{10} a(T)}}$$

$$\log_{10} |E^*(f_R)| = 3.9412 + \frac{2.7590}{1 + e^{-0.2964 - 0.4089 \log_{10}(f_R) + (0.4089)(-0.8848)}}$$

$$\log_{10} |E^*(f_R)| = 3.9412 + \frac{2.7590}{1 + e^{-0.6582 - 0.4089 \log_{10}(f_R)}}$$

2. Determine the dynamic modulus value at a reduced frequency of 1 Hz.

$$\log_{10} |E^*(f_R)| = 3.9412 + \frac{2.7590}{1 + e^{-0.6582 - 0.4089 \log_{10}(f_R)}}$$

$$\log_{10} |E^*(f_R = 1 \text{ Hz})| = 3.9412 + \frac{2.7590}{1 + e^{-0.6582 - 0.4089 \log_{10}(1)}}$$

$$\log_{10} |E^*(f_R = 1 \text{ Hz})| = 3.9412 + \frac{2.7590}{1 + e^{-0.6582 - 0.4089 \log_{10}(1)}}$$

$$\log_{10} |E^*(f_R = 1 \text{ Hz})| = 3.9412 + \frac{2.7590}{1 + e^{-0.6582}}$$

$$\log_{10} |E^*(f_R = 1 \text{ Hz})| = 5.7590$$

$$|E^*(f_R = 1 \text{ Hz})| = 5.7409 \cdot 10^5 \text{ psi}$$

3. Calculate the layer coefficient using the equation from the 1993 AASHTO Pavement Design Guide.

$$a = 0.171 \cdot \ln(|E^*(f_R = 1 \text{ Hz})|) - 1.784$$

$$a = 0.171 \cdot \ln(5.7409 \cdot 10^5) - 1.784$$

$$a = 0.4836$$

## **APPENDIX B. PROPOSED STANDARD OPERATING PROCEDURE FOR OPERATION OF UGA-PAVE FOR DYNAMIC MODULUS BACKCALCULATION**

### **GENERAL**

The purpose of this Standard Operating Procedure is to outline the methodology to conduct FWD Backcalculation via UGA-PAVE. The software is capable of generating Level 1  $|E^*|$  (dynamic modulus) inputs and Level 2  $D(t)$  (creep compliance) inputs for AASHTOWare PavementME. First, a comprehensive outline of how to use UGA-PAVE is provided, including how to prepare the FWD data, running the application, and exporting the backcalculated data into files for use in PavementME. Then, an example with pictures are provided to demonstrate all three parts of the procedure.

### **BACKCALCULATION PROCEDURE**

The following lists contain the step-by-step guidelines for conducting FWD backcalculations UGA-PAVE. First, the way to prepare the data from a Dynatest FWD for UGA-PAVE is covered. Then, the procedure for using UGA-PAVE is given. Finally, the steps for exporting backcalculated results to files ready for use in PavementME are provided.

#### **A. Preparing Dynatest FWD Data for UGA-PAVE**

1. Use Microsoft Access to open the Microsoft database (“.mdb”) file containing Dynatest FWD data.
2. In the left-hand pane called “Tables”, double-click the “Histories” tab.
3. In the pane at the top side of the page, click “External Data”, then click “Excel”.

4. In the “Export – Excel Spreadsheet” window, click the “Browse...” button and select the location you would like to save the new FWD data file.
5. At the bottom right of the “Export – Excel Spreadsheet” page, click “OK”.
  - a. Note: Do **NOT** check the “Export data with formatting and layout.” option.
6. Wait for a few moments (typically takes up to one minute) until the “Save Export Steps” window pops up, and click “Close” in the bottom right.
7. The data will now be saved to the location specified in Step 4 and is ready for use in UGA-PAVE.

## **B. Conducting FWD Backcalculation with UGA-PAVE**

1. Start UGA-PAVE.
2. On the opening page, click the “**START NEW PROJECT**” button; the **DATA IMPORT WIZARD** screen will appear.
3. On the **DATA IMPORT WIZARD** screen, click the “**Select File**” button. In the file explorer window that appears, navigate to the location of the FWD data (saved as a “.xlsx” file) and click “**Open**”.
  - a. To prepare the FWD data from a Dynatest FWD for UGA-PAVE as a “.xlsx” file, follow the steps outlined in Section **II.B**.
  - b. You will need to wait a while as UGA-PAVE imports the FWD data. This takes approximately 1 second per FWD station in the data (usually 1-1.5 minutes).
4. By default, no FWD data will be selected for the backcalculation analysis; to do so, you need to use the dropdown boxes labeled “**Station:**” and “**Drop:**”, as well as the 8 buttons in the center of the screen (e.g., “**Include Station 1 Drop 1**”).
  - a. Description of Plots:

- i. **Deflection (mils) vs Time (ms)** – Plots the FWD deflections of the Station/Drop combination selected via the dropdown boxes.
  - ii. **Max Deflection (mils) vs Station** – Plots the peak FWD deflections measured at each station to quickly identify comparative strength of the road at each station.
- b. Description of Buttons:
- i. **Select File** – Used to point UGA-PAVE to location of FWD data for backcalculation analysis.
  - ii. **Station** – Selects the X'th FWD station.
  - iii. **Drop** – Selects the Y'th FWD drop from the currently selected X'th station.
  - iv. **Include/Remove Station X Drop Y** – Adds/removes the current Station/Drop combination selected via the dropdown boxes to/from the data selected for backcalculation.
  - v. **Include/Remove ALL Stations Drop Y** – Adds/removes the Y'th drop recorded for all FWD stations to/from the data selected for backcalculation.
  - vi. **Include/Remove Station X ALL Drops** – Adds/removes all drops recorded for the X'th FWD station to/from the data selected for backcalculation.
  - vii. **Include/Remove ALL Stations ALL Drops** – Adds/removes all drops from all stations to/from the data selected for backcalculation.
  - viii. **Expand/Collapse all** – Expands/collapses the list of FWD stations and drops selected for backcalculation for easier viewing.

5. Once the desired FWD stations and drops are selected for analysis, click the **PROPS** tab in the left-hand side of the screen. On this page, the user should input the correct material properties to the best of their knowledge for each station. Parameters in **magenta** are varied by UGA-PAVE for backcalculation, whereas the parameters in **blue** remain constant throughout the analysis.
  - a. Primary Inputs for User to Change:
    - i. All “**t (in.)**” values
    - ii. Any “**p (pcf)**” values if known (e.g., from ground-penetrating radar).
    - iii. All **Sensor Distances** on the right-hand side of the page.
  - b. Optional Inputs for User to Change:
    - i. Sigmoidal coefficients ( **$\delta, \alpha, \beta, \gamma$** )
    - ii. Elastic Moduli of Foundation Layers ( **$E$** )
    - iii. Poisson Ratios ( **$\nu$** ).
  - c. Description of Buttons:
    - i. **Station** – Select the station that the material properties will be applied to.
    - ii. **-/+** – Used to remove/add Asphalt and Foundation Layers to/from the pavement model for the backcalculation analysis.
    - iii. **Apply values to all stations** – Copies the current material properties (number of Asphalt/Foundation layers, values) for the current station and sets them for all stations selected in **Step 4**.
    - iv. **Sensor Distances Check Boxes** – Sensors with checked boxes will be used for the backcalculation. Un-checking a box will remove that deflection from



the backcalculation analysis for the station (useful for sensors with erroneous measurements).

d. Description of Parameters:

- i.  $\delta, \alpha, \beta, \gamma$  – [ $\log_{10}$  psi] Sigmoidal coefficients used for modeling Dynamic Modulus of the corresponding Asphalt Layer. The sigmoidal fitting function is shown at the top-right of the page.
- ii.  $t$  – [inches] Thickness of the corresponding pavement layer.
- iii.  $\nu$  – Poisson ratio of the corresponding pavement layer.
- iv.  $\rho$  – [pcf] Density of the corresponding pavement layer.
- v.  $E$  – [psi] Elastic modulus of the corresponding Foundation Layer.
- vi.  $d_i$  – [inches] Distance of the  $i^{\text{th}}$  FWD sensor from the loading plate.

6. Once all material properties are set and verified, click the “**BACKCALC**” tab in the left-hand pane; the **FWD BACKCALCULATION** screen will appear. Click the “**BACKCALCULATE**” button to begin the dynamic FWD backcalculation analysis.

- a. The backcalculation will run for a while—approximately 5 minutes per drop.
- b. A status light is displayed to show the current status of the backcalculation

i. **Red:**

Scenario 1. Setup from previous pages is incomplete (no FWD data has been selected).

Scenario 2. Backcalculation was aborted prematurely by user. Click the “**BACKCALCULATE**” button to restart backcalculation when ready.

- ii. **Green:** Setup is complete and backcalculation can begin.

- iii. **Yellow**: Backcalculation is currently in progress.
  - iv. **Blue**: Backcalculation is complete, and results are ready for viewing.
- c. Description of Buttons:
- i. **BACKCALCULATE**: Begins the FWD backcalculation.
  - ii. **STOP** – Aborts the backcalculation procedure. ALL RESULTS COMPUTED BEFOREHAND WILL BE DISCARDED AND HAVE TO BE CALCULATED AGAIN.
- d. Description of Plots:
- i. **Deflection (mils) vs Time (ms)** – Plots the FWD load, FWD deflections, and current backcalculated deflections (“VW”- for ViscoWave) for the current Station and Drop.
  - ii. **Run Info** – Prints out various information pertaining to the current backcalculation (e.g., current station, drop, iteration, sum of squared errors).
7. Once all data selected on the **DATA IMPORT WIZARD** page have been backcalculated, results may be viewed on the following pages. (In-depth descriptions of how to export results are covered in Section **II.C.**)
- a. **|E\*| CURVE** – Plots the dynamic modulus mastercurve that was backcalculated for the Station selected in the dropdown box at the top of the page. This can be used for Level 1 |E\*| Inputs in PavementME.
  - b. **D(t) CURVE** – Plots the creep compliance curve that was backcalculated for the Station selected in the dropdown box at the top of the page. This can be used for Level 2 D(t) inputs in PavementME.

- c. **VARIATION** – Plots the dynamic and elastic moduli backcalculated at each station to visualize their variation. The “**EXPORT PLOT**” button can be used to save a file containing the values used to create the variation graph.
- 8. [Optional Step] The setup information (and results, if backcalculated) for the current project can be saved and returned to later. To do so, click the **MAIN** tab in the left-hand pane. Then, click the “**SAVE CURRENT PROJECT**” button. A file explorer window will appear; navigate to the location where you would like to save the current project file and click “**OK**”.
  - a. The project data will be saved as a “.mat” file. Once saved, the UGA-PAVE application can be closed and restarted later.
  - b. To resume the project, run UGA-PAVE (if not already running), and on the **MAIN** tab, click the “**LOAD EXISTING PROJECT**” button. In the file explorer window that appears, navigate to the “.mat” file where the desired project is saved, and click “**OK**”. After a few seconds, UGA-PAVE will load the data from the file and the user can resume where they left off.

### **C. Exporting Results for PavementME**

- 1. Level-1 |E\*| (Dynamic Modulus)
  - a. Primary Inputs for User to Change:
    - i. **Station Temp** – Input the temperature of the pavement surface measured by the FWD equipment for proper Time-Temperature Superposition shifting.
  - b. Optional Inputs for User to Change:

- i.  $T_1/T_2/T_3/T_4$  – Temperatures used for Time-Temperature Superposition shifting to create L1  $|E^*|$  inputs for PavementME. These temperatures are automatically set to PavementME defaults; however, the user may change the temperatures if desired.

*(Note: The rows in the table at the bottom-right of the page correspond to these temperatures.)*

- ii.  $\alpha_1/\alpha_2/\alpha_3$  – Coefficients of the Time-Temperature Superposition model used to construct each  $|E^*|$  mastercurve. They are set to HMA averages by default, and the user may change them if desired (such as when a TTS model is known for the asphalt material).

c. Description of Buttons:

- i. **Station Dropdown** – Select which Station’s results to view.
- ii. **Log Scale Checkbox** – When checked: plot both axes in logarithmic scale.  
When unchecked: plot only the X-axis in logarithmic scale.
- iii. **Export** – Used to save the data tabulated above the button in a “.xlsx” file to be used as L1  $|E^*|$  inputs for PavementME. The data in the table changes based on the asphalt layer selected in the dropdown box to the left of the button.

d. Description of Plots:

- i.  $|E^*|$  (psi) vs **Reduced Frequency (Hz)** – An  $|E^*|$  mastercurve is plotted for each Asphalt Layer (specified for the station on the **PROPS** tab) based on the **Station Dropdown** selection.

2. Level-2 D(t) (Creep Compliance)

- a. Primary Inputs for User to Change:
  - i. **Station Temp** – Input the temperature of the pavement surface measured by the FWD equipment for proper Time-Temperature Superposition shifting.
  
- b. Optional Inputs for User to Change:
  - i. **Shifted Temp** – Temperatures used for Time-Temperature Superposition shifting to create L2 D(t) inputs for PavementME. The Shifted Temp is automatically set to the PavementME default; however, the user may change the temperature if desired.  
  
*(Note: The row in the table at the bottom-right of the page corresponds to this temperature.)*
  - ii.  $\alpha_1/\alpha_2/\alpha_3$  – Coefficients of the Time-Temperature Superposition model used to shift each D(t) curve. They are set to HMA averages by default, and the user may change them if desired (such as when a TTS model is known for the asphalt material).
  
- c. Description of Buttons:
  - i. **Station Dropdown** – Select which Station’s results to view.
  - ii. **Log Scale Checkbox** – When checked: plot only the Y-axis in logarithmic scale. When unchecked: plot both axes in linear scale.
  - iii. **Export** – Used to save the data tabulated above the button in a “.xlsx” file to be used as L2 D(t) inputs for PavementME. The data in the table changes based on the asphalt layer selected in the dropdown box to the left of the button.

d. Description of Plots:

- i. **D(t) (psi<sup>-1</sup>) vs Loading Time (s)** – A D(t) curve is plotted for each Asphalt Layer (specified for the station on the **PROPS** tab) based on the **Station Dropdown** selection at the value specified in the **Shifted Temp** input field.

## EXAMPLES

In this section, an example of the procedures covered in the previous section are provided with screenshots to demonstrate a typical backcalculation.

### A. Preparing Dynatest FWD Data for UGA-PAVE

1. Open the Microsoft database (“.mdb”) file containing Dynatest FWD data.
2. In the left-hand pane called “Tables”, double-click the “Histories” tab.

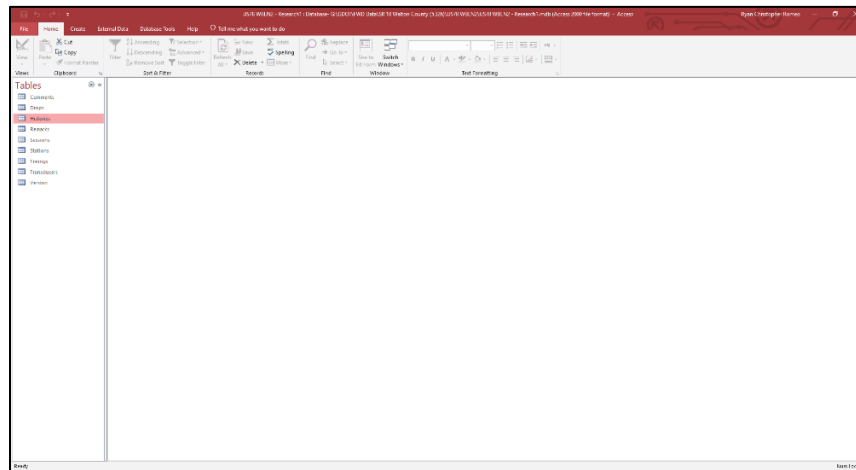


**Figure 38.** Screen. Initial Microsoft Access after opening FWD data database file.

3. In the pane at the top side of the page, click “External Data”, then click “Excel”.

Original	Imported	Time	Address	Format	03	04	05	06	07	08	09	10	11	12	13	14	15
241	240001	0.00	0.0	0	0.00	0.00	0.00	0.00	0.00	0.00	0.00	0.00	0.00	0.00	0.00	0.00	0.00
41	242	280201	0.00	0.0	0	0.00	0.00	0.00	0.00	0.00	0.00	0.00	0.00	0.00	0.00	0.00	0.00
40	236	280101	0.00	0.0	0	0.00	0.00	0.00	0.00	0.00	0.00	0.00	0.00	0.00	0.00	0.00	0.00
40	239	280501	0.00	0.0	0	0.00	0.00	0.00	0.00	0.00	0.00	0.00	0.00	0.00	0.00	0.00	0.00
40	232	280201	0.00	0.0	0	0.00	0.00	0.00	0.00	0.00	0.00	0.00	0.00	0.00	0.00	0.00	0.00
40	235	280801	0.00	0.0	0	0.00	0.00	0.00	0.00	0.00	0.00	0.00	0.00	0.00	0.00	0.00	0.00
40	240	280801	0.00	0.0	0	0.00	0.00	0.00	0.00	0.00	0.00	0.00	0.00	0.00	0.00	0.00	0.00
41	245	280801	0.00	0.0	0	0.00	0.00	0.00	0.00	0.00	0.00	0.00	0.00	0.00	0.00	0.00	0.00
40	238	280401	0.00	0.0	0	0.00	0.00	0.00	0.00	0.00	0.00	0.00	0.00	0.00	0.00	0.00	0.00
41	243	280901	0.00	0.0	0	0.00	0.00	0.00	0.00	0.00	0.00	0.00	0.00	0.00	0.00	0.00	0.00
41	246	290401	0.00	0.0	0	0.00	0.00	0.00	0.00	0.00	0.00	0.00	0.00	0.00	0.00	0.00	0.00
41	248	280401	0.00	0.0	0	0.00	0.00	0.00	0.00	0.00	0.00	0.00	0.00	0.00	0.00	0.00	0.00
39	234	270601	0.00	0.0	0	0.00	0.00	0.00	0.00	0.00	0.00	0.00	0.00	0.00	0.00	0.00	0.00
42	249	280901	0.00	0.0	0	0.00	0.00	0.00	0.00	0.00	0.00	0.00	0.00	0.00	0.00	0.00	0.00
44	260	310801	0.00	0.0	0	0.00	0.00	0.00	0.00	0.00	0.00	0.00	0.00	0.00	0.00	0.00	0.00
42	247	290501	0.00	0.0	0	0.00	0.00	0.00	0.00	0.00	0.00	0.00	0.00	0.00	0.00	0.00	0.00
44	259	290601	0.00	0.0	0	0.00	0.00	0.00	0.00	0.00	0.00	0.00	0.00	0.00	0.00	0.00	0.00
42	252	301201	0.00	0.0	0	0.00	0.00	0.00	0.00	0.00	0.00	0.00	0.00	0.00	0.00	0.00	0.00
43	253	302401	0.00	0.0	0	0.00	0.00	0.00	0.00	0.00	0.00	0.00	0.00	0.00	0.00	0.00	0.00
42	248	290401	0.00	0.0	0	0.00	0.00	0.00	0.00	0.00	0.00	0.00	0.00	0.00	0.00	0.00	0.00
43	258	300401	0.00	0.0	0	0.00	0.00	0.00	0.00	0.00	0.00	0.00	0.00	0.00	0.00	0.00	0.00
42	251	300001	0.00	0.0	0	0.00	0.00	0.00	0.00	0.00	0.00	0.00	0.00	0.00	0.00	0.00	0.00
43	257	307201	0.00	0.0	0	0.00	0.00	0.00	0.00	0.00	0.00	0.00	0.00	0.00	0.00	0.00	0.00
43	244	280601	0.00	0.0	0	0.00	0.00	0.00	0.00	0.00	0.00	0.00	0.00	0.00	0.00	0.00	0.00
43	256	300601	0.00	0.0	0	0.00	0.00	0.00	0.00	0.00	0.00	0.00	0.00	0.00	0.00	0.00	0.00
42	250	280801	0.00	0.0	0	0.00	0.00	0.00	0.00	0.00	0.00	0.00	0.00	0.00	0.00	0.00	0.00
43	255	300801	0.00	0.0	0	0.00	0.00	0.00	0.00	0.00	0.00	0.00	0.00	0.00	0.00	0.00	0.00
45	270	320801	0.00	0.0	0	0.00	0.00	0.00	0.00	0.00	0.00	0.00	0.00	0.00	0.00	0.00	0.00
45	266	310801	0.00	0.0	0	0.00	0.00	0.00	0.00	0.00	0.00	0.00	0.00	0.00	0.00	0.00	0.00
46	269	321801	0.00	0.0	0	0.00	0.00	0.00	0.00	0.00	0.00	0.00	0.00	0.00	0.00	0.00	0.00
44	263	310401	0.00	0.0	0	0.00	0.00	0.00	0.00	0.00	0.00	0.00	0.00	0.00	0.00	0.00	0.00
44	262	310201	0.00	0.0	0	0.00	0.00	0.00	0.00	0.00	0.00	0.00	0.00	0.00	0.00	0.00	0.00
44	271	320401	0.00	0.0	0	0.00	0.00	0.00	0.00	0.00	0.00	0.00	0.00	0.00	0.00	0.00	0.00
44	273	320401	0.00	0.0	0	0.00	0.00	0.00	0.00	0.00	0.00	0.00	0.00	0.00	0.00	0.00	0.00
44	268	310401	0.00	0.0	0	0.00	0.00	0.00	0.00	0.00	0.00	0.00	0.00	0.00	0.00	0.00	0.00
45	265	310801	0.00	0.0	0	0.00	0.00	0.00	0.00	0.00	0.00	0.00	0.00	0.00	0.00	0.00	0.00
46	272	320201	0.00	0.0	0	0.00	0.00	0.00	0.00	0.00	0.00	0.00	0.00	0.00	0.00	0.00	0.00

Figure 39. Screen. Histories tab of the imported FWD data.

4. In the “Export – Excel Spreadsheet” window, click the “Browse...” button and select the location you would like to save the new FWD data file.

Export - Excel Spreadsheet

Select the destination for the data you want to export

Specify the destination file name and format.

File name:

File format:

Specify export options.

We will not import table relationships, calculated columns, validation rules, default values, and columns of certain legacy data types such as OLE Object.

Search for "Import" in Access 2016 Help for more information.

Export data with formatting and layout.  
Select this option to preserve most formatting and layout information when exporting a table, query, form, or report.

Open the destination file after the export operation is complete.  
Select this option to view the results of the export operation. This option is available only when you export formatted data.

Export only the selected records.  
Select this option to export only the selected records. This option is only available when you export formatted data and have records selected.

Figure 40. Screen. Example of the “Export – Excel Spreadsheet” window.

5. At the bottom right of the “Export – Excel Spreadsheet” page, click “OK”.
  - a. Note: Do **NOT** check “Export data with formatting and layout.”

6. Wait for a few moments (typically takes up to one minute) until the “Save Export Steps” window appears, and click “Close” in the bottom right.

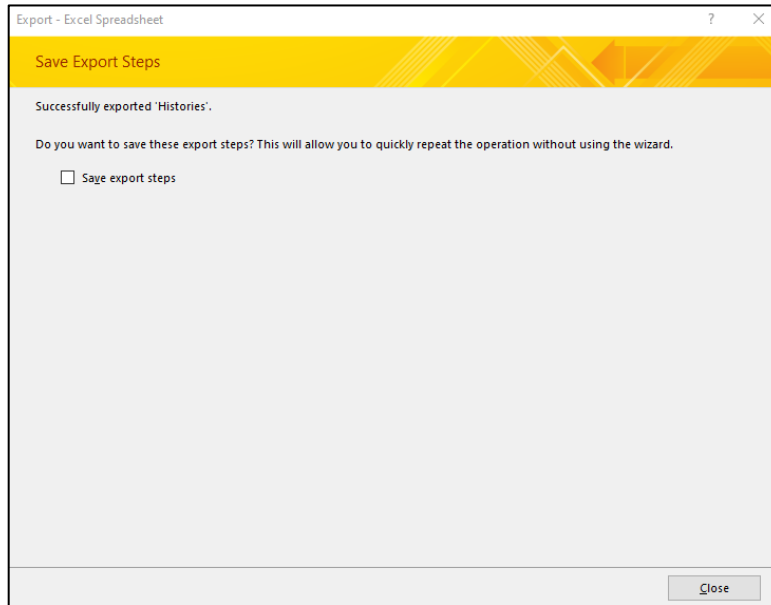


**Figure 41.** Screen. FWD data export confirmation window.

7. The data will now be saved to the location specified in Step 4 and is ready for use in UGA-PAVE.

## **B. Conducting FWD Backcalculation with UGA-PAVE**

1. Start UGA-PAVE.
2. Click the “**START NEW PROJECT**” button.



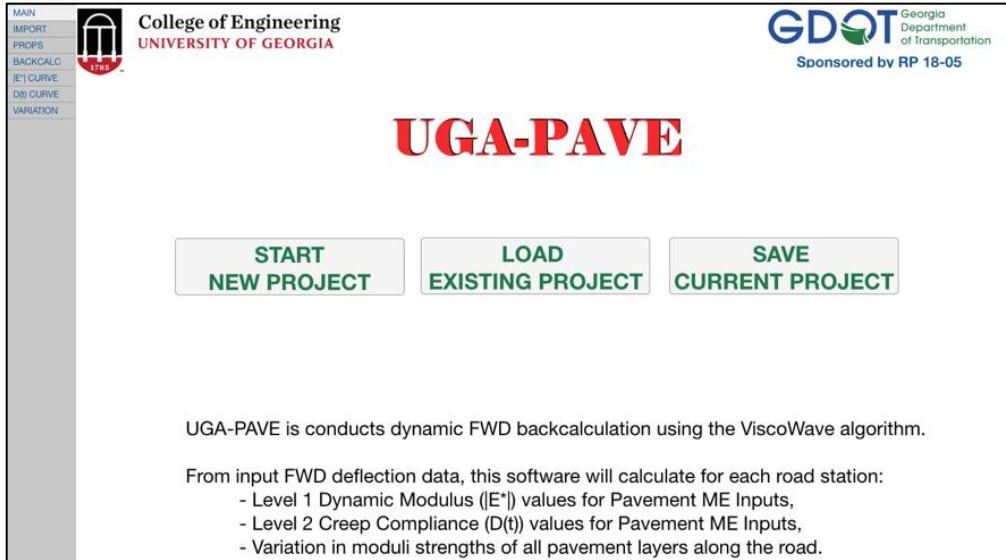


**Figure 42.** Screen. The UGA-PAVE starting page.

3. Open the FWD data file.



**Figure 43.** Screen. UGA-PAVE data import wizard prior to importing FWD data.

4. Select FWD Stations and Drops for analysis. Four total FWD drops are selected in the below example: the third and fifth drops from Station 1, and the second and fourth drops from Station 55. This will lead to four total backcalculations.

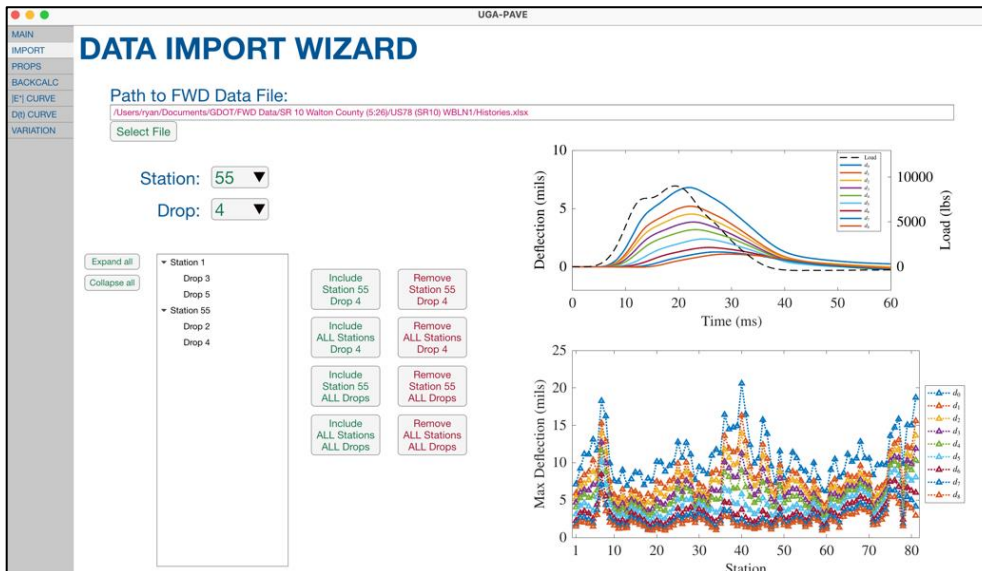


**Figure 44.** Screen. Import wizard after selecting and importing FWD data.

5. Set the material properties for each station selected. In the below example, different properties are set for Stations 1 and 55.

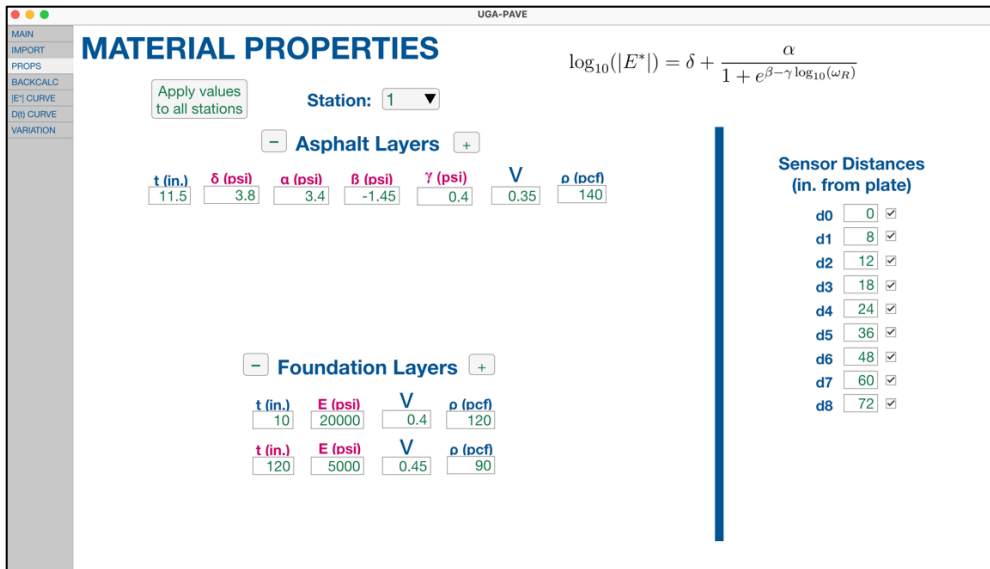


Figure 45. Screen. Example of setting material properties for Station 1.

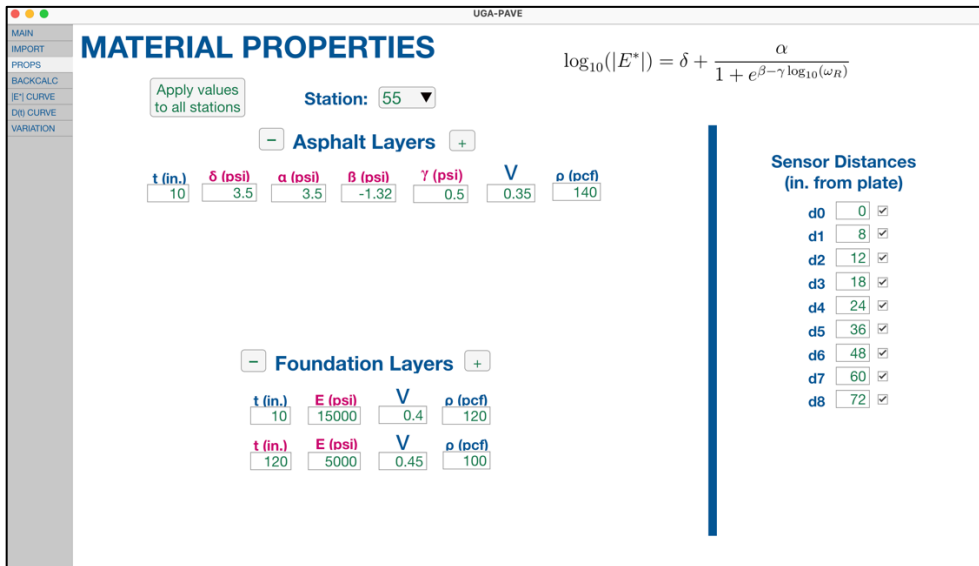
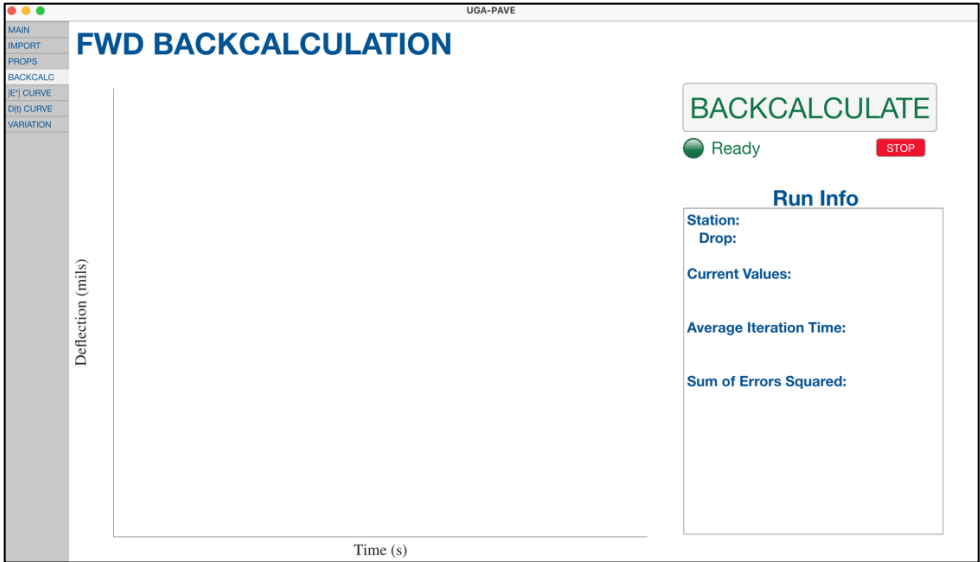


Figure 46. Screen. Example of setting material properties for Station 55.

- With the material properties set, the program is now ready for backcalculation. Click the **BACKCALC** tab, and then click the “**BACKCALCULATE**” button.



**Figure 47.** Screen. Example of runtime window prior to starting backcalculation.

- Once the backcalculation completes, the results pages (**|E\*| CURVE**, **D(t) CURVE**, and **VARIATION**) are now ready to view.

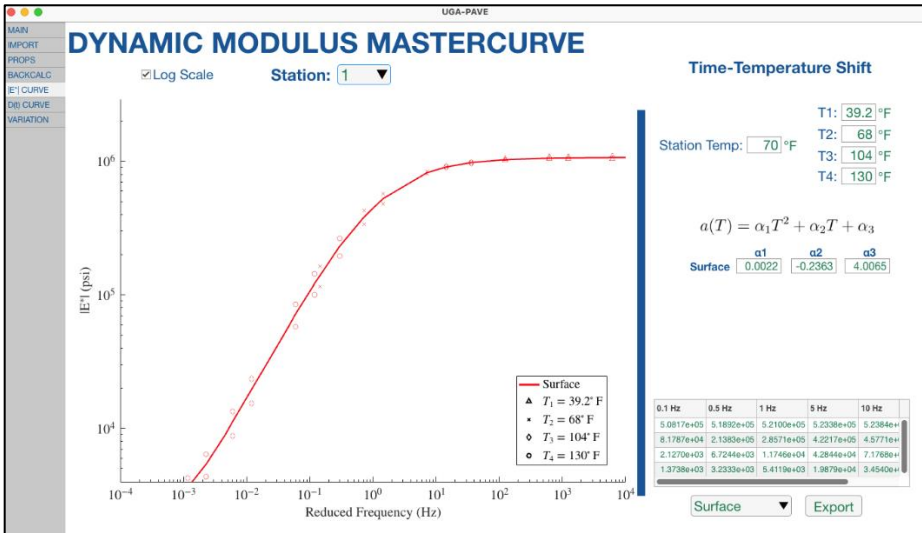


**Figure 48.** Screen. Example of |E\*| results page after backcalculation completes.

## C. Exporting Results for PavementME

The example here will cover how to export backcalculated  $|E^*|$  results for use as Level 1 Dynamic Modulus inputs for PavementME. The steps for  $D(t)$  are the same as for  $|E^*|$ ; however, the creep compliance input is instead Level 2.

1. In the dropdown box in the bottom-right, select the asphalt layer for export.
  - a. If the pavement model at the current station only had one asphalt layer, then the correct asphalt layer will already be selected.
2. Click the “Export” button. In the file explorer window that appears, select the location to save the data, and click “OK”.

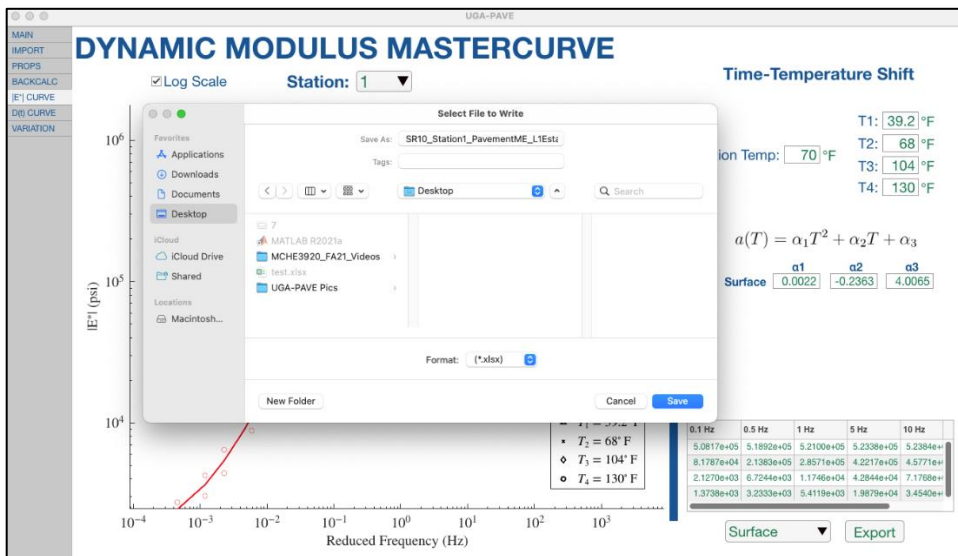


**Figure 49.** Screen. Demonstration of exporting  $|E^*|$  result from UGA-PAVE.

3. The data is now saved and immediately ready to be input to PavementME. An example of what the export should look like is given below.

	A	B	C	D	E	F	G	H	I	J	K	L	M	N	O	P
1	508171.229	518918.117	520996.175	523382.943	523844.239	524210.789										
2	81787.1418	213828.308	285705.841	422174.335	457706.747	487542.626										
3	2126.98099	6724.42157	11746.3292	42843.7666	71768.1756	132994.794										
4	1373.78751	3233.3248	5411.86712	19879.3908	34539.5475	69428.9707										
5																
6																
7																
8																
9																
10																
11																
12																
13																
14																
15																
16																
17																
18																
19																
20																
21																
22																
23																

Figure 50. Screen. Example of exported |E\*| data from UGA-PAVE to an Excel file.

## **ACKNOWLEDGMENTS**

The University of Georgia acknowledges the financial support for this work provided by the Georgia Department of Transportation (GDOT). The authors thank the technical manager, Mr. Ian Rish, and his Office of Materials and Testing (OMAT) team members, Mr. Phillip Snider and Mr. Jason Waters, for research support and partnership. Special thanks also to the project manager, Mr. Sunil Thapa, who advised the research team in successfully performing the study and assisted in the coordination of project meetings with GDOT. Finally, the team expresses thanks for the continuous support from Supriya Kamatkar and her leadership in the Performance-based Management and Research Office.

## REFERENCES

- [1] AASHTO (1972). *AASHTO Interim Guide for Design of Pavement Structures*. American Association of State Highway and Transportation Officials, Washington, D.C.
- [2] AASHTO (1986). *Guide for Design of Pavement Structures*. American Association of State Highway and Transportation Officials, Washington, D.C.
- [3] Janoo, V.C. (1994). *Layer Coefficients for NHDOT Pavement Materials*. Technical Report 94-30, U.S. Army Corps of Engineers, Cold Regions Research & Engineering Laboratory. Available online: <http://hdl.handle.net/11681/12334>.
- [4] Rohde, G.T. (1994). "Determining Pavement Structural Number from FWD Testing." *Transportation Research Record: Journal of the Transportation Research Board*, 1448(10), pp. 61–68. Available online: <https://onlinepubs.trb.org/Onlinepubs/trr/1994/1448/1448-008.pdf>.
- [5] Schnoor, H. and Horak, E. (2012). "Possible Method of Determining Structural Number for Flexible Pavement with the Falling Weight Deflectometer." *Proceedings of the 31st Southern African Transport Conference*, Pretoria, South Africa, pp. 94–109. Available online: <http://hdl.handle.net/2263/20033>.
- [6] Kim, M.Y., Kim, D.Y., and Murphy, M.R. (2013). "Improved Method for Evaluating the Pavement Structural Number with Falling Weight Deflectometer Deflections." *Transportation Research Record: Journal of the Transportation Research Board*, 2366(1), pp. 120–126. Available online: <https://doi.org/10.3141/2366-14>.
- [7] Bahia, H.U., Bosscher, P.J., Christensen, J., and Hu, Y.H. (2000). *Layer Coefficients for New and Reprocessed Asphaltic Mixes*. Report No. WI/SPR 04-00, Wisconsin Department of Transportation, Madison, WI. Available online: <https://wisconsindot.gov/documents2/research/97-02layercoefficients.pdf>.
- [8] Peters-Davis, K. and Timm, D.H. (2009). *Recalibration of the Asphalt Layer Coefficient*. Report 09-03, National Center for Asphalt Technology, Auburn University, Auburn, AL. Available online: <https://www.eng.auburn.edu/research/centers/ncat/files/technical-reports/rep09-03.pdf>.
- [9] Taylor, R.K. (2019). *Structural Coefficient for High Polymer Modified Asphalt Mixes*. Final Report BE321, Florida Department of Transportation, Tallahassee, FL.



- [10] Katicha, S.W., Shrestha, S., Flintsch, G.W., and Diefenderfer, B.K. (2020). *Network Level Pavement Structural Testing with the Traffic Speed Deflectometer*. Final Report VTRC 21-R4, Virginia Department of Transportation, Richmond, VA. Available online: [https://www.virginiadot.org/vtrc/main/online\\_reports/pdf/21-r4.pdf](https://www.virginiadot.org/vtrc/main/online_reports/pdf/21-r4.pdf).
- [11] Nemati, R., Dave, E.V., and Sias, J.E. (2021). "Generalized Methodology to Develop Mechanistically Informed Asphalt Mixture Layer Coefficients for AASHTO 1993 Pavement Design Approach." *Transportation Research Record*, (published online) September 22. Available online: <https://doi.org/10.1177%2F03611981211041597>.
- [12] Ceylan, H., Gopalakrishnan, K., and Guclu, A. (2007). "Advanced Approaches to Characterizing Nonlinear Pavement System Responses." *Transportation Research Record: Journal of the Transportation Research Board*, 2005(1), pp. 86–94. Available online: <http://dx.doi.org/10.3141/2005-10>.
- [13] Zaghoul, S. and White, T. (1993). "Use of a Three-dimensional, Dynamic Finite Element Program for Analysis of Flexible Pavement." *Transportation Research Record*, 1388, pp. 60–69. Available online: <https://onlinepubs.trb.org/Onlinepubs/trr/1993/1388/1388-008.pdf>.
- [14] Saltan, M. and Karaşahin, M. (2006). "A Finite Element Based Backcalculation Program for Flexible Pavements." *Indian Journal of Engineering & Materials Sciences*, 13(3), pp. 221–230. Available online: <http://nopr.niscair.res.in/bitstream/123456789/7552/1/IJEMS%2013%283%29%20221-230.pdf>.
- [15] Goktepe, A.B., Agar, E., and Lav, A.H. (2006). "Advances in Backcalculating the Mechanical Properties of Flexible Pavements." *Advances in Engineering Software*, 37(7), pp. 421–431. Available online: <https://doi.org/10.1016/j.advengsoft.2005.10.001>.
- [16] Liang, R. and Zeng, S. (2002). "Efficient Dynamic Analysis of Multilayered System During Falling Weight Deflectometer Experiments." *Journal of Transportation Engineering*, 128(4), pp. 366–374. Available online: [https://doi.org/10.1061/\(ASCE\)0733-947X\(2002\)128:4\(366\)](https://doi.org/10.1061/(ASCE)0733-947X(2002)128:4(366)).
- [17] Gopalakrishnan, K., Kim, S., Ceylan, H., and Kaya, O. (2014). *Development of Asphalt Dynamic Modulus Master Curve Using Falling Weight Deflectometer Measurements*. InTrans Project 13-471 Final Report, Iowa Department of Transportation, Ames, IA. Available online: [http://publications.iowa.gov/17832/1/IADOT\\_InTrans\\_TR-659\\_Ceylan\\_Devo\\_Aspphalt\\_Dynamic\\_Modulus\\_Master\\_Curve\\_FWD\\_2014\\_report.pdf](http://publications.iowa.gov/17832/1/IADOT_InTrans_TR-659_Ceylan_Devo_Aspphalt_Dynamic_Modulus_Master_Curve_FWD_2014_report.pdf).

- [18] Meier, R.W. and Rix, G.J. (1995). "Backcalculation of Flexible Pavement Moduli from Dynamic Deflection Basins Using Artificial Neural Networks." *Transportation Research Record*, 1473, pp. 72–81. Available online: <https://onlinepubs.trb.org/Onlinepubs/trr/1995/1473/1473-009.pdf>.
- [19] Chatti, K., Ji, Y., and Harichandran, R. (2004). "Dynamic Time Domain Backcalculation of Layer Moduli, Damping, and Thicknesses in Flexible Pavements." *Transportation Research Record: Journal of the Transportation Research Board*, 1869(1), pp. 106–116. Available online: <https://doi.org/10.3141%2F1869-13>.
- [20] Varma, S., Kutay, M.E., and Levenberg, E. (2013). "Viscoelastic Genetic Algorithm for Inverse Analysis of Asphalt Layer Properties from Falling Weight Deflections." *Transportation Research Record: Journal of the Transportation Research Board*, 2369(1), pp. 38–46. Available online: <https://doi.org/10.3141%2F2369-05>.
- [21] Lee, H.S., Ayyala, D., and Von Quintus, H.L. (2017). "Dynamic Backcalculation of Viscoelastic Asphalt Properties and Master Curve Construction." *Transportation Research Record: Journal of the Transportation Research Board*, 2641(1), pp. 29–38. Available online: <http://dx.doi.org/10.3141/2641-05>.
- [22] Madsen, S.S. and Levenberg, E. (2018). "Dynamic Backcalculation with Different Load-Time Histories." *Road Materials and Pavement Design*, 19(6), pp. 1314–1333. Available online: <https://doi.org/10.1080/14680629.2017.1307263>.
- [23] Li, M. and Wang, H. (2018). "Prediction of Asphalt Pavement Responses from FWD Surface Deflections Using Soft Computing Methods." *Journal of Transportation Engineering*, 144(2), p. 04018014. Available online: <https://doi.org/10.1061/JPEODX.0000044>.
- [24] Berenger, J-P. (1994). "A Perfectly Matched Layer for the Absorption of Electromagnetic Waves." *Journal of Computational Physics*, 114(2), pp. 185–200. Available online: <https://doi.org/10.1006/jcph.1994.1159>.
- [25] Basu, U. and Chopra, A.K. (2003). "Perfectly Matched Layers for Time-Harmonic Elastodynamics of Unbounded Domains: Theory and Finite-Element Implementation." *Computer Methods in Applied Mechanics and Engineering*, 192(11–12), pp. 1337–1375. Available online: [https://doi.org/10.1016/S0045-7825\(02\)00642-4](https://doi.org/10.1016/S0045-7825(02)00642-4).
- [26] Madsen, S.S., Krenk, S., and Hededal, O. (2013). "Perfectly Matched Layer (PML) for Transient Wave Propagation in a Moving Frame of Reference." Presented at the 4th ECCOMAS Thematic Conference on Computational Methods in Structural Dynamics and Earthquake Engineering (COMPdyn 2013), Kos Island, Greece, June 12–14.

- [27] Kohno, H., Bathe, K.-J., and Wright, J.C. (2010). "A Finite Element Procedure for Multiscale Wave Equations with Application to Plasma Waves." *Computers and Structures*, 88(1–2), pp. 87–94. Available online: <https://doi.org/10.1016/j.compstruc.2009.05.001>.
- [28] Ham, S. and Bathe, K.-J. (2012). "A Finite Element Method Enriched for Wave Propagation Problems." *Computers and Structures*, 94–95, pp. 1–12. Available online: <https://doi.org/10.1016/j.compstruc.2012.01.001>.
- [29] Thomson, W.T. (1950). "Transmission of Elastic Waves Through a Stratified Solid Medium." *Journal of Applied Physics*, 21, pp. 89–93. Available online: <https://doi.org/10.1063/1.1699629>.
- [30] Haskell, N.A. (1953). "The Dispersion of Surface Waves on Multilayered Media." *Bulletin of Seismological Society of America*, 43(1), pp. 17–34. Available online: <https://doi.org/10.1785/BSSA0430010017>.
- [31] Kausel, E. and Roesset, J.M. (1981). "Stiffness Matrices for Layered Soils." *Bulletin of the Seismological Society of America*, 71(6), pp. 1743–1761. Available online: <https://doi.org/10.1016/0148-9062%2883%2991665-0>.
- [32] Rizzi, S.A. and Doyle, J.F. (1992). "A Spectral Element Approach to Wave Motion in Layered Solids." *Journal of Vibration and Acoustics*, 114(4), pp. 569–577. Available online: <https://doi.org/10.1115/1.2930300>.
- [33] Doyle, J.F. (1997). *Wave Propagation in Structures: Spectral Analysis Using Fast Discrete Fourier Transforms*. Mechanical Engineering Series, Springer, New York.
- [34] Al-Khoury, R., Scarpas, A., Kasbergen, C., and Blaauwendraad, J. (2001). "Spectral Element Technique for Efficient Parameter Identification of Layered Media. I. Forward Calculation." *International Journal of Solids and Structures*, 38(9), pp. 1605–1623. Available online: [http://dx.doi.org/10.1016/S0020-7683\(00\)00112-8](http://dx.doi.org/10.1016/S0020-7683(00)00112-8).
- [35] Al-Khoury, R., Scarpas, A., Kasbergen, C., and Blaauwendraad, J. (2001). "Spectral Element Technique for Efficient Parameter Identification of Layered Media. Part II: Inverse Calculation." *International Journal of Solids and Structures*, 38(48–49), pp. 8753–8772. Available online: [https://doi.org/10.1016/S0020-7683\(01\)00109-3](https://doi.org/10.1016/S0020-7683(01)00109-3).
- [36] Al-Khoury, R., Scarpas, A., Kasbergen, C., and Blaauwendraad, J. (2002). "Spectral Element Technique for Efficient Parameter Identification of Layered Media. Part III: Viscoelastic Aspects." *International Journal of Solids and Structures*, 39(8), pp. 2189–2201. Available online: [https://doi.org/10.1016/S0020-7683\(02\)00079-3](https://doi.org/10.1016/S0020-7683(02)00079-3).

- [37] Chatti, K. and Yun, K.K. (1996). "SAPSI-M: Computer Program for Analyzing Asphalt Concrete Pavements Under Moving Arbitrary Loads." *Transportation Research Record: Journal of the Transportation Research Board*, 1539(1), pp. 88–95. Available online: <https://doi.org/10.1177%2F0361198196153900112>.
- [38] Ji, Y. (2005). *Frequency and Time Domain Backcalculation of Flexible Pavement Layer Parameters*. Ph.D. Dissertation, Michigan State University, East Lansing, MI.
- [39] Zhang, W., Drescher, A., and Newcomb, D.E. (1997). "Viscoelastic Analysis of Diametral Compression of Asphalt Concrete." *Journal of Engineering Mechanics*, 123(6), pp. 596–603. Available online: [https://doi.org/10.1061/\(ASCE\)0733-9399\(1997\)123:6\(596\)](https://doi.org/10.1061/(ASCE)0733-9399(1997)123:6(596)).
- [40] Zhang, W., Drescher, A., and Newcomb, D.E. (1997). "Viscoelastic Behavior of Asphalt Concrete in Diametral Compression." *Journal of Transportation Engineering*, 123(6), pp. 495–502. Available online: [https://doi.org/10.1061/\(ASCE\)0733-947X\(1997\)123:6\(495\)](https://doi.org/10.1061/(ASCE)0733-947X(1997)123:6(495)).
- [41] Bendat, J.S. and Piersol, A.G. (2010). *Random Data: Analysis and Measurement Procedures*. John Wiley & Sons, Inc., Hoboken, NJ.
- [42] Lee, H.S. (2013). *Development of a New Solution for Viscoelastic Wave Propagation of Pavement Structures and Its Use in Dynamic Backcalculation*. Ph.D. Dissertation, Michigan State University, East Lansing, MI.
- [43] Lee, H.S. (2014). "Viscowave—A New Solution for Viscoelastic Wave Propagation of Layered Structures Subjected to an Impact Load." *International Journal of Pavement Engineering*, 15(6), pp. 542–557. Available online: <https://doi.org/10.1080/10298436.2013.782401>.
- [44] Kabanikhin, S.I. (2008). "Definitions and Examples of Inverse and Ill-posed Problems." *Journal of Inverse and Ill-Posed Problems*, 16(4), pp. 317–357. Available online: <http://dx.doi.org/10.1515/JIIP.2008.019>.
- [45] Hua, X.G., Ni, Y.Q., and Ko, J.M. (2009). "Adaptive Regularization Parameter Optimization in Output-error-based Finite Element Model Updating." *Mechanical Systems and Signal Processing*, 23(3), pp. 563–579. Available online: <http://dx.doi.org/10.1016%2Fj.ymssp.2008.05.002>.
- [46] Sivanesarwan, N., Kramer, S.L., and Mahoney, J.P. (1991). "Advanced Backcalculation Using a Nonlinear Least Squares Optimization Technique." *Transportation Research Record*, 1293, pp. 93–102. Available online: <http://onlinepubs.trb.org/Onlinepubs/trr/1991/1293/1293-010.pdf>.

- [47] Pellinen, T., Witczak, M., and Bonaquist, R. (2002). "Asphalt Mix Master Curve Construction Using Sigmoidal Fitting Function with Non-linear Least Squares Optimization." 15th ASCE Engineering Mechanics Division Conference, New York, June 4. Available online: [https://doi.org/10.1061/40709\(257\)6](https://doi.org/10.1061/40709(257)6).
- [48] Gould, N.I.M. and Toint, P.L. (2007). "FILTRANE, a Fortran 95 Filter-Trust-Region Package for Solving Nonlinear Least-Squares and Nonlinear Feasibility Problems." *ACM Transactions on Mathematical Software*, 33(1), pp. 3–25. Available online: <https://doi.org/10.1145/1206040.1206043>.
- [49] More, J. and Sorensen, D.C. (1983). "Computing a Trust Region Step." *SIAM Journal on Scientific and Statistical Computing*, 4(3), pp. 553–572. Available online: <https://doi.org/10.1137/0904038>.
- [50] Byrd, R.H., Schnabel, R.B., and Shultz, G.A. (1988). "Approximate Solution of the Trust Region Problem by Minimization over Two-dimensional Subspaces." *Mathematical Programming*, 40(1), pp. 247–263. Available online: <https://doi.org/10.1007/BF01580735>.
- [51] Branch, M.A. (1995). *Inexact Reflective Newton Methods for Large-scale Optimization Subject to Bound Constraints*. Ph.D. Dissertation, Cornell University, Ithaca, NY.
- [52] Macconi, M., Morini, B., and Porcelli, M. (2009). "A Gauss–Newton Method for Solving Bound-constrained Underdetermined Nonlinear Systems." *Optimization Methods and Software*, 24(2), pp. 219–235. Available online: <https://doi.org/10.1080/10556780902753031>.
- [53] Bellavia, S., Macconi, M., and Pieraccini, S. (2012). "Constrained Dogleg Methods for Nonlinear Systems with Simple Bounds." *Computational Optimization and Applications*, 53, pp. 771–794. Available online: <https://doi.org/10.1007/s10589-012-9469-8>.
- [54] Branch, M.A., Coleman, T.F., and Li, Y. (1999). "A Subspace, Interior, and Conjugate Gradient Method for Large-scale Bound-constrained Minimization Problems." *SIAM Journal on Scientific Computing*, 21(1), pp. 1–23. Available online: <https://doi.org/10.1137/S1064827595289108>.
- [55] Bellavia, S. and Riccietti, E. (2018). "On an Elliptical Trust-Region Procedure for Ill-posed Nonlinear Least-Squares Problems." *Journal of Optimization Theory and Applications*, 178(3), pp. 824–859. Available online: <https://doi.org/10.1007/s10957-018-1318-1>.
- [56] Georgia Department of Transportation (GDOT). (2021). "Road & Traffic Data." (website) GDOT, Atlanta, GA. Available online: <http://www.dot.ga.gov/DS/Data#tab-4>.
- [57] Cornille, P. (1972). "Computation of Hankel Transforms." *SIAM Review*, 14(2), pp. 278–285. Available online: <https://doi.org/10.1137/1014032>.

- [58] Kim, J. (2011). "General Viscoelastic Solutions for the Multilayered Systems Subjected to Static and Moving Loads." *Journal of Materials in Civil Engineering*, 23(7), pp. 1007–1016. Available online: [https://doi.org/10.1061/\(ASCE\)MT.1943-5533.0000270](https://doi.org/10.1061/(ASCE)MT.1943-5533.0000270).
- [59] Valkó, P.P. and Abate, J. (2004). "Multi-precision Laplace Transform Inversion." *International Journal for Numerical Methods in Engineering*, 60(5), pp. 979–993. Available online: <https://doi.org/10.1002/nme.995>.
- [60] Conn, A.R., Gould, N.I., and Toint, P.L. (2000). *Trust-Region Methods*. MOS-SIAM Series on Optimization, Mathematical Programming Society/Society for Industrial and Applied Mathematics, Philadelphia, PA. Available online: <https://doi.org/10.1137/1.9780898719857>.
- [61] Lanotte, M.A. and Kutay, M.E. (2017). "Determination of AASHTO 1993 Layer Coefficients Considering Time- and Temperature-dependency of the Asphalt Mixture." 10th International Conference on the Bearing Capacity of Roads, Railways and Airfields (BCCRA 2017), Athens, Greece, June 28–30.
- [62] Abd El-Raof, H.S., Abd El-Hakim, R.T., El-Badawy, S.M., and Afify, H.A. (2018). "Simplified Closed-form Procedure for Network-level Determination of Pavement Layer Moduli from Falling Weight Deflectometer Data." *Journal of Transportation Engineering, Part B: Pavements*, 144(4). Available online: <https://doi.org/10.1061/JPEODX.0000080>.
- [63] Fu, G., Zhao, Y., Zhou, C., and Liu, W. (2020). "Determination of Effective Frequency Range Excited by Falling Weight Deflectometer Loading History for Asphalt Pavement." *Construction and Building Materials*, 235, 117792. Available online: <http://dx.doi.org/10.1016/j.conbuildmat.2019.117792>.